NOAA Technical Report NWS 19

A Point Energy and Mass Balance Model of a Snow Cover

Eric A. Anderson

February 1976

U.S. DEPARTMENT OF COMMERCE
National Oceanic and Atmospheric Administration
National Weather Service

NOAA TECHNICAL REPORTS

National Weather Service Series

The National Weather Service (NWS) makes observations and measurements of atmospheric phenomena, develops and distributes forecasts of weather conditions and warnings of adverse weather, and collects and disseminates weather information to meet the needs of the public and specialized users. The NWS develops the national meteorological service system and the improved procedures and techniques for weather and hydrologic measurements and forecasts and for their dissemination.

NWS series of NOAA Technical Reports is a continuation of the former series, ESSA Technical Report Weather Bureau (WB).

Reports 1 to 3 are available from the National Technical Information Service, U.S. Department of Commerce, Sills Bldg., 5285 Port Royal Road, Springfield, Va. 22151. Prices vary. Order by accession number (at end of each entry). Beginning with 4, Reports are available from the Superintendent of Documents, U.S. Government Printing Office, Washington, D.C. 20402.

ESSA Technical Reports

WB 1 Monthly Mean 100-, 50-, 30-, and 10-Millibar Charts January 1964 through December 1965 of the IQSY Period. Staff, Upper Air Branch, National Meteorological Center, February 1967 (AD 651 101)

WB 2 Weekly Synoptic Analyses, 5-, 2-, and 0.4-Mb Surfaces for 1964 (based on observations of the Meteorological Rocket Network during the IQSY). Staff, Upper Air Branch, National Meteorological Center, April 1967 (AD 652 696)

WB 3 Weekly Synoptic Analyses, 5-, 2-, and 0.4-Mb Surfaces for 1965 (based on observations of the Meteorological Rocket Network during the IQSY). Staff, Upper Air Branch, National Meteorological Center, August 1967 (AD 662 053)

WB 4 The March-May 1965 Floods in the Upper Mississippi, Missouri, and Red River of the North Basins. J. L. H. Paulhus and E. R. Nelson, Office of Hydrology, August 1967. Price $0.60.

WB 5 Climatological Probabilities of Precipitation for the Conterminous United States. Donald L. Jorgensen, Techniques Development Laboratory, December 1967. Price $0.40.

WB 6 Climatology of Atlantic Tropical Storms and Hurricanes. M. A. Alaka, Techniques Development Laboratory, May 1968. Price $0.20.

WB 7 Frequency and Areal Distributions of Tropical Storm Rainfall in the United States Coastal Region on the Gulf of Mexico. Hugo V. Goodyear, Office of Hydrology, July 1968. Price $0.35.

WB 8 Critical Fire Weather Patterns in the Conterminous United States. Mark J. Schroeder, Weather Bureau, January 1969. Price $0.40.

WB 9 Weekly Synoptic Analyses, 5-, 2-, and 0.4-Mb Surfaces for 1966 (based on meteorological rocketsonde and high-level rawinsonde observations). Staff, Upper Air Branch, National Meteorological Center, January 1969. Price $1.50.

WB 10 Hemispheric Teleconnections of Mean Circulation Anomalies at 700 Millibars. James F. O'Connor, National Meteorological Center, February 1969. Price $1.00.

WB 11 Monthly Mean 100-, 50-, 30-, and 10-Millibar Charts and Standard Deviation Maps, 1966-1967. Staff, Upper Air Branch, National Meteorological Center, April 1969. Price $1.25.

WB 12 Weekly Synoptic Analyses, 5-, 2-, and 0.4-Millibar Surfaces for 1967. Staff, Upper Air Branch, National Meteorological Center, January 1970. Price $1.50.

NOAA Technical Reports

NWS 13 The March-April 1969 Snowmelt Floods in the Red River of the North, Upper Mississippi, and Missouri Basins. Joseph L. H. Paulhus, Office of Hydrology, October 1970. Price $1.25. (COM-71-50269)

NWS 14 Weekly Synoptic Analyses, 5-, 2-, and 0.4-Millibar Surfaces for 1968. Staff, Upper Air Branch, National Meteorological Center, May 1971. Price $1.50. (COM-71-50383)

NWS 15 Some Climatological Characteristics of Hurricanes and Tropical Storms, Gulf and East Coasts of the United States. Francis P. Ho, Richard W. Schwerdt, and Hugo V. Goodyear, May 1975. (COM-75-11088)

(Continued on inside back cover)

NOAA Technical Report NWS 19

A Point Energy and Mass Balance Model of a Snow Cover

Eric A. Anderson
February 1976

Office of Hydrology
National Weather Service
Silver Spring, Md.

U.S. DEPARTMENT OF COMMERCE
Elliot L. Richardson, Secretary

National Oceanic and Atmospheric Administration
Robert M. White, Administrator

National Weather Service
George P. Cressman, Director

PREFACE

This report is basically a reproduction of the author's Ph.D. dissertation from Stanford University, California. The only significant difference is that the appendix containing a complete listing of the computer program is not included in this report. This is because of the length of the program (71 pages) and because a detailed program listing is probably only of interest to a few individuals. A copy of the program listing can be obtained by procuring a copy of the dissertation from University Microfilms in Ann Arbor, Michigan, 48106.

ACKNOWLEDGMENTS

The detailed verification of the snow cover energy and mass balance model is possible only because of the existence of the cooperative snow research project being conducted by the National Oceanic and Atmospheric Administration (NOAA) and the Agricultural Research Service (ARS). The contributions of the many people who have assisted in this project should be acknowledged.

Martin L. Johnson, Edwin T. Engman, and Ronald Whipkey of the ARS have played significant roles in the establishment and continued operation of the project. Carl T. Machell, Darwin Heath, and the late Roland Berube assisted in the construction of many of the project facilities and have provided valuable technician support services.

Max A. Kohler, Tor Nordenson, and Walter T. Wilson of NOAA were instrumental in the establishment of the project. The continued operation and growth of the project has been under the supervision and guidance of Dr. Eugene L. Peck. Charles Hoffeditz, Donald Baker, and Richard Farnsworth have provided valuable assistance and expertise on the procurement and operation of the many sensors and recording systems. Doris Brown has provided most of the technical support during the processing of the data.

Hugh Greenan has been the meteorological technician in charge of the NOAA-ARS snow research station since the station was established. Instrument installation and maintenance plus data collection are difficult under the climatic conditions that can occur at the snow research station. The continuity and high quality of the data are largely due to the efforts of Hugh Greenan. His devotion to excellence has contributed immeasurably to the project.

The comments and encouragement of Professor Ray K. Linsley throughout the preparation of this report are sincerely appreciated. The author would also like to thank: Professors Joseph B. Franzini and Robert L. Street, plus Dr. Eugene L. Peck for reviewing the final draft and providing suggestions for improving the presentation; my wife Melba for the many hours she spent typing draft copies; and Christy Cusimano and Kathryn Carey for typing the final report.

TABLE OF CONTENTS

TABLE OF CONTENTS (Continued)

TABLE OF CONTENTS (Continued)

LIST OF TABLES

LIST OF ILLUSTRATIONS

LIST OF SYMBOLS

Symbol	Description	Units
A	Activation energy of the snow	$cal \cdot mol^{-1}$
A_s	Albedo of snow expressed as a decimal fraction	
C	Concentration of water vapor	grams of vapor per cm^3 of air
C_D	$= D_{eo} \cdot \frac{1000}{P_a \cdot (273.16)^{n_d}}$	$cm^2 \cdot sec^{-1} \cdot {}^\circ K^{-n_d}$
C_H	Bulk transfer coefficient for heat	
$(C_H)_N$	Value of C_H under neutral conditions	
C_M	Bulk transfer coefficient for momentum (drag coefficient)	
$(C_M)_N$	Value of C_M under neutral conditions	
C_W	Bulk transfer coefficient for water vapor	
$(C_W)_N$	Value of C_W under neutral conditions	
C_d	Layer thickness parameter	
C_e	Experimental constant in Clasius-Clapeyron equation	mb
C_k	Effective thermal conductivity parameter	$cal \cdot cm^5 \cdot {}^\circ K^{-2} \cdot sec^{-1} \cdot gm^{-2}$
C_t	Theoretically based wind function coefficient with stability adjustment	$mm \cdot mb^{-1} \cdot km^{-1}$
$C_{t'}$	Theoretically based wind function coefficient without a stability adjustment	$mm \cdot mb^{-1} \cdot km^{-1}$
C_ν	Extinction coefficient parameter	$cm^2 \cdot mm^{1/2} \cdot gm^{-1}$
C_1	Fractional increase in density per cm of load at zero density and a temperature of 0°C	$cm^{-1} \cdot hr^{-1}$
C_2	Compaction parameter for snow	$cm^3 \cdot gm^{-1}$

C_3	Fractional settling rate for snow at 0°C for densities less than ρ_d	hr^{-1}
C_4	Settling parameter for snow	$°K^{-1}$
C_5	Ratio of fractional settling rate for wet snow as compared to dry snow	
CW_1	Maximum allowable lag time for water moving through snow	hr
CW_2	Lag time parameter	cm^{-1}
CW_3	Recession parameter for water moving through snow	hr
CW_4	Attenuation parameter for water moving through snow	$cm^3 \cdot gm^{-1}$
D_e	Effective diffusion coefficient for water vapor in snow	$cm^2 \cdot sec^{-1}$
D_{eo}	Effective diffusion coefficient for water vapor in snow at 0°C and 1000-mb pressure	$cm^2 \cdot sec^{-1} \cdot mb \cdot °K^{-n_d}$
D_v	Diffusion coefficient for water vapor	$cm^2 \cdot sec^{-1}$
D_z	Desirable thickness of the snow cover layers	cm
E	Water vapor flux	$gm \cdot cm^{-2} \cdot sec^{-1}$
E_n	The finite-difference equation for a given snow cover layer	
F1	$k_c + L_S \cdot D_v \cdot f'$	$cal \cdot cm^{-1} \cdot °K^{-1} sec^{-1}$
F2	$= T^{n_d} \cdot f'$	$gm \cdot cm^{-3} \cdot °K^{n_d - 1}$
F4	$= T^{n_d} \cdot f''$	$gm \cdot cm^{-3} \cdot °K^{n_d - 2}$
G_1	Grain size parameter	mm
G_2	Grain size parameter	$mm \cdot cm^6 \cdot gm^{-2}$
G_3	Grain size parameter	$mm \cdot cm^{12} \cdot gm^{-4}$
H	Sensible heat flux	$cal \cdot cm^{-2} \cdot sec$
I	Solar radiation flux	$cal \cdot cm^{-2} \cdot sec^{-1}$

I_n	Amount of solar radiation absorbed in layer n during a given time interval	$cal \cdot cm^{-2}$
I_o	Solar radiation flux at the snow surface	$cal \cdot cm^{-2} \cdot sec^{-1}$
I_z	Solar radiation flux at a depth z below the snow surface	$cal \cdot cm^{-2} \cdot sec^{-1}$
K_H	Eddy transfer coefficient for heat	$cm^2 \cdot sec^{-1}$
K_M	Eddy transfer coefficient for momentum	$cm^2 \cdot sec^{-1}$
K_v	Thermal diffusivity	$cm^2 \cdot sec^{-1}$
K_W	Eddy transfer coefficient for water vapor	$cm^2 \cdot sec^{-1}$
L	Monin-Obukhov length	cm
L_f	Latent heat of fusion (79.7)	$cal \cdot gm^{-1}$
L_s	Latent heat of sublimation (677)	$cal \cdot gm^{-1}$
L_W	Lag time for water moving through snow	hr
$L_{W_{max}}$	Maximum lag for the given snow cover conditions	hr
M	Snowmelt	mm
O_s	Snow cover outflow	mm
O_t	Snow cover outflow	$cm \cdot hr^{-1}$
P_a	Atmospheric pressure	mb
P_x	Precipitation	mm
Q_a	Incoming longwave radiation	$cal \cdot cm^{-2}$
Q_e	Latent heat transfer	$cal \cdot cm^{-2}$
Q_g	Snow-soil heat transfer	$cal \cdot cm^{-2}$
Q_h	Sensible heat transfer	$cal \cdot cm^{-2}$
Q_i	Incoming solar radiation	$cal \cdot cm^{-2}$
Q_{ir}	Incoming minus reflected all-wave radiation	$cal \cdot cm^{-2}$
Q_m	Advected heat	$cal \cdot cm^{-2}$
Q_n	Net radiation transfer	$cal \cdot cm^{-2}$
Q_r	Reflected solar radiation	$cal \cdot cm^{-2}$

ΔQ	Change in heat storage of the snow cover	$cal \cdot cm^{-2}$
R	The gas constant	$cal \cdot mol^{-1} \cdot {}^{\circ}K^{-1}$
Ri	Gradient Richardson number	
$(Ri)_B$	Bulk Richardson number	
Ri_{cr}	Critical Richardson number	
R_f	Flux Richardson number	
R_w	Gas constant for water vapor (0.110226)	$cal \cdot {}^{\circ}K^{-1} \cdot gm^{-1}$
S	Excess water in storage	cm
SCF	Ratio of the increase in water-equivalent of the snow cover to the catch in the precipitation gage	
T	Temperature	°K
T_g	Soil temperature	°K
T_o	Snow surface temperature	°K
T_s	Snow temperature	°K
T_w	Wet-bulb temperature	°K
U	Wind travel	km
U_n	Unknown variable for a given snow cover layer	
ΔU_n	Correction to be applied to U_{n_j} to get $U_{n_{j+1}}$	
V	Water vapor transfer between snow and air	mm
V_g	Vapor transfer between snow and soil	mm
W	Amount of liquid-water in the snow cover	mm
W_L	Amount of lagged excess water	cm
W_s	Weight of snow above a given layer expressed in terms of water equivalent	cm

W_e	Fractional liquid-water-holding capacity for snow	
$W_{e_{max}}$	Maximum value of W_e	
$W_{e_{min}}$	Minimum value of W_e	
W_f	Fractional amount of liquid-water in snow	
W_x	Amount of excess liquid-water in snow	cm
ΔWE	Change in water-equivalent of the snow cover	mm
$\underline{a}$	Empirically determined amount of vapor transfer with no wind	$mm \cdot mb^{-1}$
$\underline{b}$	Slope of empirical U versus $V/(e_a-e_o)$ relationship	$mm \cdot mb^{-1} \cdot km^{-1}$
c_i	Specific heat of ice	$cal \cdot gm^{-1} \cdot {}^\circ K^{-1}$
c_p	Specific heat of dry air	$cal \cdot gm^{-1} \cdot {}^\circ K^{-1}$
c_w	Specific heat of water (1.0)	$cal \cdot gm^{-1} \cdot {}^\circ K^{-1}$
d	Snow depth or layer thickness	cm
d_g	Depth below ground of soil temperature measurement	cm
d_s	Snow grain diameter	mm
e	Vapor pressure of air	mb
e_i	Saturation vapor pressure over ice	mb
e_o	Vapor pressure at the snow surface	mb
f(U)	Wind function	$mm \cdot mb^{-1}$
f'	Partial of water vapor concentration with respect to temperature $(\partial C/\partial T)$	$gm \cdot cm^{-3} \cdot {}^\circ K^{-1}$
f''	$\partial^2 C/\partial T^2$	$gm \cdot cm^{-3} \cdot {}^\circ K^{-2}$
f'''	$\partial^3 C/\partial T^3$	$gm \cdot cm^{-3} \cdot {}^\circ K^{-3}$
g	Acceleration of gravity	$cm \cdot sec^{-2}$
k	von Karman's constant (0.4)	
k_c	Thermal conductivity	$cal \cdot cm^{-1} \cdot sec^{-1} \cdot {}^\circ K^{-1}$

k_e	Effective thermal conductivity	$cal \cdot cm^{-1} \cdot sec^{-1} \cdot {}^{\circ}K^{-1}$
k_s	Intrinsic permeability	mm^2
m	Net sublimation	$gm \cdot cm^{-3} \cdot sec^{-1}$
n_d	Temperature exponent in the expression for the effective diffusion coefficient for water vapor in snow	
q	Specific humidity	grams of water vapor per gram of air
q_c	Conduction heat transfer	$cal \cdot cm^{-2} \cdot sec^{-1}$
r	Reflectivity of snow for longwave radiation (0.01)	
r_n	Residual when E_n is evaluated at the value of U_{n_j}	
t	Time	sec
Δt	Computational time interval	sec
Δt_h	Time interval	hr
u	Wind speed	$cm \cdot sec^{-1}$
u_*	Friction velocity	$cm \cdot sec^{-1}$
w	Amount of liquid water	$gm \cdot cm^{-3}$
z	Distance above or below the snow surface	cm
z_o	Roughness height parameter	cm
α	Experimentally determined parameter in the expression for the stability related function under stable conditions ($\alpha^{-1}=Ri_{cr}$)	
γ	$(c_p \cdot P_a)/(0.622 \cdot L_s)$	$mb \cdot {}^{\circ}K^{-1}$
ε	Emissivity of snow (0.99)	
η	Viscosity coefficient for snow	cm·hr
η_c	Viscosity coefficient when snow density is extrapolated to zero	cm·hr
η_o	Viscosity coefficient at 0°C	cm·hr
η_t	Viscosity coefficient at a given temperature	cm·hr

θ	Weighting factor for spacial derivatives in finite difference expressions	
υ	Solar radiation extinction coefficient for snow	cm^{-1}
υ_i	Extinction coefficient for clear ice	mm^{-1}
ρ_a	Density of air	$gm \cdot cm^{-3}$
ρ_d	The density below which the settling rate for snow equals C_3	$gm \cdot cm^{-3}$
ρ_e	Density above which $W_e = W_{e_{min}}$	$gm \cdot cm^{-3}$
ρ_i	Density of ice	$gm \cdot cm^{-3}$
ρ_{ns}	Density of new snow	$gm \cdot cm^{-3}$
ρ_s	Density of the ice portion of the snow	$gm \cdot cm^{-3}$
ρ_w	Density of water (1.0)	$gm \cdot cm^{-3}$
σ	Stefan-Boltzmann constant ($1.355 \cdot 10^{-12}$)	$cal \cdot cm^{-2} \cdot {}^\circ K^{-4} \cdot sec^{-1}$
τ	Shear stress	$dynes \cdot cm^{-2}$
τ_o	Shear stress at the surface	$dynes \cdot cm^{-2}$
ϕ_H	Stability-related function for heat	
ϕ_M	Stability-related function for momentum	
ϕ_W	Stability-related function for water vapor	

Appendix A

C_{H1}	$= 0.0222$	$cal \cdot gm^{-1} \cdot {}^\circ K^{-1}$
C_{H2}	$= 0.00176$	$cal \cdot gm^{-1} \cdot {}^\circ K^{-1}$
DL_1	$= z_n - z_{n-1}$	cm
DL_2	$= z_{n+1} - z_n$	cm
F3	$= T^{n_d} \cdot f'' + n_d \cdot f' \cdot T^{(n_d-1)}$	$gm \cdot cm^{-3} \cdot {}^\circ K^{n_d-2}$
F5	$= T^{n_d} \cdot f''' + n_d \cdot f'' \cdot T^{(n_d-1)}$	$gm \cdot cm^{-3} \cdot {}^\circ K^{n_d-3}$

$F6_n$	$= DL_1 \cdot T_{n+1} + (DL_2 - DL_1) \cdot T_n - DL_2 \cdot T_{n-1}$	cm·°K
$F7_n$	$= DL_1 \cdot T_{n+1} - (DL_1 + DL_2) \cdot T_n + DL_2 \cdot T_{n-1}$	cm·°K

Superscripts

t	Time at the beginning of a computational time interval	sec
$t+\Delta t$	Time at the end of a computational time interval	sec

Subscripts

a	Measurement level above snow surface when using bulk transfer coefficients
g	Soil
j	Iteration number
n	Layer number for snow cover (surface layer is layer zero)
N	Total number of snow cover layers

A POINT ENERGY AND MASS BALANCE MODEL OF A SNOW COVER

Eric A. Anderson

Office of Hydrology, National Weather Service, NOAA
Silver Spring, Md.

ABSTRACT. A point energy and mass balance model is developed for a snow cover. The model is based on two equations. These are the snow cover energy balance equation and the equation for energy transfer within a snow cover. The snow cover is divided into finite layers. Implicit finite-difference expressions, based on the two equations, are written for each layer. This set of non-linear finite-difference equations is solved by use of the Newton-Raphson iteration technique. The model also includes mathematical representations of the densification of the snow and the retention and transmission of liquid-water.

The model is tested on an extensive, high-quality set of data obtained as part of a cooperative snow research project between NOAA and the Agricultural Research Service near Danville, Vermont. Six years of data are used. The comparison of observed and computed values of snow cover outflow, water-equivalent, temperature, and density, plus snow surface temperature and density is quite good. The results obtained with this energy balance model are compared to results obtained with a temperature index snow cover model. The energy balance model gives improved results. These comparisons and the energy exchange theory suggest that an energy balance model should give improved results in open areas and under extreme conditions when adequate data are available. Index snow cover models should give completely adequate results in heavily forested areas.

CHAPTER I: INTRODUCTION

BACKGROUND

Snow is an important part of the hydrologic cycle in many parts of the world. Accurate estimates of the volume of water contained in the snow cover and of the rate of release of that water are needed for many purposes. These include river and flood forecasting, water supply forecasting, reservoir operation, watershed management, and the design of hydrologic and hydraulic structures.

Measurements of the snow cover and its properties have been made for a century or more. The first application of modern energy transfer theory to a snow cover was the investigation conducted by Sverdrup (1936) on West Spitzbergen Island in 1934. This investigation primarily dealt with turbulent heat transfer between the snow and the air, although a complete energy balance was also computed. Sverdrup's work laid the foundation for most of the snow cover energy transfer studies which were to follow.

In the 1940's the Corps of Engineers and the U.S. Weather Bureau initiated the Cooperative Snow Investigations. The purpose of these investigations was to promote a more fundamental understanding of snow hydrology for project design and streamflow forecasting, particularly in the western part of the United States. Extensive data collection and analysis were performed over a 10-year period at three research watersheds. The summary report of the Snow Investigations was the publication Snow Hydrology (1956). The results and methods included in this publication are widely referenced and form the basis of many of the snow cover models in use today.

At about the same time as the Snow Investigations, extensive studies were being conducted in the Soviet Union dealing with the physical properties, formation, and melting of a snow cover. A summary of the studies concerned with the melting of a snow cover was published by Kuzmin (1961). This publication contains a very thorough and complete discussion of snow cover energy exchange from both a theoretical and practical viewpoint. Unfortunately, this excellent publication was not translated into English until 1972.

SNOW COVER SIMULATION MODELS

After the publication of Snow Hydrology, and especially with the advent of the digital computer, emphasis has been placed on the development of conceptual simulation models of the snow accumulation and ablation process. These models are being developed for use in solving many kinds of practical hydrologic problems. In a conceptual model, each major physical process is represented by a mathematical relationship. This is in contrast to degree-day techniques which were commonly used to estimate snow cover outflow directly from air temperature data. Degree-day techniques do not include the snow accumulation process, nor do they explicitly account for heat deficits, liquid-water retention and transmission, and the areal extent of the snow cover.

Two of the earliest snow cover simulation models were developed by Rockwood (1964) as part of the SSARR model and by Anderson and Crawford (1964) for use in conjunction with the Stanford Watershed Model. Both of these models use air temperature as the sole index to energy exchange across the air-snow interface. This is also true of more recent models developed by Eggleston et al. (1971) and Anderson (1973). Snow Hydrology contains generalized snowmelt equations for various forest cover conditions. These equations are based on theoretical and empirical considerations. As the amount of forest cover decreases, the number of types of data that are required increases. These generalized snowmelt equations are used in several snow cover simulation models [Amorocho and Espildora (1966), Carlson et al. (1974), and as an option in the current SSARR model (1972)]. The net radiation balance, estimated from incoming solar radiation and air temperature, is used to compute energy exchange in the snow cover simulation model developed by Leaf and Brink (1973). This model was developed to determine the probable hydrologic effects of forest management.

All of the previously mentioned models compute snowmelt by one set of equations and the change in the heat deficit of the snow cover by a separate equation (the SSARR model does not compute the heat deficit). Thus, these models are not energy balance models. Some of these models use empirical procedures to estimate the change in the heat deficit during non-melt periods. The Eggleston et al., and the Leaf and Brink models use the one-dimensional Fourier heat-conduction equation and

the assumption that the snow surface temperature (T_o) equals the air temperature (T_a) to compute temperatures at one or two points within the snow cover. Quick (1967) also uses the heat-conduction equation and the assumption that $T_o = T_a$ to compute changes in the snow cover temperature profile during periods when depth can be considered to be constant. In addition, Quick accounts for the effect of the density profile on the snow cover temperature profile.

Recently several energy balance snow cover models have been developed [Obled (1973), Humphrey and Skau (1974), and Outcalt et al. (1975)]. The energy balance includes net radiation transfer, latent and sensible heat transfer, heat transfer by rain water, and the change in heat storage of the snow cover. The change in heat storage is also determined from the computed temperature profiles at the beginning (time t) and the end (time $t+\Delta t$) of each computational time interval (Δt). Finite-difference approximations to the Fourier heat-conduction equation are solved to determine the temperature profile at time $t+\Delta t$ knowing the profile at time t. The thermal conductivity of the snow varies with snow density. The snow surface temperature is determined by various iterative schemes which seek to reduce to an acceptable level the difference between the value of the change in heat storage term in the energy balance equation and the value of the same term as determined from changes in snow cover temperatures. None of these models include the densification of the snow cover. Humphrey and Skau use periodic measurements of the density profile to account for changes in snow density. The other two models merely use the measured total snow cover density. Only Obled compares computed and observed values of snow cover outflow and water equivalent. Humphrey and Skau, as well as Obled, show comparisons of computed and observed snow cover temperature profiles. Outcalt, et al. only make comparisons between the computed and observed dates on which melt begins and ablation is complete.

BACKGROUND OF THIS INVESTIGATION

This investigation has evolved out of an earlier study of snow cover energy exchange [Anderson (1968)]. A snow cover energy balance model was developed and tested in this earlier study. The change in heat storage was computed only in the case of the cooling of an isothermal

snow cover immediately following a period of melt. Thus the model could only be used during extended snowmelt periods or periods of daytime melt and nighttime heat loss. The model was tested on data collected as part of a lysimeter study of snowmelt at the Central Sierra Snow Laboratory during the Snow Investigations (1955). The data included all the necessary input meteorological variables plus various snow cover variables, such as water equivalent, depth, temperature, and snow cover outflow. The agreement between computed and observed values of daily snow cover outflow and of mean nighttime snow surface temperature was very good. However, there were several problems. The period of record was quite short (17 days), plus there was some uncertainty regarding the accuracy of a portion of the data. More importantly, there was almost no variability in meteorological conditions during the period (warm days and cool nights with mostly clear skies and moderate winds). Thus, it was not possible to determine if the model was valid over a wide range of meteorological conditions. Attempts at finding another high-quality data set that included measurements of all the necessary input and verification variables were unsuccessful.

Since the data needed to adequately test snow cover energy exchange models were not available, the decision was made to establish a snow research station in order to obtain the necessary data. Such a station was established as part of a cooperative research project concerned with the physical processes in snow metamorphosis and snowmelt. This project is being conducted by the National Oceanic and Atmospheric Administration (NOAA) and the Agricultural Research Service (ARS) [Johnson and Anderson (1968)]. The station is located within the ARS's Sleepers River Research Watershed near Danville, Vermont. This is not the most ideal location in terms of the amount of snow (average maximum water-equivalent of about 300 mm), but is nearly ideal in terms of the wide variety of meteorological conditions that occur during snowmelt periods. Data collection at the NOAA-ARS snow research station began in December 1968. Measurement methods have changed over time due to advances in instrumentation. Also, additional types of data have been added in order to provide more and better information for the testing of snow cover energy exchange models.

In addition to better data for model testing, additional information was becoming available on the basic energy transfer processes and on the numerical techniques needed to solve the basic snow cover energy exchange equations. Thus, it became obvious that a new, more theoretically sound, and more complete snow cover energy balance model should be developed.

PURPOSE OF THIS INVESTIGATION

The basic purpose of this investigation is to expand the understanding of snow cover energy exchange by combining the results of recent and past theoretical studies of specific energy transfer processes and to test the resulting energy and mass balance model on the data collected at the NOAA-ARS snow research station.

Even though the resulting model is a research model and is probably too complex for direct practical application, in the long term such research models should result in improved operational models. Improvements to current operational snow cover simulation models will likely be as a result of a more thorough understanding of the basic energy transfer processes and their interactions. Only with such an understanding can the effect of various assumptions, approximations, and simplifications which are a part of operational snow cover models be evaluated. A more complete understanding of the energy exchange processes affecting a snow cover should also enable the hydrologist to more intelligently select the appropriate type of snow cover model given the problem to be solved and the climatic and physiographic characteristics of the area. The available data could be a constraint in model selection or it could be determined that it is worth the effort and expense to obtain the additional data needed to apply the proper type of model. This decision is possible only if the process being modeled is well enough understood so that the difference in accuracy between various types of models can be reasonably determined.

CHAPTER II; SNOW COVER ENERGY EXCHANGE

INTRODUCTION

This chapter deals with the development of the equations used to estimate the gain or loss of heat by a snow cover. Of primary importance is the energy exchange at the snow-air interface. Under most conditions the energy exchange at the snow-air interface is much greater than the heat transfer at the snow-soil interface.

SNOW COVER ENERGY BALANCE EQUATION

The energy balance of a snow cover can be expressed as:

$$Q_n + Q_e + Q_h + Q_g + Q_m = \Delta Q \qquad (2.1)$$

where: Q_n = net radiation transfer,
Q_e = latent heat transfer,
Q_h = sensible heat transfer,
Q_g = heat transfer across the snow-soil interface,
Q_m = heat transfer by mass changes (advected heat), and
ΔQ = change of heat storage of the snow cover.

The units of each term in Eq. (2.1) are $cal \cdot cm^{-2}$.

For a given time interval (Δt) beginning at time t, the term ΔQ can be expressed as:

$$\Delta Q = (d \cdot \rho_s)^t \cdot \left[(c_i \cdot T_s)^{t+\Delta t} - (c_i \cdot T_s)^t \right] + \frac{L_f \cdot \rho_w}{10} \cdot (W^{t+\Delta t} - W^t) \qquad (2.2)$$

where: d = depth of the snow cover (cm),
ρ_s = density of the solid (ice) portion of the snow cover ($gm \cdot cm^{-3}$),
c_i = specific heat of ice ($cal \cdot gm^{-1} \cdot °K^{-1}$),
T_s = temperature of the solid portion of the snow cover (°K),
L_f = latent heat of fusion (79.7 $cal \cdot gm^{-1}$ at 0°C),
ρ_w = density of water ($gm \cdot cm^{-3}$) (a value of 1.0 $gm \cdot cm^{-3}$ is used), and
W = the amount of liquid-water in the snow cover, expressed as a depth (mm).

Water in both the liquid and solid phases can exist in a snow cover. The liquid-water is the result of melting or rainfall. The liquid-water may freeze, remain in storage, or when the snow cover is isothermal

at 0°C and saturated (in this condition a snow cover is commonly referred to as "ripe") the excess liquid-water becomes outflow from the bottom of the snow cover.

NET RADIATION TRANSFER

Net radiation can be measured at a particular point and be used in the energy balance equation. However, net radiation is highly dependent on the surface over which it is measured. If the energy balance equation is ultimately being developed for areal application, it is more useful to break Q_n down into its components. In an areal application the incident components of net radiation can be extrapolated from one point to another by taking topography and vegetation cover into account. The outgoing components of net radiation are a function of the albedo and surface temperature of the snow cover, both of which can be highly variable over an area. The albedo of the snow cover must be measured or estimated, whereas it will be shown that the snow surface temperature can be computed from the energy balance equation.

The components of net radiation transfer for a given time interval can be expressed as:

$$Q_n = Q_i - Q_r + \varepsilon \cdot Q_a - \Delta t \cdot \varepsilon \cdot \sigma \cdot T_o^4 \qquad (2.3)$$

where: Q_i = incident (incoming) solar radiation ($cal \cdot cm^{-2}$),

Q_r = reflected (outgoing) solar radiation ($cal \cdot cm^{-2}$),

ε = emissivity in the longwave portion of the energy spectrum (a value of 0.99 is used),

Q_a = incoming (emitted by the atmosphere and terrestrial objects) longwave radiation ($cal \cdot cm^{-2}$),

σ = Stefan-Boltzmann constant ($cal \cdot cm^{-2} \cdot °K^{-4} \cdot sec^{-1}$) (a value $1.355 \cdot 10^{-12}$ is used),

Δt = the computational time interval (sec), and

T_o = snow surface temperature (°K).

It should be noted that Albedo = Q_r/Q_i and $\varepsilon = 1.0 - r$ where r is reflectivity in the longwave portion of the spectrum. Emissivity also equals absorption. Snow has been found to be nearly a perfect black-body in the longwave portion of the spectrum [Shafer and Super (1971), Snow Hydrology (1956)].

If we let

$$Q_{ir} = Q_i - Q_r + \varepsilon \cdot Q_a \tag{2.4}$$

where Q_{ir} is thus defined as the incident minus reflected all-wave radiation, then the equation for net radiation transfer becomes:

$$Q_n = Q_{ir} - \Delta t \cdot \varepsilon \cdot \sigma \cdot T_o^4 \quad . \tag{2.5}$$

TURBULENT TRANSFER BETWEEN THE SNOW AND THE ATMOSPHERE

Introduction

The purpose of this section is to outline the development of the equations used to estimate latent and sensible heat transfer between the snow cover and the atmosphere. A more detailed derivation and discussion of these equations and concepts can be found in a number of books [Rose (1966), Priestly (1959), Lumley and Panofsky (1964), Sutton (1953, 1954)] in addition to the articles referred to in this section.

Surface Boundary Layer

Under turbulent conditions the thickness of the surface boundary layer is on the order of 10 to 50 meters. Flow in the atmosphere above a snow cover, with the exception of calm periods, either at night or when the air temperature is well above 0°C, is characteristically turbulent. The surface boundary layer contains a viscous sublayer where molecular conduction processes play an important role. The thickness of this layer over a snow cover is about 1 millimeter [Sverdrup (1936), Kraus (1973)]. The remainder of the surface boundary layer is sometimes referred to as the constant flux layer. Within this layer, shear stress and the vertical fluxes of heat and water vapor are considered constant with height. This is the layer of maximum interest in estimating latent and sensible heat exchange between the snow cover and the atmosphere.

Eddy Flux

The average turbulent flux ($\overline{F}$) of any transferable conservative property (c), per unit mass of fluid, can be expressed as:

$$\overline{F} = \overline{\rho_a \cdot w \cdot c} = \overline{\rho_a \cdot w} \cdot \overline{c} + \overline{\rho_a \cdot w' \cdot c'} \tag{2.6}$$

where: w = vertical velocity,

ρ_a = density of air ($gm \cdot cm^{-3}$), bars denote averages, and primes denote random instantaneous departures from the mean.

At a height in the order of one to several meters above a uniform surface $\overline{\rho_a \cdot w}$ and thus $\overline{\rho_a \cdot w'}$ have been found to be zero over a sufficiently long period (in the order of hours). Since by definition there can be no correlation between $\overline{\rho_a \cdot w}$ and $\bar{c}$, the term $\overline{\rho_a \cdot w} \cdot \bar{c}$ must be zero. However, the value of $\overline{\rho_a \cdot w' \cdot c'}$ will not be zero if there is any correlation between $\rho_a \cdot w'$ and c'. Such a correlation exists; and therefore:

$$\bar{F} = \overline{\rho_a \cdot w' \cdot c'} \quad . \tag{2.7}$$

Eddy correlation instruments based on Eq. (2.7) have been developed to measure sensible heat and water vapor flux [Dyer (1961), Dyer and Maher (1965)]. However, it would not be at all practical to measure these fluxes by eddy correlation instruments for routine hydrologic applications. Thus, other equations, based on more easily obtainable measurements, must be used.

Transfer Coefficient Hypothesis

The hypothesis is that the mean vertical flux of any conservative quantity c is proportioned to the gradient of the mean value $\bar{c}$ of the quantity in the vertical direction. The factor of proportionally between the flux and the gradient is called an exchange coefficient, A_c. English language writers have commonly used K_t defined by $K_t = A_c/\rho_a$. K_t is referred to as a transfer coefficient. Thus we can write

$$\bar{F} = \rho_a \cdot K_t \cdot \frac{\partial \bar{c}}{\partial z} \tag{2.8}$$

where z is height above the surface (cm). Mean values will be used for the transferred quantities throughout the remainder of this report; thus the bar notation will not be used in succeeding equations.

Based on the transfer coefficient hypothesis, equations can be written for the mean flux of momentum per unit area, sensible heat, and water vapor. The equation for momentum per unit area (shear stress) is:

$$\tau = \rho_a \cdot K_M \cdot \frac{\partial u}{\partial z} \tag{2.9}$$

where: τ = shear stress (dynes$\cdot$cm^{-2}),

u = wind speed (cm$\cdot$sec^{-1}), and

K_M = eddy transfer coefficient for momentum (cm$^2\cdot$sec^{-1}).

The equation for sensible heat flux is:

$$H = -\rho_a \cdot c_p \cdot K_H \cdot \frac{\partial T}{\partial z} \tag{2.10}$$

where: H = sensible heat flux (cal$\cdot$cm$^{-2}\cdot$sec)

c_p = specific heat of dry air (cal$\cdot$gm$^{-1}\cdot{}^\circ$K^{-1}),

T = air temperature ($^\circ$K), and

K_H = eddy transfer coefficient for heat (cm$\cdot$sec^{-1}).

To be precise, potential temperature at the snow surface should be used in Eq. (2.10). However, when working with the first few meters above the snow, the difference between potential and actual temperature is insignificant.

The equation for water vapor flux is:

$$E = -\rho_a \cdot K_W \cdot \frac{\partial q}{\partial z} \tag{2.11}$$

where: E = water vapor flux (gm$\cdot$cm$^{-2}\cdot$sec^{-1}),

q = specific humidity (grams water vapor per gram air), and

K_W = eddy transfer coefficient for water vapor (cm$^2\cdot$sec^{-1}).

Turbulent Transfer under Neutral Stability

An atmosphere having an adiabatic temperature profile is neutrally stable. Under fully turbulent, neutral conditions within the constant flux layer the wind profile is logarithmic and described by the expression:

$$\frac{u}{u_*} = \frac{1}{k} \cdot \ln\left(\frac{z}{z_o}\right) \tag{2.12}$$

where: k = von Karman's constant (a value of 0.40 is used),

z_o = the roughness length (cm), and

u_* = the friction velocity defined by

$$u_* = (\tau_o/\rho_a)^{1/2} \tag{2.13}$$

where: τ_o = the shear stress at the surface (dynes$\cdot$cm^{-2}). From Eq. (2.12) we would formally regard z_o as the value of z for which $u = 0$. However, in reality there is a departure from the logarithmic profile at values of z comparable to z_o. z_o is determined from a plot of u versus ln z with neutral stability.

Differentiating Eq. (2.12) yields:

$$\frac{\partial u}{\partial z} = \frac{u_*}{k \cdot z} \quad . \tag{2.14}$$

Since shear stress is considered constant with height in the constant flux layer:

$$\tau = \tau_o = \text{constant} \quad . \tag{2.15}$$

It should also be noted that u_* can be considered constant with height within this layer. Combining Eqs. (2.9), (2.13), (2.14), and (2.15) gives:

$$K_M = k \cdot u_* \cdot z = k^2 \cdot z^2 \cdot \frac{\partial u}{\partial z} \quad . \tag{2.16}$$

The anology between turbulent transfer of momentum, heat, and matter, if assumed exact (as first suggested by Reynolds), implies that the three transfer coefficients are equal. Assuming that $K_W = K_M$ for neutral stability and by using Eqs. (2.11) and (2.16), we obtain:

$$E = -\rho_a \cdot k^2 \cdot z^2 \cdot \frac{\partial u}{\partial z} \cdot \frac{\partial q}{\partial z} \quad . \tag{2.17}$$

Specific humidity can be approximated from:

$$q = \frac{0.622 \cdot e}{P_a} \tag{2.18}$$

where: 0.622 = the molecular weight ratio of water vapor to dry air,

e = vapor pressure (mb), and

P_a = atmospheric pressure (mb).

Substituting Eq. (2.18) into Eq. (2.17) and integrating between two observational heights z_1 and z_2 yields:

$$E = -\frac{\rho_a \cdot 0.622}{P_a} \cdot k^2 \cdot \frac{(u_2 - u_1) \cdot (e_2 - e_1)}{(\ln z_2/z_1)^2} \quad . \tag{2.19}$$

The same thing can be done for sensible heat flux. Assuming $K_H = K_M$ for neutral stability, H can be expressed as:

$$H = -\rho_a \cdot c_p \cdot k^2 \cdot z^2 \cdot \frac{\partial u}{\partial z} \cdot \frac{\partial T}{\partial z} \quad . \tag{2.20}$$

Integrating between two observational heights yields:

$$H = -\rho_a \cdot c_p \cdot k^2 \cdot \frac{(u_2 - u_1) \cdot (T_2 - T_1)}{(\ln z_2/z_1)^2} \quad . \tag{2.21}$$

Generalized Turbulent Transfer

The logarithmic wind profile [Eq. (2.14)] has been generalized by Monin and Obukhov (1954) to apply under all conditions, giving:

$$\frac{\partial u}{\partial z} = \frac{u_*}{k \cdot z} \cdot \phi_M \tag{2.22}$$

where ϕ_M is an unknown stability related function to be determined by experiment. Under neutral stability, $\phi_M = 1.0$. Functions analogous to ϕ_M may also be used to describe generalized forms for temperature and humidity profiles, giving:

$$\frac{\partial T}{\partial z} = - \frac{H}{\rho_a \cdot c_p \cdot k \cdot u_* \cdot z} \cdot \phi_H \tag{2.23}$$

and

$$\frac{\partial q}{\partial z} = - \frac{E}{\rho_a \cdot k \cdot u_* \cdot z} \cdot \phi_W \tag{2.24}$$

where ϕ_H and ϕ_W are stability related functions for heat and water vapor.

From these three generalized equations for the vertical profiles of wind, temperature, and humidity, plus the basic turbulent transfer expressions [Eqs. (2.9), (2.10), and (2.11)], it can be determined that:

$$\frac{K_W}{K_M} = \frac{\phi_M}{\phi_W} \tag{2.25}$$

and

$$\frac{K_H}{K_M} = \frac{\phi_M}{\phi_H} \quad . \tag{2.26}$$

Using Eqs. (2.22) through (2.24) and the expression relating specific humidity and vapor pressure [Eq. (2.18)], generalized equations for water vapor and heat flux can be written as:

$$E = - \frac{\rho_a \cdot 0.622}{P_a} \cdot k^2 \cdot z^2 \cdot \frac{\partial u}{\partial z} \cdot \frac{\partial e}{\partial z} \cdot \frac{1}{\phi_W \cdot \phi_M} \tag{2.27}$$

and

$$H = -\rho_a \cdot c_p \cdot k^2 \cdot z^2 \cdot \frac{\partial u}{\partial z} \cdot \frac{\partial T}{\partial z} \cdot \frac{1}{\phi_H \cdot \phi_M} \quad . \tag{2.28}$$

Determination of ϕ_M, ϕ_H, and ϕ_W

Many investigators have used the Monin-Obukhov "similarity theory" [Monin and Obukhov (1954)] as a framework to define the functions ϕ_M, ϕ_H, and ϕ_W. According to this theory ϕ_M, ϕ_H, and ϕ_W should be functions of a dimensionless height ratio z/L where L is constant with height within the surface boundary layer. L is defined by:

$$L = - \frac{u_*^3 \cdot c_p \cdot \rho_a \cdot T}{k \cdot g \cdot H} \tag{2.29}$$

where g is the acceleration of gravity ($cm \cdot sec^{-2}$). The height ratio z/L is positive for stable conditions, negative for unstable, and equal to zero for neutral stability. Experimental determination of the functions $\phi_M(z/L)$, $\phi_H(z/L)$, and $\phi_W(z/L)$ are made by measuring the profiles of wind speed, temperature, and humidity plus shear stress and the fluxes of heat and water vapor. H, E, and τ can be measured by eddy correlation techniques. Shear stress at the surface can also be measured by drag plates [Bradley (1968)]. Accurate measurements of water vapor flux can be made with large weighing lysimeters [Pruitt and Angus (1960)].

There are a number of determinations of the stability-related functions which have been reported in the literature [Businger et al. (1971), Dyer (1967), Dyer and Hicks (1970), McVehil (1964), Webb (1970), Oke (1970), Pruitt et al. (1971)]. There is not complete agreement from these determinations; however, the following relationships are quite representative of the majority of the determinations. For stable conditions:

$$\phi_M = \phi_H = \phi_W = 1 + 5 \cdot \frac{z}{L} \tag{2.30}$$

which means that $K_H = K_W = K_M$ for stable conditions. For unstable conditions:

$$\phi_M = (1 - 16 \cdot z/L)^{-1/4} \tag{2.31}$$

and

$$\phi_H = \phi_W = (1 - 16 \cdot z/L)^{-1/2} \quad . \tag{2.32}$$

Eqs. (2.31) and (2.32) are frequently called the Businger-Dyer formulas.

In order to apply these functions to estimate heat and vapor fluxes when H and u_* are not measured, z/L must be related to a stability criterion that can be computed from data that are commonly available. Richardson (1920) derived a stability criterion which reflects the ratio

of the consumption of energy by the buoyancy forces to the rate of its production by wind shear. This ratio can be expressed as:

$$R_f = - \frac{g \cdot H}{c_p \cdot T \cdot \tau \cdot (\partial u / \partial z)} \tag{2.33}$$

where R_f is referred to as the flux form of the Richardson number. Using Eqs. (2.9) and (2.13) the ratio of z/L to R_f is:

$$\frac{z/L}{R_f} = \frac{k \cdot z \cdot (\partial u / \partial z)}{u_*} = \phi_M \quad . \tag{2.34}$$

Using Eqs. (2.9) and (2.10), R_f reduces to the more familiar gradient Richardson number:

$$Ri = \frac{g \cdot (\partial T / \partial z)}{T \cdot (\partial u / \partial z)^2} \tag{2.35}$$

where

$$Ri = R_f \cdot \frac{K_M}{K_H} \quad . \tag{2.36}$$

As can be seen, the graident Richardson number can be computed from observations of temperature and wind speed. Ri will be referred to as the Richardson number, without qualification, in the rest of this report. Combining Eq. (2.34) and Eq. (2.36) the relationship between Ri and z/L is:

$$z/L = \frac{K_H}{K_M} \cdot \phi_M \cdot Ri \quad . \tag{2.37}$$

Using this relationship between z/L and Ri, plus Eq. (2.26), the ϕ functions can now be written in terms of the Richardson number. For stable conditions:

$$\phi_M = \phi_H = \phi_W = (1 - 5 \cdot Ri)^{-1} \tag{2.38}$$

and for unstable conditions:

$$\phi_M = (1 - 16 \cdot Ri)^{-1/4} \tag{2.39}$$

and

$$\phi_H = \phi_W = (1 - 16 \cdot Ri)^{-1/2} \quad . \tag{2.40}$$

It should be noted that Ri = z/L for unstable conditions using the Businger-Dyer formulas.

The expression:

$$Ri = \frac{2 \cdot g \cdot (z_2 - z_1) \cdot (T_2 - T_1)}{(T_2 + T_1) \cdot (u_2 - u_1)^2} \tag{2.41}$$

can be used to determine the Richardson number at the geometric mean height of z_2 and z_1.

The Critical Richardson Number

Eq. (2.38) can be written in a more general form as:

$$\phi_M = \phi_H = \phi_W = (1.0-\alpha \cdot Ri)^{-1} \tag{2.42}$$

where α is a parameter to be determined experimentally. As z/L in Eq. (2.30) approaches ∞, thus ϕ_M, ϕ_H, and ϕ_W approach ∞, Ri approaches α^{-1}. $Ri = \alpha^{-1}$ is an empirical expression for the critical Richardson number (Ri_{cr}). The critical Richardson number is the value of Ri beyond which turbulent conditions no longer exist.

In his original study Richardson (1920) argued that $Ri_{cr} = 1.0$. Experimental data indicates that Ri_{cr} is less than 1.0 with most investigations suggesting values in the range from 0.15-0.25 [Businger (1973)]. Brutsaert (1972) indicates that evaporation and radiation increase the critical Richardson number depending on atmospheric conditions. He indicates that there is no definite Ri_{cr}, but rather a range between 0.25, below which turbulence is very likely, and somewhat higher than 0.5, above which turbulence is improbable.

The value of the critical Richardson number is especially important in the case of snow because stable conditions should predominate over a snow cover. The air temperature normally exceeds the snow surface temperature because of the high albedo and high emissivity of snow, as well as the fact that the snow surface temperature cannot exceed 0°C.

Computation of Turbulent Transfer Using Measurements at One Level

In many applications, measurements of wind, temperature, and humidity at two levels are not available or it is not practicable to make observations at two levels. This is true in most cases when snow cover energy exchange computations are needed for hydrologic application.

In order to compute the mean flux of shear stress, sensible heat, and water vapor between the surface and some height above the surface (z_a), the integrated form of the basic transfer equations [Eqs. (2.9), (2.10), and (2.11)] are used. If these equations are integrated between z_o and z_a (assuming $u = 0$, $T = T_o$, and $e = e_o$ when $z = z_o$ and

substituting Eq. (2.18) for specific humidity), the resulting expressions are:

$$\tau = u_*^2 \cdot \rho_a = \rho_a \cdot C_M \cdot u_a^2, \tag{2.43}$$

$$H = -\rho_a \cdot c_p \cdot C_H \cdot u_a \cdot (T_a - T_o), \tag{2.44}$$

and

$$E = -\frac{\rho_a \cdot 0.622}{P_a} \cdot C_W \cdot u_a \cdot (e_a - e_o) \tag{2.45}$$

where: e_o = vapor pressure at the snow surface (mb) (assumed equal to the saturation vapor pressure at the snow surface temperature),

u_a = wind speed at a height z_a ($cm \cdot sec^{-1}$),

T_a = air temperature at z_a (°K),

e_a = vapor pressure of the air at z_a (mb),

C_M = a dimensionless coefficient referred to as the drag coefficient, and

C_H and C_W are the coefficients equivalent to the drag coefficient for sensible heat and water vapor flux. Deardorff (1968) calls these coefficients "bulk" transfer coefficients.

Under neutral conditions, assuming $K_H = K_W = K_M$, and using Eq. (2.16) for K_M, the integration of Eqs. (2.9), (2.10), and (2.11) yields:

$$(C_H)_N = (C_W)_N = (C_M)_N = \frac{k^2}{\left(\ln \frac{z_a}{z_o}\right)^2} \tag{2.46}$$

where the subscript N signifies neutral conditions.

Deardorff (1968) computed the ratio of each of the bulk transfer coefficients to its value under neutral conditions. For unstable conditions these ratios were computed by first integrating the genearlized profile relationships [Eqs. (2.22), (2.23), and (2.24) with ϕ_M given by Eq. (2.31) and ϕ_H and ϕ_W given by Eq. (2.32)] from z_o to z_a. The results of this integration when changed to bulk transfer coefficient form can be expressed as:

$$\frac{C_M}{(C_M)_N} = \left[1.0 - \frac{(C_M)_N^{1/2}}{k} \cdot \left(\ln\left(\frac{1+x^2}{2}\right) + 2 \cdot \ln\left(\frac{1+x}{2}\right) - 2 \cdot \tan^{-1}(x) + \frac{\pi}{2}\right)\right]^{-2} \tag{2.47}$$

and

$$\frac{C_H}{(C_H)_N} = \frac{C_W}{(C_W)_N} = \left(\frac{C_M}{(C_M)_N}\right)^{1/2} \cdot \left[1.0 - \frac{2}{k}\cdot(C_M)_N^{1/2}\cdot\ln\left(\frac{1+x^2}{2}\right)\right]^{-1} \qquad (2.48)$$

where

$$x = (1-16\cdot\frac{z}{L})^{1/4} \quad . \qquad (2.49)$$

In order to compute these ratios using observations at the surface and a height z_a, z/L needs to be related to an easily computed stability index. This index is the bulk Richardson number $(Ri)_B$, defined as:

$$(Ri)_B = \frac{2\cdot g\cdot z_a\cdot(T_a-T_o)}{(T_a+T_o)\cdot u_a^2} \quad . \qquad (2.50)$$

If Eqs. (2.43) and (2.44) are substituted into Eq. (2.29), the Monin-Obukhov length can be expressed as:

$$L = \frac{C_M^{3/2}\cdot T\cdot u_a^2}{C_H\cdot k\cdot g\cdot(T_a-T_o)} \quad . \qquad (2.51)$$

By dividing the numerator and denominator by $(C_M)_N^{3/2}$, the relationship between z/L and the bulk Richardson number can be written as:

$$\frac{z_a}{L} = \frac{k\cdot C_H/(C_M)_N}{(C_M)_N^{1/2}\cdot\left(\frac{C_M}{(C_M)_N}\right)^{3/2}}\cdot(Ri)_B \quad . \qquad (2.52)$$

For stable conditions Deardorff gives the ratios for the general case, i.e., when $\phi_M \neq \phi_H \neq \phi_W$. If $\phi_M = \phi_H = \phi_W$ as in Eq. (2.42), the resulting ratios can be expressed as:

$$\frac{C_W}{(C_W)_N} = \frac{C_H}{(C_H)_N} = \frac{C_M}{(C_M)_N} = \left[1.0-\alpha\cdot(Ri)_B\right]^2 \quad . \qquad (2.53)$$

Fig. 2.1 shows the ratio of the bulk transfer coefficients to their values under neutral conditions as a function of the bulk Richardson number. For unstable conditions, the ratio is a function of the value of the bulk transfer coefficient under neutral conditions. In Fig. 2.1, neutral transfer coefficients were computed from Eq. (2.46) using several values of z_o which have been obtained for snow. To compute the ratios for unstable conditions, values of x and $(C_M)_N$ are first specified. Then $C_M/(C_M)_N$ is calculated from Eq. (2.47), $C_H/(C_H)_N$ and $C_W/(C_W)_N$ from Eq. (2.48), and $(Ri)_B$ from Eq. (2.52).

For stable conditions, $\alpha = 5$ ($Ri_{cr} = 0.2$) is used for Fig. 2.1.

EMPIRICAL WIND FUNCTIONS

The turbulent transfer equations in the previous section show that water vapor transfer is predominantly a function of wind speed and the vapor pressure gradient. This relationship can be expressed in an equation attributed to Dalton as:

$$V = f(U_a) \cdot (e_a - e_o) \tag{2.54}$$

where: V = water vapor transfer expressed as a depth (mm), and

$f(U_a)$ = a function of the wind speed ($mm \cdot mb^{-1}$).

A positive V indicates vapor transfer toward the snow cover (condensation-frost formation) while a negative V indicates a loss from the snow cover (sublimation-evaporation). It has been common to determine $f(U_a)$ empirically from simultaneous observations of vapor transfer, wind speed, and the vapor pressure gradient. For a snow cover, the amount of vapor gained or lost is usually measured by inserting a pan filled with snow into the snow cover so that the top of the pan is flush with the surrounding snow cover. The vapor transfer is determined by carefully weighing the pan before and after exposure. The wind function is normally represented as:

$$f(U_a) = \underline{a} + \underline{b} \cdot U_a \tag{2.55}$$

where: U_a = wind travel (mean wind speed multiplied by the time interval) (km),

$\underline{b}$ = an empirical constant ($mm \cdot mb^{-1} \cdot km^{-1}$), and

$\underline{a}$ = an empirical constant which indicates the amount of vapor transfer with no wind ($mm \cdot mb^{-1}$).

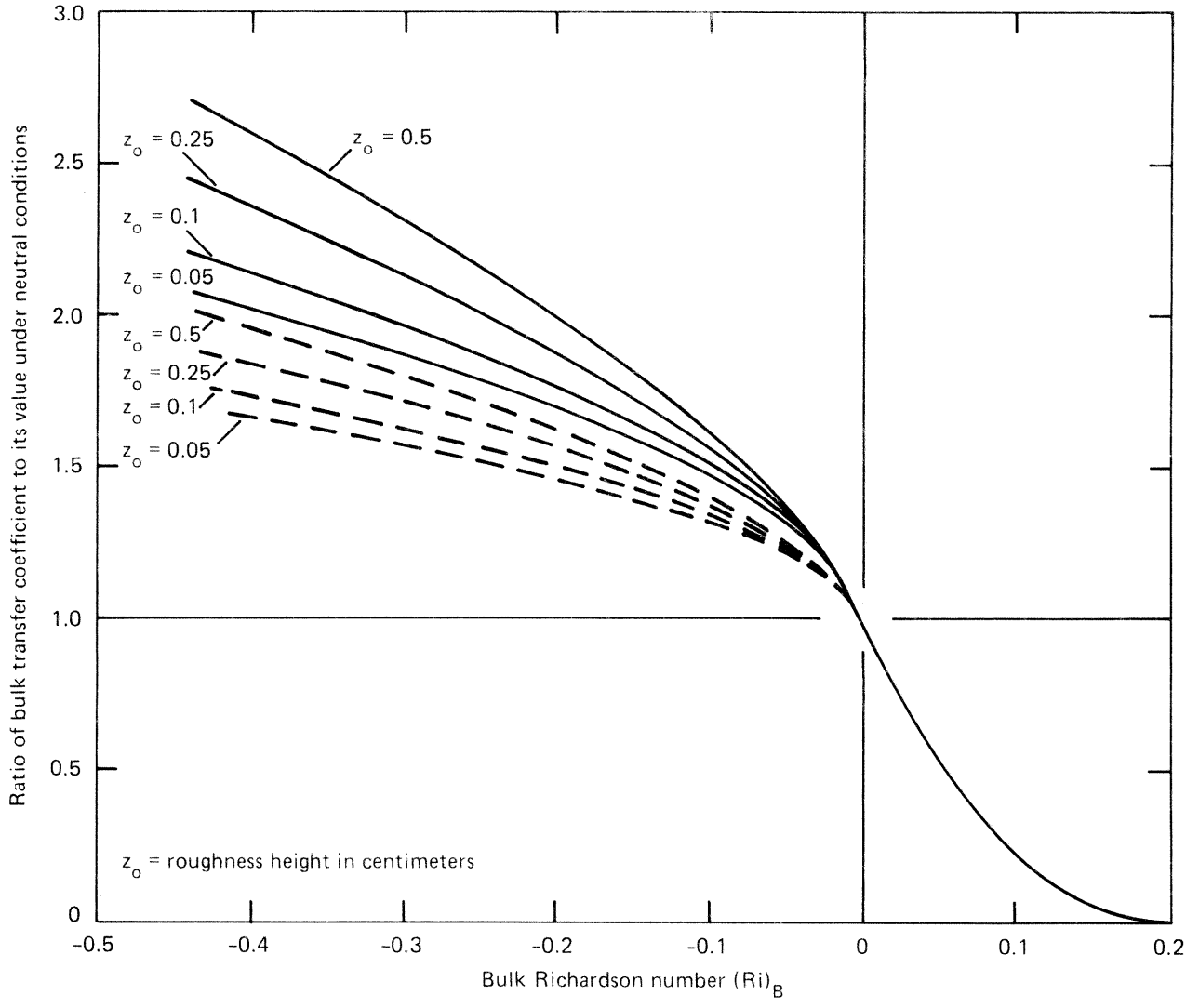

Figure 2.1.--Ratios of the bulk transfer coefficients to their values under neutral conditions over a wide range of stability. [Neutral values computed from Eq. (2.46) with z_a = 1 m. Solid lines represent $C_W/(C_W)_N$ and $C_H/(C_H)_N$. Dashed lines represent $C_M/(C_M)_N$.]

The value of a is dependent on the time interval being used. It is difficult to make a direct comparison of reported values of the constants a and b because of several factors, including:

1. variations in the heights at which the wind speed and vapor pressure of the air are measured,
2. variations in the method and the accuracy of measuring snow surface temperature, and
3. variations in the predominating stability conditions and surface roughness between measurement sites.

Determinations of $f(U_a)$ for the evaporation of water typically result in a finite value of the constant a. This reflects evaporation during calm, unstable periods caused by radiative heating of the surface. Since stable conditions should tend to predominate over a snow cover, the constant a should be near zero.

Table 2.1 presents a summary of some of the determinations of a and b found in the literature. In addition to the determined values an attempt is made to compare the values by reducing the measurement levels of wind and vapor pressure to a constant height of 1 meter above the snow surface. A commonly used extrapolation formula:

$$\frac{u_2}{u_1} = \frac{e_2}{e_1} = \left(\frac{z_2}{z_1}\right)^n \tag{2.56}$$

is used. In reality, n varies with such factors as surface roughness, height, and stability; thus, a strict comparison of the empirical constants is impossible. In computing a and b for Table 2.1 at 1 meter height, a value of n=0.17 was arbitrarily selected.

SENSIBLE AND LATENT HEAT TRANSFER

The theoretical turbulent transfer equation for water vapor flux [Eq. (2.45)] can be expressed in the form of the Dalton-type equation. In this case the wind function becomes:

$$f(U_a) = C_t \cdot U_a \tag{2.57}$$

where:

$$C_t = \frac{\rho_a \cdot 0.622}{P_a \cdot \rho_w} \cdot 10^6 \cdot C_w \quad . \tag{2.58}$$

Table 2.1.--Comparison of empirical wind function constants for a snow cover

Reference	$\underline{a}$ ($mm \cdot mb^{-1} \cdot hr^{-1}$)	$\underline{b}$ ($mm \cdot mb^{-1} \cdot km^{-1}$)	Measurement height (m)		Value of coefficients for a measurement height of 1.0 m	
			Wind	Vapor pressure	$\underline{a}$	$\underline{b}$
Kuzmin (1961) based on data from USSR plus measurements by Kohler (1950)	0.0075	0.00114	10	2	0.0084	0.0019
Snow Investigations (1955):						
a. Central Sierra Snow Laboratory	0.0	0.00242	0.3	2.4-3.6 avg.=3	0.0	0.00239
b. Based on data collected by M. deQuervain, Switzerland	0.0	0.0055	0.1	1.5	0.0	0.00398
Meiman and Grant (1974) Colorado	0.0	0.00457	0.6-1.25 avg.=0.8	0.6-1.25 avg.=0.8	0.0	0.00423

The latent heat transfer is the amount of heat required to change the snow into a vapor or the heat released when water vapor condenses on the snow surface. Thus latent heat transfer can be expressed as:

$$Q_e = \frac{L_s \cdot \rho_w}{10} \cdot V = \frac{L_s \cdot \rho_w}{10} \cdot f(U_a) \cdot (e_a - e_o) \qquad (2.59)$$

where L_s = latent heat of sublimation (677 cal·gm^{-1}).

The ratio of sensible heat flux to latent heat flux (commonly referred to as Bowen's ratio [Bowen (1926)] can be written as:

$$\frac{Q_h}{Q_e} = \frac{H}{L_s \cdot E} = \frac{P_a \cdot c_p}{0.622 \cdot L_s} \cdot \frac{(T_a - T_o)}{(e_a - e_o)} \quad . \qquad (2.60)$$

It should be noted that Eq. (2.60) assumes that $K_H = K_W$ (also $C_H = C_W$), but does not assume that $K_M = K_H$ or K_W. Experimental evidence seems to indicate that $K_H = K_W$ is a reasonable assumption for all stability conditions that have been investigated [Dyer (1967), Pruitt et al. (1971)]. For unstable conditions the evidence indicates that $K_M \neq K_H$ or K_W (thus $C_M \neq C_H$ or C_W) as different expressions for ϕ_M [Eq. (2.39)] as opposed to ϕ_H and ϕ_W [Eq. (2.40)] would indicate. Substituting Eq. (2.59) into Eq. (2.60) sensible heat transfer can be expressed as:

$$Q_h = \frac{L_s \cdot \rho_w}{10} \cdot \gamma \cdot f(U_a) \cdot (T_a - T_o) \qquad (2.61)$$

where:

$$\gamma = \frac{c_p \cdot P_a}{0.622 \cdot L_s} \quad . \qquad (2.62)$$

The units of γ are mb·°K^{-1}. γ is essentially a constant for a given location.

HEAT TRANSFER BY MASS CHANGES

The mass balance of a snow cover can be expressed as:

$$P_x - O_s + V + V_g = \Delta WE \qquad (2.63)$$

where: P_x = water-equivalent of precipitation (mm),
O_s = liquid-water outflow from the bottom of the snow cover (mm),
V = vapor transfer between the snow and the air (mm),
V_g = vapor transfer between the snow and the soil (mm), and
ΔWE = change in the water-equivalent of the snow cover (mm).

When computing the energy balance of the snow cover [Eq. (2.1)], the water-equivalent of the snow cover should be held constant. Mass changes can be computed prior to or after the energy balance computations. Thus, as far as the energy balance computations are concerned, it is only necessary to consider the heat transferred by mass changes. If the temperature of snow cover outflow is assumed to be 0°C and the heat content of the transferred vapor is assumed negligible, then only the heat transferred by precipitation need be considered. New snowfall can be added to the snow cover prior to the energy balance computations. The initial temperature of the new snow is assumed equal to the temperature of the precipitation. The wet-bulb temperature should be a good approximation of the temperature of precipitation because of the analogy between falling precipitation and a ventilated wet-bulb thermometer. The heat transferred to the snow cover by rain is heat released as the rain is cooled from its temperature upon reaching the snow cover to 0°C. Thus the advected heat which must be considered in the energy balance computations is:

$$Q_m = \frac{c_w \cdot \rho_w \cdot P_x}{10} \cdot (T_w - 273.16) \qquad (2.64)$$

where: c_w = specific heat of water ($cal \cdot gm^{-1} \cdot °K^{-1}$) (a value of 1.0 is used),

T_w = wet-bulb temperature (°K), and

273.16 = 0°C on the Kelvin scale.

SNOW COVER ENERGY BALANCE

By substituting Eqs. (2.5), (2.59), (2.61), (2.64), and (2.2) into Eq. (2.1), the energy balance of a snow cover can be written as:

$$Q_{ir} - \Delta t \cdot \varepsilon \cdot \sigma \cdot T_o^4 + \frac{L_s \cdot \rho_w}{10} \cdot f(U_a) \cdot \left[(e_a - e_o) + \gamma \cdot (T_a - T_o) \right]$$

$$+ \frac{c_w \cdot \rho_w}{10} \cdot P_x \cdot (T_w - 273.16) + Q_g - (d \cdot \rho_s)^t \cdot \left[(c_i \cdot T_s)^{t+\Delta t} - (c_i \cdot T_s)^t \right]$$

$$- \frac{L_f \cdot \rho_w}{10} \cdot (W^{t+\Delta t} - W^t) = 0.0 \quad . \qquad (2.65)$$

If Q_{ir}, U_a, e_a, T_a, P_x, and T_w are measured or estimated and the conditions at time t are known, then $W^{t+\Delta t}$, Q_g, T_o, and $(c_i \cdot T_s)^{t+\Delta t}$ are unknowns in this general expression. The next two chapters will describe how these unknowns can be evaluated so that the energy balance equation can be solved. There is one important case, however, for which a solution can immediately be written. This is the case when an isothermal snow cover is melting. In this case T_o = 273.16 °K, $(c_i \cdot T_s)^{t+\Delta t} = (c_i \cdot T_s)^t$ and Q_g is negligible compared to the energy exchange at the snow air interface. The amount of melt is then the difference between $W^{t+\Delta t}$ and W^t. The amount of melt in the time interval Δt_h can be expressed as:

$$M = 0.125 \cdot Q_{ir} - 3.37 \cdot \Delta t_h + 0.0125 \cdot P_x \cdot (T_w - 273.16)$$
$$+ 8.5 \cdot f(U_a) \cdot \left[(e_a - 6.11) + \gamma \cdot (T_a - 273.16) \right] \qquad (2.66)$$

where: M = snowmelt (mm), and t_h is the time interval in hours.

CHAPTER III: HEAT TRANSFER WITHIN THE SNOW COVER

INTRODUCTION

This chapter deals with the development of the equations used to estimate heat transfer within the snow cover. The heat transfer within the snow cover must be estimated so that the change in heat storage can be determined. The major mechanisms involved in the transfer of heat within a snow cover are heat conduction, the penetration of solar radiation, and heat transferred by phase changes (solid-vapor, liquid-solid, and vice versa). Very small amounts of liquid-water may exist in snow at temperatures below 0°C. However, this water has a negligible effect on heat transfer and is thus neglected. The equations which quantify these mechanisms involve coefficients that are related to physical characteristics of the snow cover. These physical characteristics include density, grain size, and crystal structure. Most of these relationships are not precisely defined, plus grain size and crystal structure are not commonly measured for hydrologic purposes. Thus, density is used as the sole index to the physical structure of the snow cover. Therefore, in order to compute heat transfer on a continuous basis, the change in density of the snow cover must be continually estimated.

Many of the publications that are referred to in this chapter contain more detailed derivations and discussions of these equations and concepts. A particularly good summary of snow cover heat transfer and related properties is that prepared by Yen (1969).

HEAT TRANSFER EQUATION

Heat Conduction

Fourier's heat-conduction equation can be used to compute the heat change for a volume of snow. Heat transfer in a snow cover is essentially one-dimensional. The equation for one-dimensional heat transfer by conduction for a uniform snow cover is:

$$c_i \cdot \rho_s \cdot \frac{\partial T}{\partial t} = k_e \cdot \frac{\partial^2 T}{\partial z^2} \qquad (3.1)$$

where: c_i = specific heat of ice ($cal \cdot gm^{-1} \cdot {}^\circ K^{-1}$),

ρ_s = density of the solid (ice) portion of the snow cover ($gm \cdot cm^{-3}$),

T = snow temperature ($^\circ K$),

t = time (sec),

z = distance from the snow-air interface (cm), and

k_e = the effective thermal conductivity of snow ($cal \cdot cm^{-1} \cdot {}^\circ K^{-1} \cdot sec^{-1}$).

The term effective thermal conductivity is usually used for snow instead of just thermal conductivity to indicate the combined effect of conduction through the ice grains, conduction through the air in the void spaces, and radiant energy exchange across the void spaces. It is not possible to separate these heat transfer mechanisms during experimental determinations of the thermal conductivity of snow.

If k_e varies with depth, as would be the case in most natural layered snow covers, the heat conduction equation becomes:

$$c_i \cdot \rho_s \cdot \frac{\partial T}{\partial t} = k_e \cdot \frac{\partial^2 T}{\partial z^2} + \frac{\partial k_e}{\partial z} \cdot \frac{\partial T}{\partial t} \quad . \tag{3.2}$$

Heat Transferred by Sublimation

If saturated vapor is present (as with a moist porous media like snow), certain corrections must be applied to Eq. (3.2). If the medium is heated, the vapor contained in the heated portion is no longer saturated. Evaporation begins in the unsaturated portion and a vapor pressure gradient develops. As a result, the water vapor diffuses towards the cooler parts of the medium, where, due to oversaturation, condensation takes place and latent heat is released. This process proceeds in the direction of the decreasing temperature gradient. Sulakvelidze (1959) derived the correction which must be applied to Eq. (3.2) to account for heat transferred by the sublimation which results when temperature gradients are present within a snow cover. With the addition of this correction, Eq. (3.2) becomes:

$$c_i \cdot \rho_s \cdot \frac{\partial T}{\partial t} = k_e \cdot \frac{\partial^2 T}{\partial z^2} + \frac{\partial k_e}{\partial z} \cdot \frac{\partial T}{\partial z} + L_s \cdot m \tag{3.3}$$

where: L_s = latent heat of sublimation (677.0 cal·gm^{-1}), and

m = the net sublimation (the net amount of vapor that undergoes a phase change) (gm·cm^{-3}·sec^{-1}).

Heat transferred due to the specific heat of the vapor is negligible and ignored in Eq. (3.3).

The net sublimation (positive indicates a vapor gain) is the amount of vapor which diffuses into the volume of snow, minus the change in concentration of vapor within the volume. The equation for net sublimation can be derived and is similar in form to the heat conduction equation. For the case where the diffusion coefficient for water vapor in snow varies with depth, net sublimation can be expressed as:

$$m = D_e \cdot \frac{\partial^2 C}{\partial z^2} + \frac{\partial D_e}{\partial z} \cdot \frac{\partial C}{\partial z} - \frac{\partial C}{\partial t} \tag{3.4}$$

where: C = concentration of water vapor (grams of vapor per cm^3 of air), and

D_e = effective diffusion coefficient for water vapor in snow (cm^2·sec^{-1}).

The term effective diffusion coefficient is used to distinguish between the movement of water vapor in snow and the diffusion of water vapor in air.

Substituting Eq. (3.4) for m in Eq. (3.3) gives:

$$c_i \cdot \rho_s \cdot \frac{\partial T}{\partial t} = k_e \cdot \frac{\partial^2 T}{\partial z^2} + \frac{\partial k_e}{\partial z} \cdot \frac{\partial T}{\partial z} + L_s \cdot D_e \cdot \frac{\partial^2 C}{\partial z^2}$$

$$+ L_s \cdot \frac{\partial D_e}{\partial z} \cdot \frac{\partial C}{\partial z} - L_s \cdot \frac{\partial C}{\partial t} \quad . \tag{3.5}$$

In a saturated porous media like snow, the concentration of water vapor is solely a function of the temperature of the snow. Thus,

$$\frac{\partial C}{\partial z} = \frac{\partial C}{\partial T} \cdot \frac{\partial T}{\partial z} = f' \cdot \frac{\partial T}{\partial z} \tag{3.6}$$

where f' denotes $\partial C/\partial T$. Also,

$$\frac{\partial C}{\partial t} = \frac{\partial C}{\partial T} \cdot \frac{\partial T}{\partial t} = f' \cdot \frac{\partial T}{\partial t} \quad . \tag{3.7}$$

The second partial of C with respect to z can be expressed as:

$$\frac{\partial^2 C}{\partial z^2} = \frac{\partial\left(f' \cdot \frac{\partial T}{\partial z}\right)}{\partial z} = f' \cdot \frac{\partial^2 T}{\partial z^2} + f'' \cdot \left(\frac{\partial T}{\partial z}\right)^2 \tag{3.8}$$

where f'' denotes the second derivative of C with respect to T.

Substituting Eqs. (3.6), (3.7), and (3.8) into Eq. (3.5), we obtain:

$$(c_i \cdot \rho_s + L_s \cdot f') \cdot \frac{\partial T}{\partial t} = (k_e + L_s \cdot D_e \cdot f') \cdot \frac{\partial^2 T}{\partial z^2}$$

$$+ \left(\frac{\partial k_e}{\partial z} + L_s \cdot f' \cdot \frac{\partial D_e}{\partial z}\right) \cdot \frac{\partial T}{\partial z} + L_s \cdot D_e \cdot f'' \cdot \left(\frac{\partial T}{\partial z}\right)^2 \quad . \tag{3.9}$$

Comparing the magnitude of $c_i \cdot \rho_s$ and $L_s \cdot f'$, we find $c_i \cdot \rho_s >> L_s \cdot f'$ (at least 100 times greater). Ignoring $L_s \cdot f'$ in the term on the left side of Eq. (3.9), the change in temperature within a snow cover with respect to time can be expressed as:

$$\frac{\partial T}{\partial t} = \left(\frac{k_e + L_s \cdot D_e \cdot f'}{c_i \cdot \rho_s}\right) \cdot \frac{\partial^2 T}{\partial z^2} + \left(\frac{\frac{\partial k_e}{\partial z} + L_s \cdot f' \cdot \frac{\partial D_e}{\partial z}}{c_i \cdot \rho_s}\right) \cdot \frac{\partial T}{\partial z}$$

$$+ \frac{L_s \cdot D_e \cdot f''}{c_i \cdot \rho_s} \cdot \left(\frac{\partial T}{\partial z}\right)^2 \quad . \tag{3.10}$$

Heat Sources and Sinks

In addition to heat conduction and latent heat transfer due to water vapor diffusion, sources and sinks of heat must be included. An external source of heat is solar radiation which penetrates into the snow cover. The change in the amount of liquid-water within the snow cover can be a source of heat (heat released by freezing, i.e., liquid-water decreasing) or a sink (heat required to melt ice, i.e., liquid-water increasing). The heat released during freezing or required for melting is equal to the latent heat of fusion multiplied by the change in the amount of liquid-water. With the addition of absorbed solar radiation and changes in the amount of liquid-water, the final equation for heat transfer within a snow cover can be expressed as:

$$\frac{\partial T}{\partial t} + \frac{L_f \cdot \frac{\partial w}{\partial t}}{c_i \cdot \rho_s} - \frac{\frac{\partial I}{\partial z}}{c_i \cdot \rho_s} - \left(\frac{k_e + L_s \cdot D_e \cdot f'}{c_i \cdot \rho_s} \right) \cdot \frac{\partial^2 T}{\partial z^2}$$

$$- \left(\frac{\frac{\partial k_e}{\partial z} + L_s \cdot f' \cdot \frac{\partial D_e}{\partial z}}{c_i \cdot \rho_s} \right) \cdot \frac{\partial T}{\partial z} - \frac{L_s \cdot D_e \cdot f''}{c_i \cdot \rho_s} \cdot \left(\frac{\partial T}{\partial z} \right)^2 = 0.0 \qquad (3.11)$$

where: I = shortwave (solar) radiation flux ($cal \cdot cm^{-2} \cdot sec^{-1}$),

L_f = latent heat of fusion (79.7 $cal \cdot gm^{-1}$ at 0°C), and

w = amount of liquid-water ($gm \cdot cm^{-3}$).

PHYSICAL COEFFICIENTS AND CONSTANTS

Coefficient of Effective Thermal Conductivity

The effective thermal conductivity of snow does not depend on density alone. The size, shape, and distribution of snow crystals are also important. However, all of the experimental determinations of thermal conductivity of snow have been empirically correlated with density as the sole parameter. Summaries of representative experimental determinations of the effective thermal conductivity of snow can be found in several sources including Mellor (1964) and Kondrat'eva (1945). The results of these investigations are listed in Table 3-1 and also plotted in Fig. 3-1. In all these studies, the effect of vapor movement on heat transfer was not considered though obviously present. Yen (1967) showed that vapor movement increases the rate of temperature propogation by a significant amount for densities less than about 0.3. He computed that for a snow with a density of 0.1, the thermal diffusivity ($k_e / \rho_s \cdot c_i$) is about 3.33 times that of the same snow without vapor movement. Thus, the previously mentioned experimental determinations of k_e may be too high for low density snow. Yen (1965) included vapor movement when determining the effective thermal conductivity and water vapor diffusion coefficient for ventilated snow. Air movement in a natural snow cover should be near zero, except possibly for the top few centimeters during windy periods. By extrapolating the air flow rate to zero, Yen determined that $k_e = 0.0077 \cdot \rho_s^2$. This value is also included in Table 3-1 and Fig. 3-1. In addition to experimental determinations of effective thermal conductivity, theoretical expressions for the thermal conductivity of snow have been derived. Schwerdtfeger (1963) derived such an expression (composite and interpolated curve

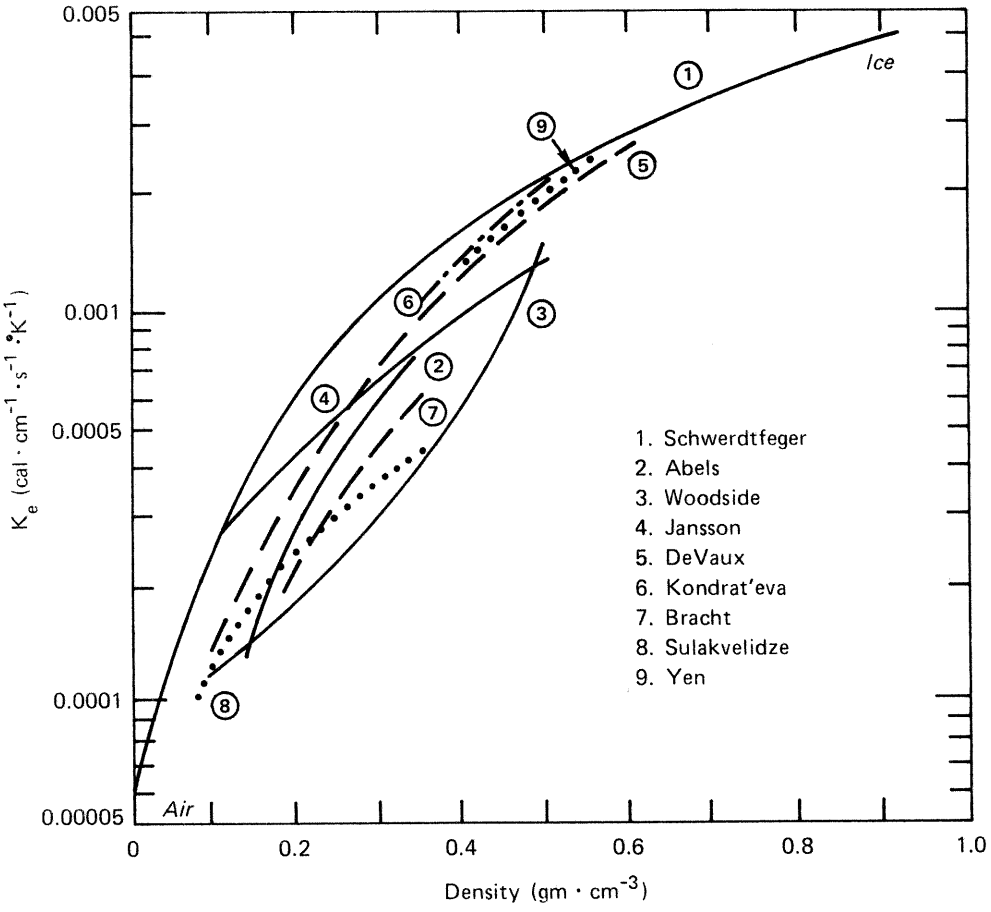

Figure 3.1.--Effective thermal conductivity of snow.

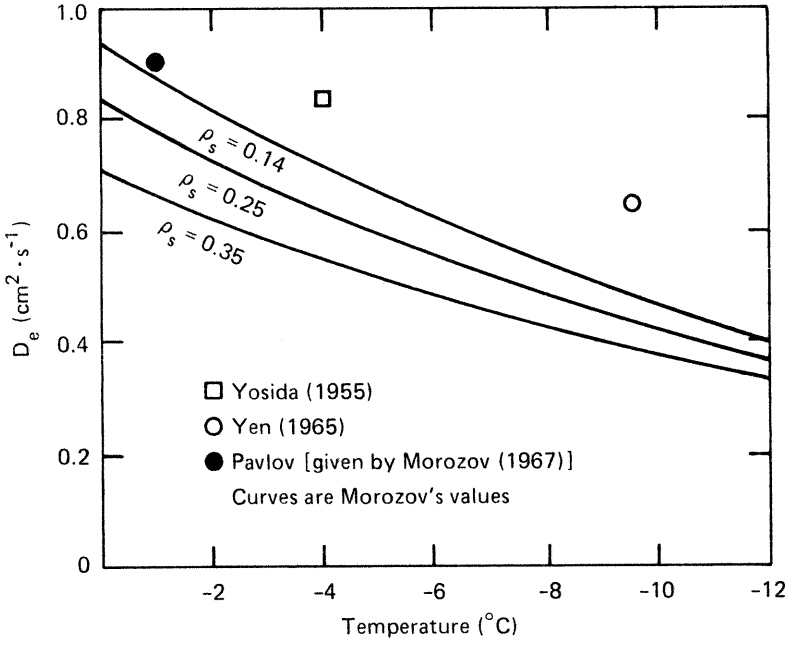

Figure 3.2.--Effective diffusion coefficient for water vapor in snow.

shown in Fig. 3-1) by considering three situations: ice containing spherical air bubbles, snow crystals enclosing parallelipiped air spaces, and air containing snow crystals. Woodside (1958) derived an expression for the case of a cubic lattice of identical spherical ice particles in air (curve, with vapor movement contributions omitted, is shown in Fig. 3-1).

Since k_e is assumed to be solely a function of density, the change in k_e with depth can be written as:

$$\frac{\partial k_e}{\partial z} = \frac{\partial k_e}{\partial \rho_s} \cdot \frac{\partial \rho_s}{\partial z} \quad . \tag{3.12}$$

Table 3-1.--Effective thermal conductivity of snow
(Units are $cal \cdot cm^{-1} \cdot sec^{-1} \cdot {}^{\circ}K^{-1}$.)

Investigator	Date	Expression	Density range
Abels	1894	$k_e=0.0068 \cdot \rho_s^2$	$0.14<\rho_s<0.34$
Jansson	1901	$k_e=0.00005+0.0019 \cdot \rho_s$ $+0.006 \cdot \rho_s^4$	$0.08<\rho_s<0.5$
Van Dusen	1929	$k_e=0.00005+0.001 \cdot \rho_s$ $+0.0052 \cdot \rho_s^3$	
DeVaux	1933	$k_e=0.00007+0.007 \cdot \rho_s^2$	$0.1<\rho_s<0.6$
Kondrat'eva	1945	$k_e=0.0085 \cdot \rho_s^2$	$0.35<\rho_s<0.5$
Bracht	1949	$k_e=0.0049 \cdot \rho_s^2$	$0.19<\rho_s<0.35$
Sulakvelidze	1958	$k_e=0.00122 \cdot \rho_s$	$\rho_s<0.35$
Yen	1965	$k_e=0.0077 \cdot \rho_s^2$	$0.52<\rho_s<0.59$

Effective Diffusion Coefficient for Water Vapor in Snow

There have been far fewer experimental determinations of the effective diffusion coefficient for water vapor in snow than measurements of effective thermal conductivity. Yosida and his colleagues (1955) were the first to investigate the diffusion of water vapor through snow. Yosida determined that the effective diffusion coefficient for water vapor in snow (D_e) is four or five times as large as the diffusion coefficient of water vapor through air. He explained the increase by noting that since the thermal conductivity of ice is about one hundred times as large as that of air the actual temperature gradient must exist in the air

spaces and not in the ice particles. In addition, unlike sand grains which hinder the movement of water vapor diffusing through sand, ice grains can produce or absorb the diffusing water vapor by the sublimation process. In other words, the water vapor is delivered "hand to hand" by each of the ice particles, the only thing it must do by itself is to diffuse across the narrow spaces between ice particles. Yosida's experiments also indicated that D_e seems to be independent of density over a range of densities from 0.08 to 0.51. Yosida determined a mean value of $D_e = 0.85\ cm^2 \cdot sec^{-1}$. The mean temperature of the snow during these measurements was -4°C.

Yen (1965) determined that $D_e = 0.65\ cm^2 \cdot sec^{-1}$ while investigating heat transfer through ventilated snow. The mean temperature of the snow during these measurements was about -9.5°C.

Morozov (1967) measured D_e for three snow samples ranging in density from 0.13 to 0.30. His measurements indicated that D_e varies with temperature and to a lesser degree, density. Morozov also presented other determinations of D_e made in the USSR.

Fig. 3-2 summarizes the determinations of D_e. The diffusion coefficient for water vapor in air is a function of temperature and is inversely proportional to the atmospheric pressure [Smithsonian Tables (1968)]. Ignoring any variation in D_e with snow density (the experimental data does not clearly indicate that a relationship exists over the range of densities commonly observed in seasonal snow covers), the relationship between D_e, temperature, and atmospheric pressure can be expressed as:

$$D_e = D_{eo} \cdot \frac{1000}{P_a} \cdot \left(\frac{T}{273.16}\right)^{n_d} \qquad (3.13)$$

where: D_{eo} = the effective diffusion coefficient for water vapor in snow at 0°C and 1000 mb pressure ($cm^2 \cdot sec^{-1} \cdot mb \cdot °K^{-n_d}$),

P_a = atmospheric pressure (mb), and

n_d = temperature exponent.

Assuming that D_e varies only with temperature for a given location, the change in D_e with depth can be written as:

$$\frac{\partial D_e}{\partial z} = \frac{\partial D_e}{\partial T} \cdot \frac{\partial T}{\partial z} \quad . \qquad (3.14)$$

Substituting Eqs. (3.12) and (3.14) into Eq. (3.11), the heat transfer within a snow cover can now be expressed as:

$$\frac{\partial T}{\partial t} + \frac{L_f \cdot \frac{\partial w}{\partial t}}{c_i \cdot \rho_s} - \frac{\frac{\partial I}{\partial z}}{c_i \cdot \rho_s} - \left(\frac{k_e + L_s \cdot D_e \cdot f'}{c_i \cdot \rho_s} \right) \cdot \frac{\partial^2 T}{\partial z^2} - \left(\frac{\frac{\partial k_e}{\partial \rho_s} \cdot \frac{\partial \rho_s}{\partial z}}{c_i \cdot \rho_s} \right) \cdot \frac{\partial T}{\partial z}$$

$$- \left(\frac{L_s \cdot f' \cdot \frac{\partial D_e}{\partial T} + L_s \cdot D_e \cdot f''}{c_i \cdot \rho_s} \right) \cdot \left(\frac{\partial T}{\partial z} \right)^2 = 0.0 \quad . \tag{3.15}$$

Penetration of Solar Radiation - Extinction Coefficient

Water and clear ice are highly transparent for solar radiation. However, ice in the granular form, as in the case of snow, returns a high percentage of solar energy by direct or multiple reflections and by scattering. The same processes affect the attenuation of penetrating radiation with gradual absorption taking place. For simplicity, it is usually assumed that snow behaves as a homogeneous diffusing medium. Thus, the net solar radiation flux at a depth z can be expressed as:

$$I_a = I_o \cdot \exp(-\nu \cdot z) \tag{3.16}$$

where: I_o = shortwave radiation flux at the surface ($cal \cdot cm^{-2} \cdot sec^{-1}$), and

ν = a coefficient, usually referred to as the extinction coefficient (sometimes called absorption coefficient) (cm^{-1}).

Eq. (3.16) fits observations quite well for deep snow covers [Gerdel (1948), O'Neill and Gray (1973)]. The extinction of penetrating solar radiation should deviate from this simple expression for snow covers containing layers with significantly different optical properties and for very shallow snow covers [Giddings and LaChapelle (1961), O'Neill and Gray (1973)]. In the case of a shallow snow cover, part of the solar radiation penetrates through the snow cover and is absorbed by the uppermost soil layer. A portion of this absorbed energy is returned to the snow by conduction. The remainder is retained by the soil.

Determinations of the extinction coefficient for snow have been compiled by Mantis (1951) and Mellor (1964). These determinations show a range of 0.035 to 0.54 cm^{-1} for the extinction coefficient. In most cases, snow cover properties were not tabulated, thus, making correlations

between the extinction coefficient and snow density impossible. Measurements by Gerdel (1948) and Thomas (1963) included tabulations of snow density. In these cases, the extinction coefficient decreased with increasing density. Mellor (1966) made laboratory measurements of the extinction coefficient which showed that for a given grain size the extinction coefficient increased with density until reaching a maximum, after which the extinction coefficient decreased. This should be expected since the extinction coefficient is near zero for both limits, air (density approaches zero) and ice. However, the value of the extinction coefficient for most of Mellor's laboratory determinations exceeded 1.0 cm^{-1}. This value is nearly an order of magnitude higher than previous measurements made at similar densities. Bohren and Barkstrom (1974) theoretically derived a relationship between the extinction coefficient and density, grain size, and wavelength. This relationship is:

$$\nu = 0.84 \cdot \left(\frac{\nu_i}{d_s}\right)^{1/2} \cdot \frac{\rho_s}{\rho_i} \tag{3.17}$$

where: ν_i = the extinction coefficient for clear ice (mm^{-1}) [Sauberer's data for various wavelengths are tabulated by Mantis (1951)],

d_s = grain diameter (mm),

ρ_i = density of ice (0.917 $gm \cdot cm^{-3}$), and 0.84 has units of $mm \cdot cm^{-1}$.

This relationship compares very well with the limited measurements available for comparison. In addition, Bohren and Barkstrom conclude that Mellor's laboratory determinations of the extinction coefficient were affected by sample geometry. Mellor used a cylindrical sample rather than measuring a plane-parallel slab.

Eq. (3.17) indicates that the extinction coefficient is a function of both density and grain size. For natural snow covers, there is generally a correlation between density and grain size. For the extinction coefficient to decrease as density increases, the square root of the grain diameter must increase faster than the density. Fresh snow, though not composed of spherical grains, probably has a very small effective grain diameter in terms of its optics. As metamorphism occurs, the grain size increases, perhaps by two orders of magnitude.

Thus, the square root of grain size would very likely exceed the increase in density as the snow changed from fresh snow (about 0.1 $gm \cdot cm^{-3}$) to old coarse grained snow (about 0.4 $gm \cdot cm^{-3}$). The extinction coefficient for high-density snow (0.3 to 0.5 $gm \cdot cm^{-3}$) could vary considerably depending on whether the high density is the result of metamorphism (large grains) or the result of wind packing of new snow (small grains).

In order to use Eq. (3.17) as a basis for relating the extinction coefficient to the density of the snow, a relationship between density and grain size must first be established. This relationship can vary from one location to another.

Specific Heat of Ice

Since the contribution of air and water vapor to the specific heat of snow is negligibly small, only the specific heat of the ice matrix need be considered. The specific heat of ice is a function of temperature and can be expressed as:

$$c_i = 0.0222 + 0.00176 \cdot T \quad . \tag{3.18}$$

Eq. (3.18) is within 0.001 $cal \cdot gm^{-1} \cdot {}^{\circ}K^{-1}$ of the values of the specific heat of ice tabulated in the Smithsonian Tables (1968) down to a temperature of -80°C. This expression is more than adequate over the full range of temperatures experienced in any cold region on earth.

Vapor Pressure and Water Vapor Concentration

The saturation vapor pressure can conveniently be expressed in terms of temperature by the Clausius-Clapeyron equation. For saturation vapor pressure over ice, the Clausius-Clapeyron equation can be expressed as:

$$e_i = C_e \cdot \exp\left(-\frac{L_s}{R_w \cdot T}\right) \tag{3.19}$$

where: e_i = saturation vapor pressure over ice (mb),

R_w = gas constant for water vapor (0.110226 $cal \cdot {}^{\circ}K^{-1} \cdot gm^{-1}$ or 4615 $mb \cdot cm^3 \cdot {}^{\circ}K^{-1} \cdot gm^{-1}$), and

C_e = an experimental constant (mb).

At 0°C, the saturation vapor pressure over ice is 6.11 mb; thus, $C_e = 3.5558 \cdot 10^{10}$ mb. Substituting the values of C_e, L_s, and R_w,

Eq. (3.19) becomes:

$$e_i = 3.5558 \cdot 10^{10} \cdot \exp(-6141.9/T) \quad . \tag{3.20}$$

Eq. (3.20) compares extremely well with the full range (0°C to -100°C) of values tabulated in the Smithsonian Tables (1968).

Water vapor concentration in a saturated ice medium can be expressed as [Smithsonian Tables (1968)]:

$$C = \frac{e_i}{R_w \cdot T} \quad . \tag{3.21}$$

Differentiating, the partials of water vapor concentration in snow are:

$$f' = \frac{\partial C}{\partial T} = \frac{e_i}{R_w \cdot T^2} \cdot \left(\frac{L_s}{R_w \cdot T} - 1.0 \right), \tag{3.22}$$

$$f'' = \frac{\partial^2 C}{\partial T^2} = \frac{e_i}{R_w \cdot T^3} \cdot \left(\left(\frac{L_s}{R_w \cdot T} \right)^2 - \frac{4.0 \cdot L_s}{R_w \cdot T} + 2.0 \right), \text{ and} \tag{3.23}$$

$$f''' = \frac{\partial^3 C}{\partial T^3} = \frac{e_i}{R_w \cdot T^4} \cdot \left(\left(\frac{L_s}{R_w \cdot T} \right)^3 - 9.0 \cdot \left(\frac{L_s}{R_w \cdot T} \right)^2 + \frac{18.0 \cdot L_s}{R_w \cdot T} - 6.0 \right) \quad . \tag{3.24}$$

The third partial, f''', is not mentioned in this chapter, but will be needed in the next chapter.

DENSITY CHANGES IN A SNOW COVER

Introduction

In order to estimate the total change in snow cover density with time, an understanding of the basic processes involved is necessary. One process which causes changes in density is compaction due to the weight of the overlying snow. In addition, density changes occur as a result of metamorphoric changes in the structure of the snow cover. Metamorphism of snow involves three basic processes [deQuervain (1963, 1973), Sommerfield and LaChappelle (1970)]:

1. destructive or equi-temperature metamorphism,
2. constructive or temperature-gradient metamorphism, and
3. melt metamorphism.

Increase in Density due to Compaction

The compaction of snow layers can be seen graphically in seasonal snow layer depth profiles obtained during several investigations [Bader et al. (1939), Snow Hydrology (1956)]. Kojima (1967) [also mentioned by Yosida (1963)] presents a quantitative expression for density change due to compaction. The relationship is based on many observations of the change in depth of various layers (with no change in water-equivalent) in a seasonal snow cover. The relationship can be expressed as:

$$\frac{1}{\rho_s} \cdot \frac{\partial \rho_s}{\partial t} = \frac{W_s}{\eta} \tag{3.25}$$

where: W_s = the weight of the snow above the layer for which the density change is being computed, expressed in terms of water-equivalent (cm), and

η = a constant for a given density, temperature, and snow type which is referred to as a viscosity coefficient (cm·hr).

Kojima's observations indicated that the relationship between η and density could be expressed as:

$$\eta = \eta_c \cdot \exp(C_2 \cdot \rho_s) \tag{3.26}$$

where: η_c = the viscosity coefficient when ρ_s is reduced to zero (cm·hr), and

C_2 = a constant to be determined from the observed data ($cm^3 \cdot gm^{-1}$).

Substituting Eq. (3.26) into Eq. (3.25) and letting $C_1 = \eta_c^{-1}$, the density change due to compaction can be expressed as:

$$\frac{1}{\rho_s} \cdot \frac{\partial \rho_s}{\partial t} = C_1 \cdot W_s \cdot \exp(-C_2 \cdot \rho_s) \tag{3.27}$$

where C_1 is the fractional increase in density per centimeter water-equivalent of load per hour. Kojima reported values of 0.026 to

to 0.069 $cm^{-1} \cdot hr^{-1}$ for C_1 and a value of 21 $cm^3 \cdot gm^{-1}$ for C_2. Eq. (3.27) fits the data obtained by Kojima quite well except for cases of low-density new snow layers, wind-packed snow, and depth-hoar layers. Low-density new snow increased in density at a rate faster than would be predicted by the values of C_1 and C_2 obtained for ordinary snow. The wind-packed layers also initially increased in density at a faster rate than for ordinary snow. The depth-hoar layers compacted at a much slower rate than the ordinary snow.

Mellor (1964) presents other determinations of the viscosity coefficient for natural snow. These relationships were based on observations in polar regions. The relationships between η and density are similar to that proposed by Kojima. In addition, the C_2 values are nearly identical to Kojima's value. However, the value of C_1 varies because of differences in temperature and snow type. Mellor indicates that the ratio between the viscosity coefficient (η_t) at a temperature (T) and the coefficient (η_o) at 0°C (T_c) can be expressed as:

$$\frac{\eta_t}{\eta_o} = \exp\left(\frac{A}{R} \cdot \left(\frac{T_c - T}{T \cdot T_c}\right)\right) \tag{3.28}$$

where: A = the activation energy of the snow (in the order of 10^4 $cal \cdot mol^{-1}$), and

R = the gas constant (approximately 2 $cal \cdot mol^{-1} \cdot °K^{-1}$).

For temperatures normally experienced in areas with seasonal snow covers, $A/(R \cdot T \cdot T_c)$ would be about 0.08 $°K^{-1}$.

Taking temperature dependence into account, the density change due to compaction can be expressed as:

$$\frac{1}{\rho_s} \cdot \frac{\partial \rho_s}{\partial t} = C_1 \cdot \exp\left[-0.08 \cdot (T_c - T)\right] \cdot W_s \cdot \exp(-C_2 \cdot \rho_s) \tag{3.29}$$

where C_1 is now the fractional increase in density ($cm^{-1} \cdot hr^{-1}$) at 0°C and $\rho_s = 0.0$.

Destructive Metamorphism

Under equi-temperature conditions, water molecules move to new positions on a snow crystal in order to decrease the surface free energy [Yosida (1958)]. Snow crystals falling from the sky typically have a very large ratio of surface area to mass. Destructive metamorphism changes these star-shaped crystals into an aggregate of rounded, oblong, or irregular

smooth grains. During this process, the snow tends to settle, thus, causing an increase in density. These changes have been well documented by means of photographs [Bader et al. (1939), Yosida (1955)]. The photographs show that destructive metamorphism is temperature dependent. Changes occur more rapidly the warmer the snow. Yosida includes a plot showing the increase in grain diameter versus time at -6°C and -20°C. The rate of increase in size at -20°C is about 60 percent of that at -6°C.

In terms of changes in density, destructive metamorphism is primarily important in the early stages after the deposition of the snow. Gunn (1965) reported that layers of new snow settle at a rate of about 1 percent per hour during and immediately after a snowfall. This rate was independent of density over a density range of 0.05 to 0.15 $gm \cdot cm^{-3}$. Yen (1969) indicates that destructive metamorphism is of minor importance for densities in excess of 0.25 $gm \cdot cm^{-3}$.

No mathematical expression of the increase in density resulting from destructive metamorphism could be found in the literature. However, it should be possible to formulate a reasonable expression based on the previously cited information. The information suggests the following relationship:

$$\frac{1}{\rho_s} \cdot \frac{\partial \rho_s}{\partial t} = C_3 \cdot \exp\left[-C_4 \cdot (T_c - T)\right] \tag{3.30}$$

for densities less than ρ_d, and

$$\frac{1}{\rho_s} \cdot \frac{\partial \rho_s}{\partial t} = C_3 \cdot \exp\left[-C_4 \cdot (T_c - T)\right] \cdot \exp\left[-46 \cdot (\rho_s - \rho_d)\right] \tag{3.31}$$

for densities greater than ρ_d. In these equations:

C_3 = the fractional settling rate at 0°C for densities less than ρ_d (hr^{-1}),

C_4 = a constant to be determined by calibration ($°K^{-1}$),

46 = the constant ($cm^3 \cdot gm^{-1}$) necessary to reduce the settling rate by a factor of 100 when ρ_s exceeds ρ_d by 0.1 $gm \cdot cm^{-3}$, and

ρ_d = a density to be determined by calibration ($gm \cdot cm^{-3}$).

Constructive Metamorphism

Constructive metamorphism is the process of vapor transfer within the snow cover due to a temperature gradient. The transfer of water vapor

results in changes in density since vapor is removed by evaporation from one crystal and deposited by condensation on another. The change in density with respect to time is:

$$\frac{\partial \rho_s}{\partial t} = m + \frac{\partial C}{\partial t} \quad . \tag{3.32}$$

The term $\partial C/\partial t$ is included because some of the net sublimation may not be transferred, but instead be used to satisfy the change in the saturated vapor capacity. Substituting from Eq. (3.4), the change in density can be expressed as:

$$\frac{\partial \rho_s}{\partial t} = D_e \cdot \frac{\partial^2 C}{\partial z^2} + \frac{\partial D_e}{\partial z} \cdot \frac{\partial C}{\partial z} \quad . \tag{3.33}$$

Substituting Eqs. (3.6) and (3.8) gives the change in density due to constructive metamorphism in terms of the temperature gradient as:

$$\frac{\partial \rho_s}{\partial t} = D_e \cdot f' \cdot \frac{\partial^2 T}{\partial z^2} + f' \cdot \frac{\partial D_e}{\partial z} \cdot \frac{\partial T}{\partial z} + D_e \cdot f'' \cdot \left(\frac{\partial T}{\partial z}\right)^2 \quad . \tag{3.34}$$

If D_e is assumed to be solely a function of temperature for a given location, Eq. (3.14) can be substituted into Eq. (3.34) giving:

$$\frac{\partial \rho_s}{\partial t} = D_e \cdot f' \cdot \frac{\partial^2 T}{\partial z^2} + \left(f' \cdot \frac{\partial D_e}{\partial T} + D_e \cdot f'' \right) \cdot \left(\frac{\partial T}{\partial z}\right)^2 \quad . \tag{3.35}$$

Under conditions of a prolonged thermal gradient near the bottom of the snow cover, constructive metamorphism leads to the formation of depth hoar. As mentioned previously, Kojima reported that well established depth-hoar layers compact at a greatly reduced rate. DeQuervain (1963) also reported that layers in a state of advanced constructive metamorphism tend not to settle unless there is structural collapse.

Melt Metamorphism

Melt metamorphism includes the change in snow structure caused by melt-freeze cycles, plus the changes in crystals due to the presence of liquid-water. Melting decreases the depth of the snow cover. All or a portion of the melt-water may be retained within the remaining

snow cover. Some of this liquid-water may in turn refreeze causing an increase in the ice portion of the snow cover. A melt-freeze cycle will increase the density of the affected portion of the snow cover by several percent. The exact change can be computed as a by-product of the energy balance computations of melt and subsequent decreases in the amount of liquid-water due to freezing.

Wakahama (1968) studied the metamorphism of wet snow and found that the grain size increased at a faster rate as the amount of water was increased. However, density did not increase except when a weight was applied (initial density of the samples was 0.39 $gm \cdot cm^{-3}$). Colbeck (1973) studied wet snow from a theoretical point of view and arrived at essentially the same conclusions in regard to grain growth and densification. Kojima (1967) showed that the rate of increase in density due to compaction was essentially the same for wet snow and dry snow. Wakahama's experimental results and Colbeck's theory indicate that when water saturation is high the rate of compaction should increase. However, such conditions do not normally occur in a snow cover except over impermeable ice layers and at interfaces. Thus, at least for high density snow with near spherical grains, the rate of increase in density should be similar to dry snow. In the case of low density fresh snow, it seems reasonable that the presence of liquid-water will add to the destructive metamorphism process and thus increase the settling rate. In order to quantify this process, a parameter (C_5) is introduced. The fractional settling rate, as computed from Eq. (3.30) or Eq. (3.31), is multiplied by C_5 whenever liquid-water is present. The value of C_5, which is greater than or equal to 1.0, is determined by calibration.

CHAPTER IV: POINT SNOW COVER MODEL

INTRODUCTION

This chapter describes the digital computer simulation model of a snow cover at a point. This energy and mass balance model is built around the equation for snow cover energy exchange developed in Chapter II and the equation for heat transfer within the snow cover developed in Chapter III. In order to combine and solve these equations the snow cover is divided into finite layers. The energy balance equation for each layer is expressed in an implicit finite-difference form. The equations are solved by using the Newton-Raphson iteration technique. The thickness of each layer varies with time because of the dynamic nature of a snow cover. These variations are kept within reasonable limits so that the numerical accuracy of the computations is not seriously affected.

In addition to computing the energy exchange for a snow cover, the model includes mathematical representations of the other processes which affect the energy and mass balance. These processes are: the addition of new snow, compaction and metamorphic changes, and the retention and transmission of liquid-water.

FINITE-DIFFERENCE FORMULATION OF THE ENERGY EXCHANGE EQUATIONS

Introduction

The energy balance for each layer of the snow cover for a given time interval (Δt) can be expressed in terms of the state of each layer at the beginning of the interval (time t) and the end (time $t+\Delta t$). In addition, the magnitude of the meteorological variables (air temperature, vapor pressure, wind speed, radiation, and precipitation) during the time interval must be known. The unknown for each layer is either the temperature or liquid-water content of the layer at time $t+\Delta t$. If the unknown is expressed solely in terms of the condition of the snow cover at time t, the result is termed an explicit formulation, i.e., the unknown is expressed only in terms of known quantities. If the unknown is expressed in terms of the state of the snow cover at both time t and $t+\Delta t$, the result is termed an implicit expression. If only conditions at time $t+\Delta t$ are used, the expression is said to be fully implicit. For convenience a factor θ can be used in the finite-difference expressions which allows the weight placed on the spatial derivatives at times t and $t+\Delta t$ to be varied. Conditions at time $t+\Delta t$ are given a weight equal to θ and

conditions at time t a weight of 1.0-θ. Thus if θ is zero we have an explicit expression. A θ of 1.0 yields a fully implicit expression. Theoretically the most accurate expression occurs when θ =0.5. Unless specified, θ =0.5 is used in all computations in this report.

The effects of new snow, compaction and metamorphic changes, and liquid-water retention and transmission are accounted for prior to or immediately after each time step. This simplifies the energy balance equations to a workable form. It means that time t values of layer thickness and density can be used during the entire time interval.

Finite-Difference Analogues for Derivatives

The following finite-difference expressions are used to represent the derivatives that appear in the energy balance equations.

1. Spatial derivatives

   a. First derivatives

$$\left(\frac{\partial V}{\partial z}\right)_n = 0.5 \cdot \left(\frac{V_n - V_{n-1}}{z_n - z_{n-1}} + \frac{V_{n+1} - V_n}{z_{n+1} - z_n}\right) \quad , \tag{4.1}$$

   where:

   V = the variable that is changing with respect to depth (snow temperature and density in this case),

   z = depth measured from the snow surface, and

   n = a subscript indicating the layer number.

   V_n represents the mean value of the variable for layer n. z_n is taken as the mid-point of the layer. The derivative is positive if V increases with depth.

   b. Second derivatives

$$\left(\frac{\partial^2 V}{\partial z^2}\right)_n = \frac{2.0}{z_{n+1} - z_{n-1}} \cdot \left(\frac{V_{n+1} - V_n}{z_{n+1} - z_n} - \frac{V_n - V_{n-1}}{z_n - z_{n-1}}\right) \quad . \tag{4.2}$$

   The only variable for which a second derivative is needed in this case is snow temperature. The second derivative is positive if $\partial V/\partial z$ increases with depth.

2. Time derivatives

$$\frac{\partial V}{\partial t} = \frac{V_n^{t+\Delta t} - V_n^t}{\Delta t} \quad , \tag{4.3}$$

where:

t = time at the start of the interval, and

Δt = the length of the time interval.

Finite-Difference Equation - Surface Layer

Eq. (2.65), which is the energy balance equation for a snow cover, is the basis for the finite-difference equation for the surface layer. Eq. (2.65) represents the surface layer if the change in heat storage of the rest of the snow cover is removed. Substituting the value of the temperature and the amount of liquid-water for each layer at time t and time t+Δt into Eq. (2.65) yields

$$(d \cdot \rho_s)_o^t \cdot \left[(c_i \cdot T)_o^{t+\Delta t} - (c_i \cdot T)_o^t \right] + \frac{L_f \cdot \rho_w}{10} \cdot \left[W_o^{t+\Delta t} - W_o^t \right] - \Delta H_o = 0.0, \qquad (4.4)$$

where:

d = layer thickness (cm),

ρ_s = density of the solid (ice) portion of the snow layer ($gm \cdot cm^{-3}$),

c_i = specific heat of ice ($cal \cdot gm^{-1} \cdot {}^\circ K^{-1}$),

T = snow temperature (°K),

L_f = latent heat of fusion (79.7 $cal \cdot gm^{-1}$),

ρ_w = density of water (1.0 $gm \cdot cm^{-3}$), and

W = the amount of liquid-water, expressed as a depth (mm). The subscript zero is the layer number of the surface layer. The term ΔH_o can be expressed as

$$\begin{aligned} \Delta H_o = Q_{ir} &- \Delta t \cdot \varepsilon \cdot \sigma \cdot \left[(1-\theta) \cdot (T_o^t)^4 + \theta \cdot (T_o^{t+\Delta t})^4 \right] \\ &+ \frac{L_s \cdot \rho_w}{10} \cdot f(U_a) \cdot \left[e_a - (1-\theta) \cdot e_o^t - \theta \cdot e_o^{t+\Delta t} \right] \\ &+ \frac{L_s \cdot \rho_w}{10} \cdot f(U_a) \cdot \gamma \cdot \left[T_a - (1-\theta) \cdot T_o^t - \theta \cdot T_o^{t+\Delta t} \right] \\ &+ \frac{c_w \cdot \rho_w}{10} \cdot P_x \cdot (T_w - 273.16) + Q_g \end{aligned} \qquad (4.5)$$

$$+ \sum_{n=1}^{n=N} \left((d \cdot \rho_s)_n^t \cdot \left((c_i \cdot T)_n^t - (c_i \cdot T)_n^{t+\Delta t} \right) \right)$$

$$+ \sum_{n=1}^{n=N} \left(\frac{L_f \cdot \rho_w}{10} \cdot (W_n^t - W_n^{t+\Delta t}) \right) \quad ,$$

where:

Q_{ir} = incident minus reflected all-wave radiation for the time interval ($cal \cdot cm^{-2}$),

ε = emissivity of the snow (0.99),

σ = Stefan-Boltzmann constant ($cal \cdot cm^{-2} \cdot °K^{-4} \cdot sec^{-1}$),

$f(U_a)$ = wind function ($mm \cdot mb^{-1}$),

e_a = mean vapor pressure of the air over the time interval (mb),

e_o = vapor pressure of the snow surface (mb),

γ = a constant for a given location as defined by Eq. (2.54) ($mb \cdot °K^{-1}$),

c_w = specific heat of water (1.0 $cal \cdot gm^{-1} \cdot °K^{-1}$),

P_x = amount of rain (mm),

T_w = wet-bulb temperature (°K),

Q_g = heat transfer across the snow-soil interface ($cal \cdot cm^{-2}$), and

N = the total number of layers in the snow cover.

If both the snow cover and the soil were being modeled, an equation similar in form to Eq. (3.11) could be used to compute heat transfer within the soil. In that case, the soil would be divided into layers and computations made down to a depth where the temperature could be treated as a constant. Then Q_g would be equal to the summation of the heat storage changes in all of the soil layers. However, modeling of heat transfer within the soil is beyond the scope of this study. Therefore an approximation to Q_g is used. Since temperature in the vicinity of the snow-soil interface normally changes very slowly, the equation for steady state heat transfer by conduction between two substances with different properties can be used to estimate Q_g. This equation can be expressed as

$$q_c = \frac{2 \cdot k_{c_1} \cdot k_{c_2} \cdot (T_2 - T_1)}{k_{c_2} \cdot d_1 + k_{c_1} \cdot d_2} \quad , \qquad (4.6)$$

where:

q_c = conduction heat transfer ($cal \cdot cm^{-2} \cdot sec^{-1}$)

k_{c_1}, k_{c_2} = thermal conductivity of the two substances ($cal \cdot cm^{-1} \cdot °K^{-1} \cdot sec^{-1}$),

T_1, T_2 = temperature at the mid-point of each substance (°K), and

d_1, d_2 = thickness of the substances (cm).

Substituting conditions at times t and t+Δt yields an approximation for Q_g. This approximation is

$$Q_g = \frac{(1-\theta) \cdot \Delta t \cdot Fl_N^t \cdot Fl_g^t \cdot (T_g^t - T_N^t)}{0.5 \cdot Fl_g^t \cdot d_N + Fl_N^t \cdot d_g} + \frac{\theta \cdot \Delta t \cdot Fl_N^{t+\Delta t} \cdot Fl_g^{t+\Delta t} \cdot (T_g^{t+\Delta t} - T_N^{t+\Delta t})}{0.5 \cdot Fl_g^{t+\Delta t} \cdot d_N + Fl_N^{t+\Delta t} \cdot d_g} , \quad (4.7)$$

where:

Δt = time interval (sec)

T_g = soil temperature (°K),

d_g = depth below ground of the soil temperature measurement (cm), and

$Fl = k_c + L_s \cdot D_v \cdot f'$,

where:

k_c = thermal conductivity (for snow $k_c = k_e$, the effective thermal conductivity) ($cal \cdot cm^{-1} \cdot °K^{-1} \cdot sec^{-1}$),

D_v = diffusion coefficient for water vapor [for snow $D_v = D_e$, Eq. (3.13)] ($cm^2 \cdot sec^{-1}$), and

f' = the partial derivative of water vapor concentration with respect to temperature [Eq. (3.22)] ($gm \cdot cm^{-3} \cdot °K^{-1}$).

Subscripts N and g refer to the bottom layer of the snow cover and the soil, respectively. The term $L_s \cdot D_v \cdot f'$ is referred to as the equivalent thermal conductivity due to water vapor diffusion [the reason for this terminology can be seen by looking at the $\partial^2 T / \partial z^2$ term in Eq. (3.11)].

If the mean temperature of the bottom layer of the snow cover is 0°C (thus there is no temperature gradient within the bottom layer), heat transfer is approximated using the gradient defined by 0°C at the snow-soil interface and the temperature, T_g, at a depth, d_g, in the soil. In this case Q_g is approximated by the expression

$$Q_g = \frac{(1-\theta)\cdot\Delta t\cdot Fl_g^t\cdot\left(T_g^t - T_N^t\right)}{d_g} + \frac{\theta\cdot\Delta t\cdot Fl_g^{t+\Delta t}\cdot\left(T_g^{t+\Delta t} - T_N^{t+\Delta t}\right)}{d_g} \quad . \qquad (4.8)$$

Eqs. (4.7) and (4.8) assume that no solar radiation penetrates through the snow cover into the soil. This assumption and the use of the steady state approximation to Q_g, are very reasonable except for a very shallow snow cover. When the snow cover is very shallow some of the solar radiation undoubtedly penetrates through the snow and warms the soil. In addition, snow and soil temperatures are more transient in nature, thus making the steady state approximations less appropriate estimates of Q_g.

Finite-Difference Equation-Intermediate Layers

Eq. (3.15) is used as the basic equation for heat transfer within the snow cover. Substituting the finite-difference expression for the time derivative, the symbolic representations of the finite-difference expressions for the spatial derivatives, and the expression for the effective diffusion coefficient for water vapor in snow [Eq. (3.13)] into Eq. (3.15) yields

$$T_n^{t+\Delta t} - T_n^t + \frac{L_f\cdot\rho_w}{10\cdot(d\cdot\rho_s)_n^t}\cdot\left(\frac{W_n^{t+\Delta t}}{(c_i)_n^{t+\Delta t}} - \frac{W_n^t}{(c_i)_n^t}\right) - \Delta T_n = 0.0. \qquad (4.9)$$

The term ΔT_n can be expressed as

$$\Delta T_n = \frac{(1-\theta)\cdot I_n}{(d\cdot\rho_s\cdot c_i)_n^t} + \frac{\theta\cdot I_n}{(d\cdot\rho_s)_n^t\cdot(c_i)_n^{t+\Delta t}} + \frac{(1-\theta)\cdot\Delta t\cdot Fl_n^t}{(\rho_s\cdot c_i)_n^t}\cdot\left(\frac{\partial^2 T}{\partial z^2}\right)_n^t$$

$$+ \frac{\theta\cdot\Delta t\cdot Fl_n^{t+\Delta t}}{(\rho_s)_n^t\cdot(c_i)_n^{t+\Delta t}}\cdot\left(\frac{\partial^2 T}{\partial z^2}\right)_n^{t+\Delta t} + \frac{(1-\theta)\cdot\Delta t\cdot\left(\frac{\partial k_e}{\partial\rho_s}\right)_n^t}{(\rho_s\cdot c_i)_n^t}\cdot\left(\frac{\partial\rho_s}{\partial z}\right)_n^t\cdot\left(\frac{\partial T}{\partial z}\right)_n^t$$

$$+ \frac{\theta\cdot\Delta t\cdot\left(\frac{\partial k_e}{\partial\rho_s}\right)_n^t}{(\rho_s)_n^t\cdot(c_i)_n^{t+\Delta t}}\cdot\left(\frac{\partial\rho_s}{\partial z}\right)_n^t\cdot\left(\frac{\partial T}{\partial z}\right)_n^{t+\Delta t} \qquad (4.10)$$

$$+\frac{(1-\theta)\cdot\Delta t\cdot C_D\cdot L_s\cdot\left[\frac{n_d}{T_n^t}\cdot F2_n^t+F4_n^t\right]}{(\rho_s\cdot c_i)_n^t}\cdot\left[\left(\frac{\partial T}{\partial z}\right)_n^t\right]^2$$

$$+\frac{\theta\cdot\Delta t\cdot C_D\cdot L_s\cdot\left[\frac{n_d}{T_n^{t+\Delta t}}\cdot F2_n^t+F4_n^t\right]}{(\rho_s)_n^t\cdot(c_i)_n^{t+\Delta t}}\cdot\left[\left(\frac{\partial T}{\partial z}\right)_n^{t+\Delta t}\right]^2 \quad ,$$

where:

I_n = the amount of solar radiation absorbed in layer n during the time interval Δt ($cal\cdot cm^{-2}$),

n_d = the temperature exponent in the equation for the effective diffusion coefficient for water vapor in snow [Eq. (3.13)],

C_D = the assumed constant part of Eq. (3.13) $C_D = D_{eo}\cdot\frac{1000}{P_a\cdot(273.16)^{n_d}}$,

$F2 = T^{n_d}\cdot f'$ ($gm\cdot cm^{-3}\cdot{}^\circ K^{n_d-1}$), and

$F4 = T^{n_d}\cdot f''$ ($gm\cdot cm^{-3}\cdot{}^\circ K^{n_d-2}$) [f" is defined by Eq. (3.23)].

Finite-Difference Equation - Bottom Layer

The bottom layer of the snow cover is influenced by heat transfer across the snow-soil interface. The energy balance for the bottom layer can be expressed as

$$Q_g + Q_{N,N-1} + I_N = \Delta Q_N \qquad (4.11)$$

where:

$Q_{N,N-1}$ = heat transfer between the bottom layer and the layer above it ($cal\cdot cm^{-2}$),

I_N = the amount of solar radiation absorbed in the bottom layer ($cal\cdot cm^{-2}$), and

ΔQ_N = the change in heat storage of the bottom layer ($cal\cdot cm^{-2}$).

Eqs. (4.7) and (4.8) give the finite-difference expressions for Q_g. The equation for steady state heat transfer by conduction between two substances with different properties [Eq. (4.6)] is also used for $Q_{N,N-1}$. After making these substitutions, the finite-difference expression for the bottom layer is

$$T_N^{t+\Delta t} - T_N^t + \frac{L_f \cdot \rho_w}{10 \cdot (d \cdot \rho_s)_N^t} \cdot \left(\frac{W_N^{t+\Delta t}}{(c_i)_N^{t+\Delta t}} - \frac{W_N^t}{(c_i)_N^t} \right) - \Delta T_N = 0.0. \qquad (4.12)$$

The term ΔT_N can be expressed as

$$\Delta T_N = \frac{(1-\theta) \cdot I_N}{(d \cdot \rho_s \cdot c_i)_N^t} + \frac{\theta \cdot I_N}{(d \cdot \rho_s)_N^t \cdot (c_i)_N^{t+\Delta t}} + \frac{Q_g}{(d \cdot \rho_s)_N^t \cdot (c_i)_N^{t*}}$$

$$+ \frac{2 \cdot (1-\theta) \cdot \Delta t \cdot Fl_N^t \cdot Fl_{N-1}^t \cdot \left(T_{N-1}^t - T_N^t \right)}{(d \cdot \rho_s \cdot c_i)_N^t \cdot \left(Fl_N^t \cdot d_{N-1}^t + Fl_{N-1}^t \cdot d_N^t \right)} \qquad (4.13)$$

$$+ \frac{2 \cdot \theta \cdot \Delta t \cdot Fl_N^{t+\Delta t} \cdot Fl_{N-1}^{t+\Delta t} \cdot \left(T_{N-1}^{t+\Delta t} - T_N^{t+\Delta t} \right)}{(d \cdot \rho_s)_N^t \cdot (c_i)_N^{t+\Delta t} \cdot \left(Fl_N^{t+\Delta t} \cdot d_{N-1}^t + Fl_{N-1}^{t+\Delta t} \cdot d_N^t \right)} \quad ,$$

where t* signifies that the first term of the appropriate Q_g expression is divided by $(c_i)_N^t$, while the second term is divided by $(c_i)_N^{t+\Delta t}$.

SOLUTION TECHNIQUE

Input Data and Unknowns

The input data needed in order to solve Eqs. (4.4), (4.9), and (4.12) are:

1. Mean values over the time interval of
   a. air temperature,
   b. vapor pressure of the air,
   c. wind speed,
   d. incoming solar radiation,
   e. reflected solar radiation,
   f. incoming longwave radiation, and
   g. amount and temperature of rainfall (temperature of rain is assumed equal to the wet-bulb temperature), plus
2. soil temperature at times t and t+Δt.

In addition, the state of the snow cover must be specified when the computations first begin.

The unknowns in these equations are the temperature and the amount of liquid-water for each layer at time t+Δt. If both of these quantities

were unknown simultaneously, it would not be possible to solve the equations. However, all the liquid-water must freeze (some very small amount of liquid-water may exist even at very low temperatures, but this is of no practical consequence) before the temperature of a layer can drop below 0°C. Vice-versa, the layer must warm up to 0°C before liquid-water can occur. Thus it is assumed when $T_n^{t+\Delta t}$ is less than 0°C, $W_n^{t+\Delta t}=0.0$; and when $W_n^{t+\Delta t}$ is greater than zero, $T_n^{t+\Delta t}=0°C$.

Newton-Raphson Iteration Technique

Eqs. (4.4), (4.9), and (4.12) are non-linear with respect to the unknown $T_n^{t+\Delta t}$. It should be noted that if $W_n^{t+\Delta t}$ is the unknown for all layers, then we have a set of linear equations and the solution is elementary. However, in the general case some sort of iterative technique is needed to solve the snow cover layer equations.

For an expression y=f(x), the Newton-Raphson iteration technique may be used to find the solution to the equation, f(x)=0. In this technique, f(x) is expanded in a Taylor Series about the point x_o, which is the initial approximation to the solution. Thus

$$y = f(x) = f(x_o) + \frac{f'(x_o)\cdot(x-x_o)}{1!} + \frac{f''(x_o)\cdot(x-x_o)^2}{2!} + \dots , \qquad (4.14)$$

where the prime denotes a derivative, i.e., $f'(x_o) = df(x_o)/dx_o$. Since f(x)=0, and if the second and higher order terms of Eq. (4.14) are neglected, then

$$f(x_o) + f'(x_o)\cdot(x-x_o) = 0. \qquad (4.15)$$

Solving Eq. (4.15) for x yields

$$x = x_o - \frac{f(x_o)}{f'(x_o)} . \qquad (4.16)$$

This value of x is an approximation to the solution since the second and higher order terms of the Taylor Series were discarded. Now if the new value x is substituted for x_o in Eq. (4.16), the resulting value of x will converge toward the solution. Successive iterations will produce a value of x which is sufficiently close to the true solution. A general iterative formula for this procedure is

$$x_{j+1} = x_j - \frac{f(x_j)}{f'(x_j)} , \qquad (4.17)$$

where the subscript j denotes the iteration number. Convergence is attained when either

$$|x_{j+1}-x_j|<\varepsilon_1 \tag{4.18}$$

or

$$|f(x_j)|<\varepsilon_2 \tag{4.19}$$

where ε_1 and ε_2 are error tolerances.

Eq. (4.15) can be rewritten in a different notation as

$$\frac{\partial E_n}{\partial U_n}\cdot\Delta U_n = -r_n \tag{4.20}$$

where:

E_n = the finite difference equation for a given snow cover layer (n),

U_n = the unknown for layer n,

r_n = the residual when E_n is evaluated at a value U_{n_j}, and

ΔU_n = the correction to be applied to U_{n_j} in order to get $U_{n_{j+1}}$

In the case of a set of equations, each equation may contain more than one unknown. For example, if $T_{n-1}^{t+\Delta t}$, $T_n^{t+\Delta t}$, and $T_{n+1}^{t+\Delta t}$ are unknown, the Newton-Raphson iteration technique expression for Eq. (4.9) is

$$\frac{\partial E_n}{\partial U_{n-1}}\cdot\Delta U_{n-1}+\frac{\partial E_n}{\partial U_n}\cdot\Delta U_n+\frac{\partial E_n}{\partial U_{n+1}}\cdot\Delta U_{n+1}=-r_n\ . \tag{4.21}$$

In the general case, the corrections to be applied to the j^{th} iteration values of the unknowns for each layer of the snow cover can be expressed by the set of linear equations shown in Fig. 4-1. The terms on the left side of the equations in Fig. 4.1 form a tri-diagonal matrix except for the first row which is always complete. If the amount of liquid-water is the unknown for a given layer (n) only two values will appear in the n^{th} column of the matrix (only one value in the 1^{st} column); one in the first row and one in the n^{th} row. The corrections to be applied to the current value of the unknown for each layer are determined by solving the set of linear equations using Gauss elimination. The solution of the finite-difference equations is considered complete when the absolute values of the corrections for each layer all are less than a given tolerance. The partials of each of the finite-

$$\frac{\partial E_o}{\partial U_o}\cdot\Delta U_o + \frac{\partial E_o}{\partial U_1}\cdot\Delta U_1 + \frac{\partial E_o}{\partial U_2}\cdot\Delta U_2 + \cdots\cdots\cdots + \frac{\partial E_o}{\partial U_N}\cdot\Delta U_N = -r_o$$

$$\frac{\partial E_1}{\partial U_o}\cdot\Delta U_o + \frac{\partial E_1}{\partial U_1}\cdot\Delta U_1 + \frac{\partial E_1}{\partial U_2}\cdot\Delta U_2 = -r_1$$

$$\frac{\partial E_2}{\partial U_1}\cdot\Delta U_1 + \frac{\partial E_2}{\partial U_2}\cdot\Delta U_2 + \frac{\partial E_2}{\partial U_3}\cdot\Delta U_3 = -r_2$$

$$\vdots \qquad \vdots \qquad \vdots \qquad \vdots$$

$$\frac{\partial E_{N-1}}{\partial U_{N-2}}\cdot\Delta U_{N-2} + \frac{\partial E_{N-1}}{\partial U_{N-1}}\cdot\Delta U_{N-1} + \frac{\partial E_{N-1}}{\partial U_N}\cdot\Delta U_N = -r_{N-1}$$

$$\frac{\partial E_N}{\partial U_{N-1}}\cdot\Delta U_{N-1} + \frac{\partial E_N}{\partial U_N}\cdot\Delta U_N = -r_N$$

Fig. 4.1. Newton-Raphson iteration technique equations for a snow cover.

difference equations with respect to the unknowns contained in each equation are given in Appendix A.

Rapid convergence is normally obtained when the Newton-Raphson iteration technique is used to solve the implicit finite-difference snow cover equations. Only one or two iterations are typically required. However, when the unknown for a given layer is changing during the time interval, it was found that the solution for that layer should pause at the $T_n^{t+\Delta t} = 0°C$, $W_n^{t+\Delta t} = 0.0$ point. Difficulties were sometimes encountered when the residual portion of a correction to one unknown was applied to the other (the residual was converted to the proper units first). This was solved by waiting and determining the correction to be applied to the new unknown on the next iteration. This process increases the number of iterations required before convergence is attained, especially if the unknown is changing for a number of layers. The computer program allows for a maximum of 10 iterations.

COMPUTER PROGRAM

Introduction

The computer program is written in FORTRAN IV. The program is written for use on a CDC 6600 computer (SCOPE 3.3 operating system). However, only basic FORTRAN statements are used, thus conversion of the program for use on another computer system should be relatively easy.

A simplified flowchart of the program is shown in Fig. 4.2. In addition to the main program, there are 28 subroutines. A comment block at the beginning of the listing specifies the input cards needed to run the program. Meteorological variables are input from a sequential tape or disk file.

The program is currently dimensioned for a maximum of 100 snow layers. With this configuration, the program requires about 50K words of core storage. Run times vary primarily with the number of layers needed and with respect to how often the snow cover profile is printed. For a case where 20 to 50 layers are needed over the course of several months of simulation and the snow cover profile is printed once per day, the CPU time is about 1.5 seconds per day.

Program Components

This section contains a brief description of each of the main components of the program.

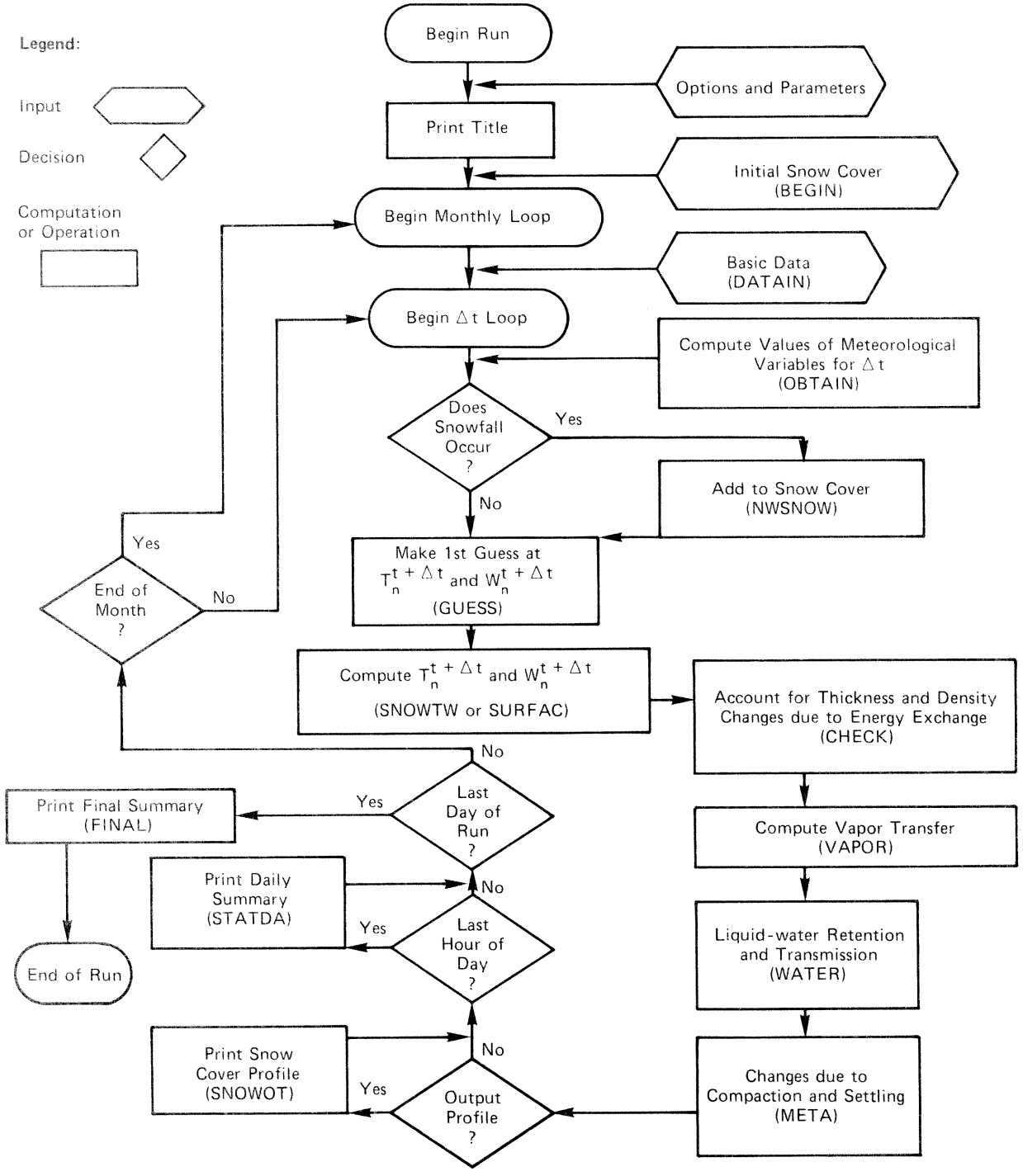

Figure 4.2.--Simplified flowchart of the point snow cover model computer program. [Subroutine names are in parentheses.]

1. Main program.

Function: The main program contains statements which input the control options and parameter values, as well as print a title sheet. The rest of the main program is a series of subroutine calls which control the operations to be performed during each time interval.

2. Subroutine BEGIN

Function: This subroutine is used to input the initial state of the snow cover (number of layers, plus thickness, temperature, density, and amount of liquid-water for each layer) at the beginning of each run.

3. Subroutine DATAIN

Function: This subroutine is used to input the required data on a monthly basis. Soil temperature is input from cards. The remainder of the data are read off a sequential tape or disk file. The data are stored in hourly arrays for use by the rest of the program.

The required format of the sequential file is described by a comment block in subroutine DATAIN. If another data set, which is stored in a differently formatted file, were being accessed, the file READ statements would have to be changed. However, only portions of subroutine DATAIN would need to be changed, as this subroutine is the sole link between the file containing the basic data and the rest of the program.

4. Subroutine OBTAIN

Function: This subroutine computes the value of each meteorological variable for the current time interval from the data stored in the hourly arrays. The program has the option to vary the computational time interval from a minimum of 1 hour to a maximum of 24 hours (only intervals divisible into 24 are allowed).

If precipitation occurs during the interval, the wet-bulb temperature is used to determine if the precipitation is rain or snow. If the wet-bulb temperature is 1°C or less, precipitation is assumed to be snow. The density of new snow is based on a plot of new snow density versus temperature for Alta, Utah [LaChapelle (1969)]. This plot is based on samples of new snow collected within 2 hours of deposition. A mathematical expression which reasonably fits the plotted data is

$$\rho_{ns} = 0.05 + 0.0017 \cdot (T_w - 258.16)^{1.5} , \qquad (4.22)$$

where:

ρ_{ns} = density of new snow, and

T_w = wet-bulb temperature (assumed to be the temperature of the precipitation) (°K).

The program allows the user to change the density of new snow or alter the form of precipitation for selected periods if observations indicate that such changes are necessary.

5. Subroutine GUESS

Function: This subroutine provides a first guess for the unknowns, $T_n^{t+\Delta t}$ and $W_n^{t+\Delta t}$, for each layer of the snow cover.

Technique used: The first guess for the surface layer is computed by solving Eq. (4.4) by assuming Q_g and the change in heat storage for the rest of the snow cover are zero. The first guess for the other layers is a linear projection of the change in temperature during the previous interval. When $W_n^{t+\Delta t}$ is the unknown in one of these layers, the first guess is W_n^t plus the melt due to solar radiation absorbed by the layer.

A provision is included to further refine the first guess for the upper three layers. These are the layers where the greatest change occurs. For the surface layer, the change in heat storage from the previous interval is used rather than assuming that the change in heat storage for the rest of the snow cover is zero. For the next two layers, the temperature gradient as defined by the temperature of the layer above and the given layer is used. The ratio of the gradient for the current time interval to the gradient for the previous interval is used in an attempt to refine the initial projection. Not enough tests have been made to determine if this technique for refining the first guess saves a significant amount of computer time. Early indications are that it does not.

In testing the program it was found that numerical errors (which damped out with time) resulted when a sudden large temperature change occurred. To rectify this, subroutine GUESS causes the time interval to be subdivided whenever the projected temperature change in the top two layers exceeds a preset value.

If $\theta = 0.0$, thus the finite-difference equations are expressed in an explicit form, the stability criterion

$$\Delta t_c = \frac{\Delta z^2}{4 \cdot K_v} \tag{4.23}$$

is used [Yen (1967)]. In Eq. (4.23)

Δt_c = the computational time interval (sec),

Δz = layer thickness (taken as the thickness of the smallest layer) (cm), and

K_v = thermal diffusivity ($K_v = k_e/c_i \cdot \rho_s$)($cm^2 \cdot sec^{-1}$).

This program is not designed for the efficient solution of explicit finite-difference equations. Explicit formulations require the use of much shorter time intervals than implicitly formulated equations, but they do not require the use of an iterative solution technique. This program goes through the Newton-Raphson iteration technique even when θ=0.0.

6. Subroutine SNOWTW

Function: This subroutine computes $T_n^{t+\Delta t}$ and $W_n^{t+\Delta t}$ for each layer.

Technique used: Subroutine SNOWTW uses the Newton-Raphson iteration technique to solve Eqs. (4.4), (4.9), and (4.12).

7. Subroutine SURFAC

Function: This subroutine computes $T_o^{t+\Delta t}$ and $W_o^{t+\Delta t}$ for use as a first guess or when the snow cover consists of only one layer.

Technique used: Subroutine SURFAC uses the Newton-Raphson iteration technique to solve Eq. (4.4). When computing a first guess for the surface layer, the term Q_g is set to zero.

8. Auxiliary subroutines

Function: There are 10 auxiliary subroutines that are primarily used to compute various terms contained in Eq. (4.4), (4.9), and (4.12). These include such terms as z_n, $\partial\rho_s/\partial z$, c_i, Fl_g, $f(U_a)$, T_w, k_e, $\partial k_e/\partial\rho_s$, I_n, and Fl_n through $F7_n$.

Expressions used: The expressions for most of these terms have been given previously; however, in a few cases the specific expression used in the program has not been given.

a. effective thermal conductivity of snow. The expression for k_e used in the program is

$$k_e = 0.00005 + C_k \cdot \rho_s^{\,2} \quad , \tag{4.24}$$

where C_k is a parameter that can be varied by the program user. By varying C_k, Eq. (4.24) can reasonably represent the relationships shown in Fig. 3-1 over the range of densities encountered in

seasonal snow covers. Using Eq. (4.24) the partial of k_e with respect to density becomes

$$\partial k_e/\partial \rho_s = 2 \cdot C_k \cdot \rho_s . \tag{4.25}$$

b. extinction coefficient. The expression used in the program for the extinction coefficient (ν) is

$$\nu = C_\nu \cdot \rho_s \cdot d_s^{-1/2} \quad , \tag{4.26}$$

where C_ν is a parameter that can be varied. Eq. (4.26) is based on Eq. (3.17). Since grain size (d_s) is not input or computed by the program, a relationship between grain size and density (ρ_s) is needed. Such a relationship would be location dependent and could be quite complex. The next chapter describes the simple relationship used for the Danville, Vermont test site.

c. wind function. The program can use an empirical or a theoretically based wind function. The program uses Eq. (2.55) with $\underline{a}$ = 0.0 to represent the empirical wind function.

Eq. (2.57) is used to compute the theoretically based wind function. The bulk transfer coefficient for neutral conditions $(C_W)_N$ is computed from Eq. (2.46) with the roughness height (z_o) being an input parameter. At the beginning of each run Eqs. (2.47), (2.48), (2.49), and (2.52) are used to generate a table giving $C_W/(C_W)_N$ as a function of the bulk Richardson number, $(Ri)_B$, for unstable conditions. This table is then used throughout the run to determine C_W for each computed negative value of $(Ri)_B$. The critical Richardson number is also an input parameter so that the stability correction computed by Eq. (2.53) for stable conditions can be varied from run to run.

If an empirical wind function is used, $f(U_a)$ is computed at the start of each time interval and used throughout that interval. When a theoretically based wind function is used, $f(U_a)$ varies for each iteration since the computed value of $T_o^{t+\Delta t}$ changes. When $T_o^{t+\Delta t}$ changes, the bulk Richardson number varies, which makes C_W vary, thus causing $f(U_a)$ to change. Variations in $f(U_a)$ can increase the number of iterations required for convergence.

9. Subroutine NWSNOW

Function: Subroutine NWSNOW adds snowfall to the existing snow cover.

Technique used: The program allows the user to select a desirable thickness for the snow cover layers (D_z, units are cm.). The actual thickness is allowed to vary from 55 to 155 percent of the desired thickness. When new snow causes the surface layer to exceed $1.55 \cdot D_z$, the surface layer is subdivided. The lower portion is set to $0.9 \cdot D_z$, while the remainder forms the new surface layer. If the remainder still exceeds $1.55 \cdot D_z$, it continues to be split until the new surface layer is less than the allowable maximum thickness. A weighted value of temperature, density, and amount of liquid-water is used for the layer which contains some old snow and some new snow. New snow is assumed to contain no liquid-water.

10. Subroutine VAPOR

Function: This subroutine computes vapor transfer within the snow cover and vapor transfer across the air-snow interface.

Equations used: Eq. (3.35) is used to compute the change in density of each layer due to vapor transfer within the snow cover. Vapor transfer across the air-snow interface is based on Eq. (2.59). The latent heat transfer (Q_e) is divided by the appropriate latent heat multiplied by ρ_w. When liquid-water is present in the surface layer the latent heat of vaporization is used, otherwise the latent heat of sublimation is used.

11. Subroutine CHECK

Function: This subroutine changes the thickness and density of each layer based on the results of the energy balance computations for the time interval.

Technique used: A given layer can increase in density due to the freezing of liquid-water, or decrease in thickness due to melt, or not change in terms of thickness or density. If $W_n^{t+\Delta t}$ is less than W_n^t, then a portion of the liquid-water in the layer at the beginning of the time interval has been frozen. Thus density needs to be increased. If $W_n^{t+\Delta t}$ is greater than W_n^t, some or all of the layer has melted. In this case, the density of the layer remains the same, but the depth decreases. If the entire layer melts, the excess melt is subtracted from the next layer below.

After making the appropriate thickness and density changes, the thickness of each layer is checked to make sure it is still within the

allowable range. The desired thickness (D_z) specified by the user applies to the top 30 centimeters of the snow cover. Below 30 centimeters, the program allows the layers to become gradually thicker since temperature fluctuations are greatly reduced in the lower portion of the snow cover. The variation of D_z with depth can be expressed as

$$D_{z_n} = D_z + C_d \cdot (z_n - 30), \tag{4.27}$$

where:

z_n = depth below snow surface to the mid-point of layer n (cm),

D_{z_n} = desired thickness of layer n (cm), and

C_d = coefficient that allows D_{z_n} to increase with depth below the top 30 centimeters.

If the thickness of a given layer exceeds $1.55 \cdot D_{z_n}$, the layer is split in half. If the thickness is less than $0.55 \cdot D_{z_n}$, the layer is combined with the smallest adjacent layer. The use of these limits keeps the splitting and combining of layers to a minimum, yet variations in layer thickness are kept within reasonable bounds.

12. Subroutine META

Function: This subroutine computes the increase in density and the decrease in thickness of each layer as a result of compaction and settling (destructive metamorphism).

Equations used: Eq. (3.29) is used to compute compaction. The finite difference form of this equation used in the program is

$$(\rho_s)_n^{t+\Delta t} = \left[1.0 + \Delta t_h \cdot C_1 \cdot W_s \cdot \exp\left(-C_2 \cdot (\rho_s)_n^t\right) \cdot \exp\left(-0.08 \cdot (T_c - T_n^{t+\Delta t})\right)\right] \cdot (\rho_s)_n^t \tag{4.28}$$

where:

Δt_h = time interval (hours)

C_1 = fractional increase in density at 0°C and ρ_s=0.0 ($cm^{-1} \cdot hr^{-1}$),

W_s = the weight of the snow above the layer for which the density change is being computed, expressed in terms of water-

equivalent (cm),

C_2 = a constant to be determined by calibration ($cm^3 \cdot gm^{-1}$), and

T_c = 0°C (273.16°K).

Eq. (3.31) is used to compute the increase in density due to settling. The finite-difference form of this equation used in the program is

$$(\rho_s)_n^{t+\Delta t} = \left[1.0 + \Delta t_h \cdot C_3 \cdot \exp\left[-C_4 \cdot (T_c - T_n^{t+\Delta t})\right] \cdot C_\rho\right] \cdot (\rho_s)_n^t \quad , \qquad (4.29)$$

where:

C_3 = the fractional settling rate at 0°C for densities less than ρ_d (hr^{-1}),

C_4 = a constant to be determined by calibration ($°K^{-1}$),

C_ρ = 1.0 when $(\rho_s)_n^t \leq \rho_d$, and

$C_\rho = \exp\left[-46 \cdot \left[(\rho_s)_n^t - \rho_d\right]\right]$ when $(\rho_s)_n^t > \rho_d$.

13. Subroutine WATER

Function: This subroutine accounts for the retention and transmission of liquid-water in the snow cover. The result is the snow cover outflow for the time interval.

Technique used: Snow holds a certain amount of liquid-water due to capillary retention after all drainage has ceased. This amount of water is referred to as the liquid-water-holding capacity, or the equilibrium free water content, or the irreducible water saturation. The fractional amount of liquid-water in the snow (W_f) can be expressed as

$$W_f = \frac{10 \cdot \rho_w \cdot W}{d \cdot \rho_s} \quad . \qquad (4.30)$$

The fractional liquid-water-holding capacity (W_e) is the value of W_f under equilibrium conditions. Values of W_e given in the literature are usually computed using the total density (ice plus liquid-water) rather than just the density of the ice portion (ρ_s). Gerdel (1948) reports values of W_e of 0.007 to 0.055 for a well-aged dense snow. Colbeck (1974) reports an irreducible water saturation of 0.07 times the pore volume for snow with a density of 0.56. In summarizing equilibrium

water content deQuervain (1973) indicates that there is no unanimous agreement on a value. He quotes values ranging from 0.01 to 0.55. There is some indication that W_e increases as ρ_s decreases and as grain size (d_s) decreases. The highest reported values probably were made partly in a zone of saturation, or in a zone of capillary rise, or when water was still in transient through the snow cover. In the program, W_e is represented as

$$W_e = W_{e_{min}} \quad , \tag{4.31}$$

when ρ_s is greater than ρ_e. When ρ_s is less than ρ_e

$$W_e = W_{e_{min}} + \left(W_{e_{max}} - W_{e_{min}} \right) \cdot \left(\frac{\rho_e - \rho_s}{\rho_e} \right) \quad , \tag{4.32}$$

where:

$W_{e_{min}}$ = the minimum value of W_e (applies to well-aged dense snow),

$W_{e_{max}}$ = the maximum value of W_e (would occur if ρ_s=0.0), and

ρ_e = density (determined by calibration) above which the snow is ripe and W_e is assumed to be at its minimum value ($gm \cdot cm^{-3}$).

Recent studies by Colbeck (1972, 1973, 1974, 1975a,b) have significantly advanced the understanding of how liquid-water moves through snow. Such studies should lead to more accurate estimates of the time distribution of snow cover outflow regardless of the initial state of the snow cover. Most of the initial work has been centered on water percolation through homogenous, ripe snow.

The equations currently used for the transmission of excess liquid-water through a snow cover are empirical equations based on a lysimeter study conducted during the Snow Investigations (1955) at the Central Sierra Snow Laboratory (CSSL). Excess liquid-water is the water remaining after any heat deficit and the liquid-water-holding capacity are satisfied. The excess liquid-water is first lagged and then attenuated. The maximum lag for a given snow cover is expressed as

$$L_{w_{max}} = CW_1 \cdot \left[1.0 - \exp(-0.0025 \cdot d/\rho_s) \right], \tag{4.33}$$

where:

$L_{w_{max}}$ = maximum lag for a snow cover with a thickness d and

density ρ_s (hr), and

CW_1 = maximum allowable lag (hr).

The actual lag is based on the amount of excess water and can be expressed as

$$L_w = \frac{L_{w_{max}}}{CW_2 \cdot W_x + 1.0} \quad , \tag{4.34}$$

where:

L_w = actual lag time (hr),

CW_2 = an empirical parameter (cm^{-1}), and

W_x = amount of excess liquid-water (cm).

The attenuated snow cover outflow is computed from the expression

$$O_t = \frac{S + W_L}{[CW_3 \cdot \exp(-CW_4 \cdot W_L \cdot \rho_s / d) + 1.0]} \quad , \tag{4.35}$$

where:

O_t = snow cover outflow ($cm \cdot hr^{-1}$),

S = excess water in storage (cm),

W_L = amount of lagged excess liquid-water (cm)

CW_3 = an empirical parameter (hr), and

CW_4 = an empirical parameter ($cm^3 \cdot gm^{-1}$).

The values of the parameters which best fit the CSSL lysimeter data were $CW_1 = 10.0$, $CW_2 = 1.0$, $CW_3 = 5.0$, and $CW_4 = 450$. Snow density was arbitrarily added to these relationships in an attempt to account for the effect of density on lag and attenuation. The density of the snow cover was essentially constant during the CSSL lysimeter study. Shimizu (1970) relates the intrinsic permeability of snow to density and grain size by the expression

$$k_s = 7.7 \cdot d_s^{\,2} \cdot \exp(-7.8 \cdot \rho_s), \tag{4.36}$$

where:

k_s = intrinsic permeability (mm^2), and

d_s = grain size (mm).

The variation of k_s with density depends on the relationship between grain size and density over the history of the snow cover. Eqs. (4.33) and (4.35) assume that lag and attenuation increase as density decreases.

14. Subroutine SNOWOT

Function: This subroutine prints the snow cover profile at those times of the day specified by the user. The thickness, density, amount of liquid-water, and temperature of each layer are printed.

15. Subroutine STATDA

Function: This subroutine computes and stores various quantities for display at the end of each day and at the end of the run. At the end of each day subroutine STATDA prints time interval and daily values of simulated and observed (when available) snow surface temperature and snow cover outflow, plus computed values of vapor transfer, net short and longwave radiation, latent and sensible heat transfer, soil-snow heat transfer, heat transferred by rain water, the change in heat storage of the snow cover, and the Richardson number.

Remark: The observed snow surface temperatures used to test the model are average hourly values. Thus, in order to make a comparison, the simulated surface temperatures need to be time interval averages. This is done by taking the average of T_o^t and $T_o^{t+\Delta t}$. An arithmetic average is good for a one-hour time interval, but is less likely to represent the true average for longer time intervals. The net longwave radiation, latent and sensible heat transfer terms, as well as, the Richardson number, are computed by using the arithmetic average snow surface temperature.

16. Subroutine FINAL

Function: This subroutine prints a summary of the run. This summary includes statistical comparisons of simulated versus observed snow surface temperature and snow cover outflow. Frequency distributions of the Richardson number and air temperature minus snow surface temperature are displayed. There is also a summary of the components of the energy and mass balances.

Remark: The mass balance which should be exactly zero usually is not. It is believed that this is due to the tremendous number of calculations involving many snow layers, each of which is changing in size by a minute amount during each time interval. The mass balance is usually less than a tenth of a centimeter.

Numerical Accuracy

In several cases analytical solutions exist for the equation for one-dimensional heat transfer by conduction in a uniform medium [Eq. (3.1)].

Two of these cases are included in the computer program. One is the solution for an instantaneous change in the surface temperature of an infinitely thick medium which is originally at the same temperature throughout. The other is when the surface temperature of an infinite medium changes according to the sin-function. The analytical solution assumes this cyclic change has occurred for an infinite time. The solutions for these cases are given in many heat transfer textbooks including Jakob and Hawkins (1942).

The analytical solutions of Eq. (3.1) for these two cases are included in the program to assist in evaluating the effect of variations in layer thickness on numerical accuracy. Two kinds of variations were used to gain an insight into the effect of layer thickness. One test involved dividing a snow cover into uniformly thick layers of various sizes. In the other test the snow cover was divided into layers of variable thickness. The effect of the variable thickness of the layers was determined by comparing the results to those obtained with the same snow cover divided into uniform layers. Tables 4.1 and 4.2 give the results of these tests. An error tolerance of 0.01°C was used to determine when convergence was attained. The basic computational time interval was one hour. This time interval was sub-divided into 5 and 4 parts during the first two hours, respectively, when an instantaneous change was applied to the surface temperature. The results of these tests indicate that, as long as the desired layer thickness (D_z) is kept reasonably small (less than 5 cm.), variations in thickness over the allowable range ($0.55 \cdot D_z$ to $1.55 \cdot D_z$) do not cause significant numerical errors.

RELATIVE MAGNITUDE OF HEAT TRANSFER PROCESSES WITHIN A SNOW COVER

A detailed examination of Eq. (3.15) would reveal the relative magnitude of conduction and vapor movement on heat transfer within a snow cover. The relative importance of these processes varies as the temperature and density profiles change. Figs. 4.3 and 4.4 illustrate the relative magnitudes of heat transfer by conduction and vapor movement as related to variations in snow cover density. These figures show the temperature profile at various times after the surface temperature of an isothermal snow cover at 0°C is suddenly lowered to -10°C. As would be expected the relative importance of heat transfer by vapor movement decreases as density increases. This occurs because while D_e does not vary

Table 4.1.--Effect of variations in the size of uniformly thick layers on computed snow cover temperature profiles.[1]

Case	Layer thickness	Absolute average and maximum deviations (°C) from the analytical solution after					
		1 hr.		6 hr.		24 hr.	
	cm	avg.	max.	avg.	max.	avg.	max.
I	1.0	.0038	.15	.0024	.02	.0044	.01
I	2.5	.0043	.05	.0008	.01	.0038	.01
I	5.0	.018	.21	.0075	.03	.004	.01
I	10.0	.071	.63	.032	.13	.016	.03
II	2.5	after 31 days: avg. = .0065, max = .03					

Table 4.2.--Effect of variable layer thickness on computed snow cover temperature profiles.[1]

Case	Repeated layer thickness pattern	The sum of absolute differences and the maximum difference (°C) (compared with a snow cover with 2.5-cm thick layers) after							
	cm	1 hr		6 hr		24 hr		120 hr.	
		sum	max.	sum	max.	sum	max.	sum	max.
I	1.5, 2.5, and 3.5	.09	.04	.03	.01	.02	.01	.34	.04
I	1.5, 3.5, 3.5, and 1.5	.15	.07	.06	.02	.06	.01	.24	.02
II	1.5, 3.5, 3.5, and 1.5	after 31 days: sum = .11, max. = .03							

[1]Note: For both tables;
Case I is an instantaneous change of -10°C, and Case II is a 24-hour sin-variation with an amplitude of 10°C. The density of the snow cover is 0.3 $gm \cdot cm^{-3}$ and the depth is 100 cm.

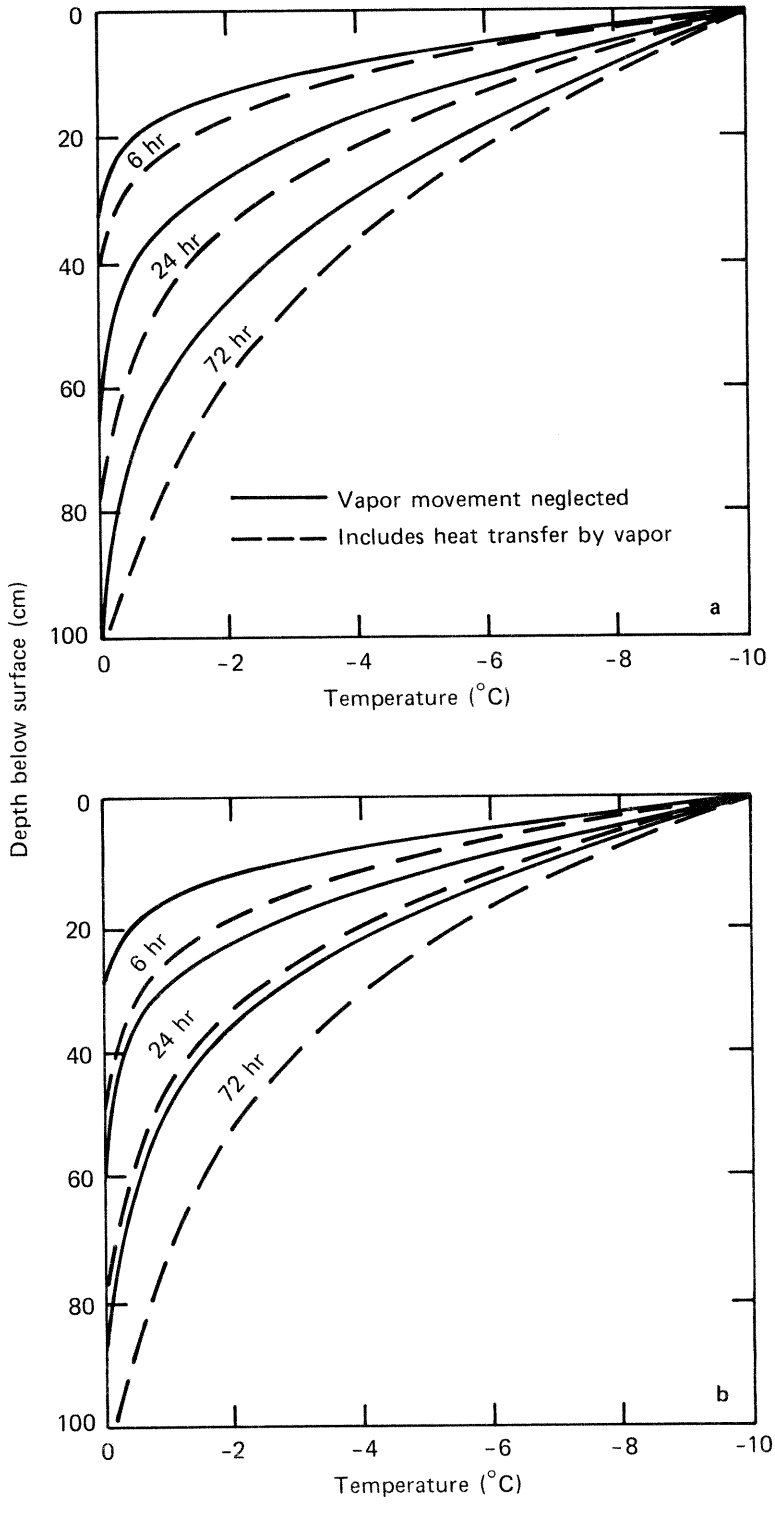

Figure 4.3.--Temperature profiles after the surface temperature of a low-density, 100-cm deep, 0°C isothermal snow cover is suddenly lowered by 10°C. (a) Uniform density of 0.15 $gm \cdot cm^{-3}$, (b) Density increases linearly with depth from 0.05 to 0.25 $gm \cdot cm^{-3}$. [$k_e = 0.00005 + 0.006 \cdot \rho_s^2$. When vapor movement is included, $D_{eo} = 0.09$, $n_d = 14$, and $P_a = 950$ mb.]

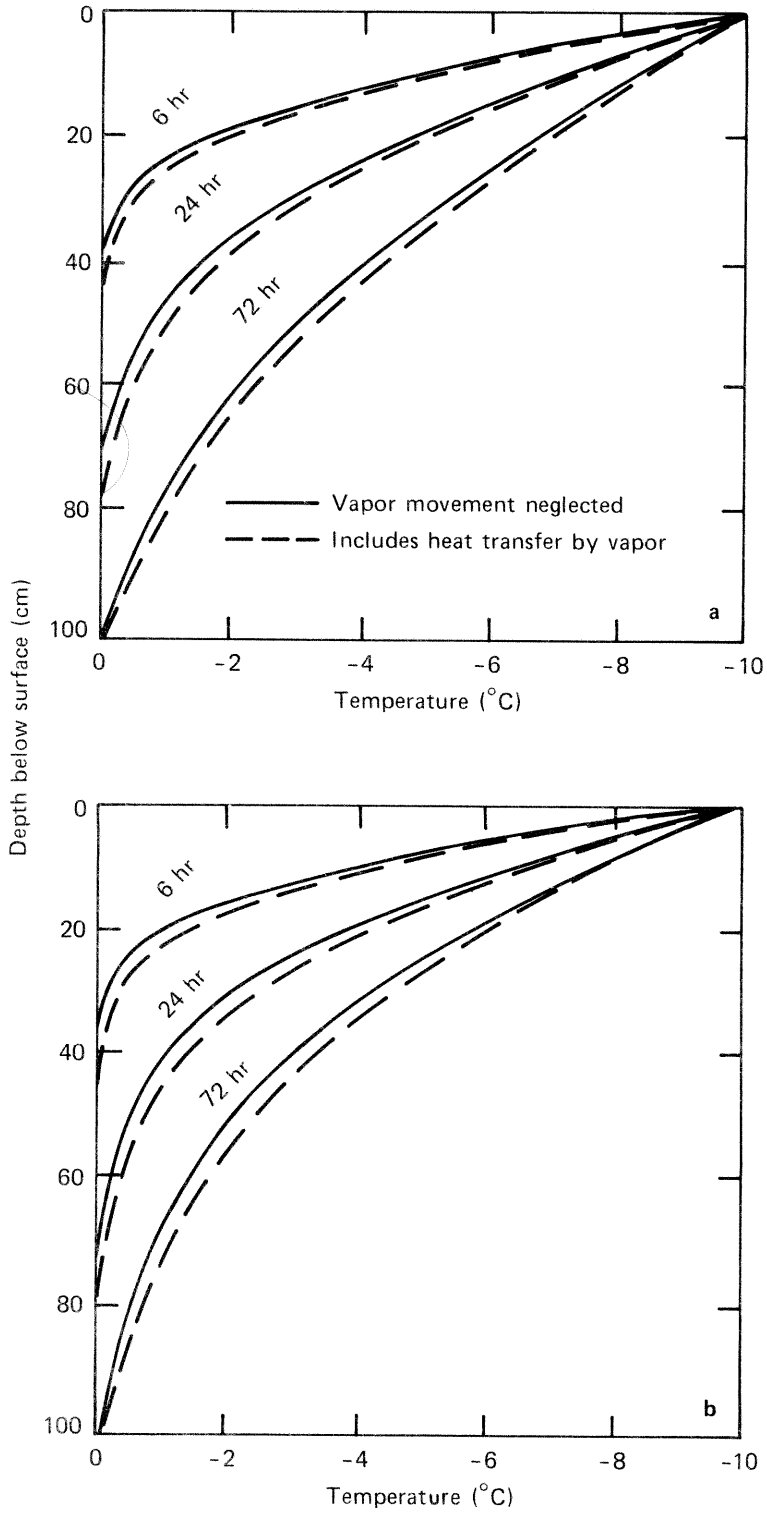

Figure 4.4.--Temperature profiles after the surface temperature of a high-density, 100-cm deep, 0°C isothermal snow cover is suddenly lowered by 10°C. (a) Uniform density of 0.35 $gm \cdot cm^{-3}$, (b) Density increases linearly with depth from 0.25 to 0.45 $gm \cdot cm^{-3}$. [$k_e = 0.00005 + 0.006 \cdot \rho_s^2$. When vapor movement is included, $D_{eo} = 0.9$, $n_d = 14$, and $P_a = 950$ mb.]

with density, k_e becomes much larger as the density of the snow cover increases. When density increases with depth (linearly in these cases), heat is transferred more rapidly in the lower portion of the snow cover where the density is the greatest. This results in relatively flat gradients near the bottom and steep gradients near the top as compared to a snow cover with uniform density.

An insight into the relative magnitudes of the various heat transfer processes under various conditions is necessary in order to properly evaluate the results of simulation runs. Simulation errors resulting from an inaccurate representation of a certain process or an improper parameter value can only be isolated under situations when the magnitude of that process is relatively large as compared to other processes which affect the results.

CHAPTER V: SIMULATION RESULTS

INTRODUCTION

This chapter presents a description of the data used and the results obtained with the snow cover simulation model. The data used to test the model were obtained as part of a cooperative research project concerned with the physical processes in snow metamorphosis and snowmelt. This project is being conducted by the National Oceanic and Atmospheric Administration (NOAA) and the Agricultural Research Service (ARS) [Johnson and Anderson (1968)]. The data used in this study were obtained at a heavily instrumented snow research station which is part of the NOAA-ARS project. The station is located within the ARS's Sleepers River Research Watershed near Danville, Vermont.

DESCRIPTION OF THE DATA

NOAA-ARS Snow Research Station

The snow research station is located about 8 kilometers NNW of Danville, Vermont, at an elevation of 552 meters. The research station site (shown in Fig. 5.1) was graded prior to the installation of the instruments. Thus the site is very flat with a slight slope to the south. This results in a very uniform snow cover over the immediate site area. However, during windy periods there is a tendency for new snow to blow off the site area. When performing mass balance computations during accumulation periods, the factor relating the increase in the water-equivalent of the snow cover to the catch in a precipitation gage varies from storm to storm and season to season. At the NOAA-ARS snow research station this factor is typically less than 1.0 on a seasonal basis. This indicates that the gage catch deficiency is exceeded by the snow which blows off the site area.

The research station is located near the eastern edge of a 0.06 square kilometer clearing. To the west, the forest is at least 175 meters from the center of the site area. The first 70 meters of this distance are free of vegetation which protrudes above the snow cover. Beyond 70 meters there are scattered clumps of small conifers. It is about 60 meters from the center of the site area to the forest in both a northeasterly and southeasterly direction. This area is also free of any vegetation which protrudes above the snow. The prevailing winds in the winter are from a westerly direction.

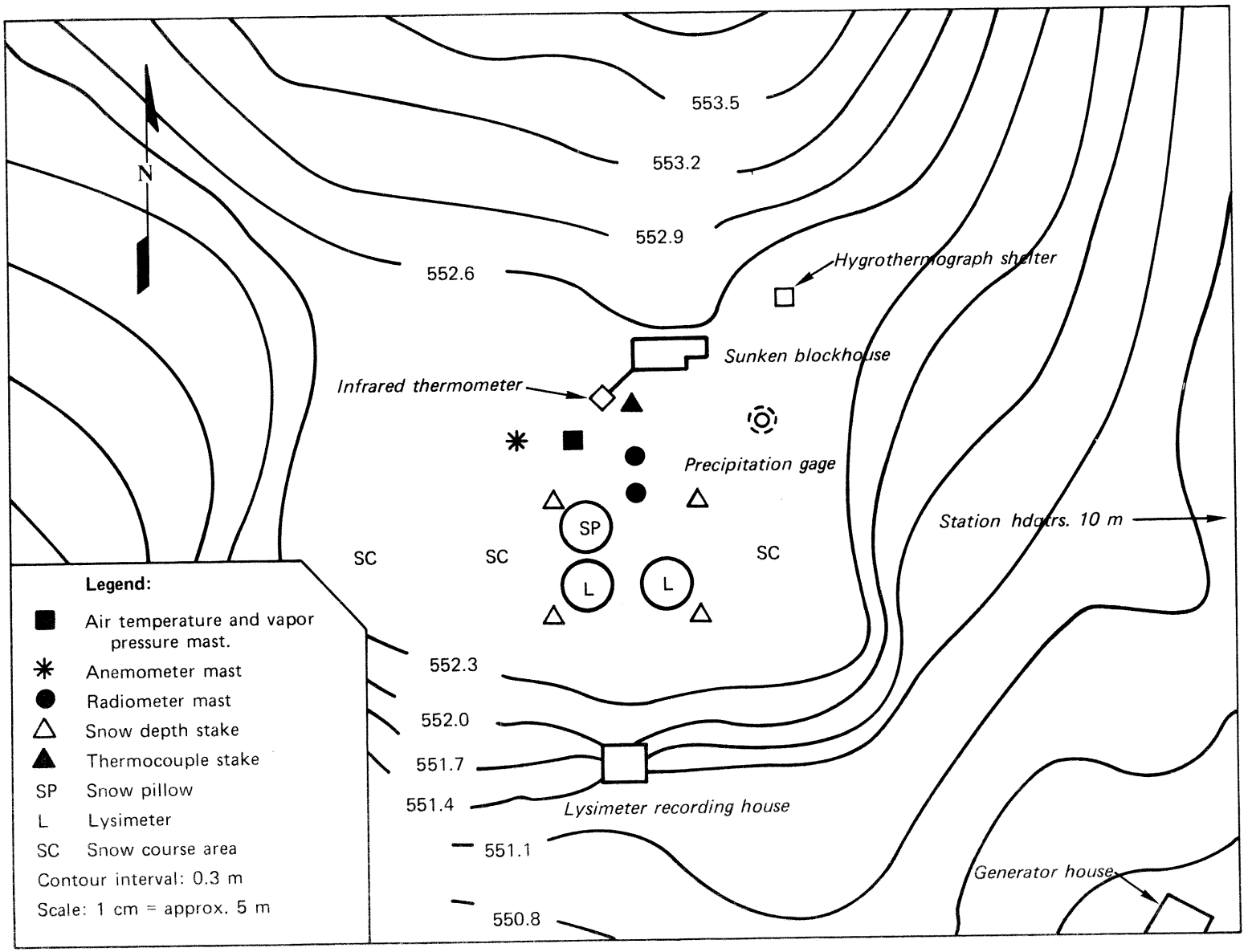

Figure 5.1.--Map of the NOAA-ARS snow research station near Danville, Vermont.

Data Used and Its Accuracy

The data needed by the snow cover simulation model are available from the NOAA-ARS snow research station for six winters beginning with 1968-69. Table 5.1 summarizes the input and verification data used to test the model. The estimated standard error between the measured and "true" value of each variable is based on a subjective evaluation of several objective factors. For the instruments these factors include comparisons between different or similar sensors measuring the same variable, calibrations of sensors against working and primary standards, repeatability of measurements, manufacturer's specifications, and a knowledge of the design and measuring principle of the instruments. The instrumental error is the combined error of the sensor and the recording system. Besides instrumental errors, the standard error estimates given in Table 5.1 include the effect of sampling errors. Sampling errors for the meteorological variables and snow cover variables, such as snow surface temperature and snow cover outflow whose values are basically determined by meteorological conditions, should be relatively small most of the time because of the uniformity and small size of the site area. The snow cover is also quite uniform over the site area. However, its variability is large enough so that sampling errors are of the same order of magnitude as instrumental errors. The estimated sampling errors for snow cover depth, density, and water-equivalent are based on the variability between individual snow course points.

The data from the NOAA-ARS snow research station are in the process of being published. The publication, besides containing data listings, will include a more detailed description of the instruments and the evaluation of their accuracy.

There are a few very short periods during the six winters when one or more of the input variables is missing. During these periods the value of the missing input variable is estimated since the model requires continuous data. These estimated values have a negligible effect on model results.

Besides the information included in Table 5.1 some brief additional comments are needed in regard to several of the variables in order to better interpret the model results.

1. Incoming (atmospheric) longwave radiation (Q_a). This has been

Table 5.1.--Summary of data used for model testing. Collected at the NOAA-ARS snow research station from December 1968 through April 1974.

Variable	Sensor	Recorder	Accuracy-estimated standard error
A. Input Variables			
1. Air temperature	a. bimetallic strip thermograph (12/68-4/69); two meters above ground	drum chart	1°C
	b. platinum resistance element in ventilated radiation shield (11/69-4/74); one meter above snow surface	strip chart	0.5°C
2. Vapor pressure	a. human hair hygrograph (12/68-4/69); 2 meters above ground	drum chart (recorded as relative humidity)	less than 5% above 0°C, and greater than 10% below -20°C.
	b. lithium chloride dewcell in ventilated radiation shield (11/69-4/74); one meter above snow surface	strip chart (recorded as dew point)	
3. Wind speed	low threshold (0.3 $m \cdot sec^{-1}$) 3-cup anemometers.	Digital printout to nearest .045 $m \cdot sec^{-1}$ (0.1 miles $\cdot hr^{-1}$)	2% or 0.1 $m \cdot sec^{-1}$, whichever is greater. (this error may be exceeded below 0.5 $m \cdot sec^{-1}$)
	a. (12/68-4/69) 0.5 meters above snow surface (data adjusted to one meter for model testing.)		
	b. (11/69-4/74) 1.0 meter above snow surface		

Table 5.1, cont'd.

Variable	Sensor	Recorder	Accuracy-estimated standard error
4. Incident solar radiation	a. 50-jct., temperature compensated, black and white concentric ring, bulb pyranometer (12/68-5/70)	electronic volt-time integrator	3%
	b. Eppley Laboratories,[1] Model 2 temperature compensated precision pyranometer (6/70-4/74)	electronic volt-time integrator	2%
5. Reflected solar radiation	a. 50-jct., temperature compensated, black and white concentric ring, bulb pyranometer (12/68-2/73)	electronic volt-time integrator	3%
	b. Eppley Laboratories, Model 2 temperature compensated precision pyranometer (3/73-4/74)	electronic volt-time integrator	2%
6. Incoming (atmospheric) longwave radiation	a. ventilated Gier and Dunkle type total hemispherical radiometer (12/68-9/71, plus 4/72-2/73)	electronic volt-time integrator	10%
	b. pyrgeometer (hemispherical infrared radiometer) with a KRS-5 dome, (10/71-3/72, plus 3/73 and 4/73)	electronic volt-time integrator	6%

[1]Trade names and commercial products or enterprises are mentioned solely for informational purpose. No endorsement by NOAA or the ARS is implied.

Table 5.1, cont'd.

Variable	Sensor	Recorder	Accuracy-estimated standard error
7. Precipitation	shielded universal gage, 2 meters above ground	drum chart	mean catch deficiency for snow is about 15%. Based on comparison with nearby gages [Larson (1972)].
8. Soil temperature	thermocouples at various depths in soil (15 cm. depth is used)	strip chart (instantaneous value every 12 minutes)	0.2 °C
B. Verification Variables			
1. Snow cover water-equivalent	a. snow course consisting of six sampling points. Adirondack snow tube is used.	spring scale	8 mm or 3%, whichever is greater
	b. 3.7 meter diameter snow pillow flush with ground surface, (12/68-5/71)	fluid level recorder	12 mm or 4%, whichever is greater
		Accuracy of snow course and snow pillow measurements varies with snow cover conditions.	
2. Snow cover depth	snow courses and snow stakes	visual	1.5 cm
3. Snow cover density	snow courses with Adirondack snow tube. (water-equivalent/depth)		0.015 $gm \cdot cm^{-3}$
4. Snow surface density	500 cm^3 CRREL tubes inserted horizontally as near to the surface as possible.	beam balance	0.02 $gm \cdot cm^{-3}$

Table 5.1, cont'd.

Variable	Sensor	Recorder	Accuracy-estimated standard error
5. Snow cover temperature	thermocouples attached to wooden stake	strip chart (instantaneous value every 12 minutes	0.3°C
6. Snow surface temperature	Barnes Engineering, Model IT-3 infrared thermometer (4/70-4/74)	strip chart (4/70-4/73) electronic volt-time integrator (1/74-4/74)	1°C at 0°C, 2°C at -10°C, and >3°C below -20°C
7. Snow cover outflow	pair of 3.05-meter diameter lysimeters	tipping bucket recorded on digital counter	within 10% or 1 mm, whichever is larger, on a daily basis.

the most difficult of the input variables to measure accurately. The ventilated radiometers are affected by wind, especially if the wind is perpendicular to, or in the opposite direction of, the forced ventilation. In addition, ventilated radiometers record much too low during rain due to evaporation from the upper surface of the thermopile plate.

The pyrgeometer seems to give good results when its dome is in a like-new condition and the amount of shortwave radiation is low. However, when the dome oxidizes and when clear skies occur, the pyrgeometer seems to record too high. This is caused by shortwave radiation being absorbed by, and thus heating, the dome.

In addition to the measured values, Q_a was computed from air temperature, vapor pressure, and the ratio of incoming solar radiation to clear sky solar radiation by the method suggested by Anderson and Baker (1967). This method has been shown to give relatively unbiased estimates of Q_a on a long-term basis.

Comparisons were made between Q_a values obtained from the ventilated radiometer and the estimation procedure with those obtained from the pyrgeometer. This was done when the pyrgeometer was new and the magnitude of shortwave radiation was low. The standard errors for the ventilated radiometer and the estimation procedure were nearly identical.

Based on these factors it was decided to use the estimated Q_a values for testing the snow cover simulation model. The main reason is that the estimated values of Q_a are consistent over the 6-year period. A few runs were made (shown later) to determine the variations caused by using measured values of Q_a.

2. Snow cover outflow. The two 3.05-meter diameter lysimeters used to measure snow cover outflow were built in the fall of 1972. The snow cover outflow drains through a pipe in the center of each lysimeter and is measured by a specially constructed tipping bucket gage. A circular pipe containing a heat cord is used to melt a 1.5 centimeter wide slot around the lysimeter. This slot separates the snow above the lysimeter from the surrounding snow cover.

Mechanical problems hindered data acquisition during the first part of 1973. Beginning on March 8, reliable measurements were obtained for most of the remainder of the season. In 1974, a thick ice layer formed in mid-winter just above the snow-soil interface. Such an ice layer is

a very unusual occurrence. When snowmelt began in March, melt-water from over a large area moved horizontally across this ice layer, over a metal lip, and into the lysimeters. As much as 430 millimeters of water per day passed through the lysimeters in early April (maximum water-equivalent during 1974 was only about 200 mm). Thus, the 1974 lysimeter data are not used to evaluate the model.

3. Snow pillows. Prior to the construction of the lysimeters several snow pillows were used each winter. Comparisons were made between the daily change in water-equivalent as measured by different pillows. The standard error computed during these comparisons ranged from 30 to 50 percent of the average daily change in water-equivalent. These large variations were one reason for constructing the lysimeters.

Snow cover water-equivalent from a snow pillow is only available for the winters of 1969, 1970, and 1971. Mechanical problems resulted in no valid snow pillow data during 1972 and 1973. The thick ice layer at the snow-soil interface resulted in extreme fluctuations during 1974.

The snow pillow readings have never returned to zero after melt (readings started at zero in the fall). The exact cause of this problem is not known, but the discrepancy seems to occur during the melt season since snow pillow and snow course values of water-equivalent are reasonably close just prior to the snowmelt period.

Description of Snow Seasons

A few brief remarks are probably needed regarding the nature of the snow cover during each of the 6 years to assist in interpreting the model results.

The first 4 years were similar in that the snow cover began accumulating early and the melt season did not begin until April. During these years there were only a few periods of rain or melt during each accumulation season. For this reason the snow covers were generally uniform with only a few thin ice layers. The exception was a thick (about 7.5 centimeter) ice layer that formed during a severe ice storm in late December 1969. This ice layer made snow tube measurements difficult and snow pillow readings erratic until it broke up when melt began in April 1970.

The year 1972-73 was similar to the previous years except melt began in March.

The snow cover during 1973-74 was the smallest during the 6 years.

Frequent rain and melt periods throughout the winter resulted in a very dense snow cover with many ice layers. An ice layer which built up at the base of the snow cover caused several measurement problems as mentioned previously. Also, because the snow cover was relatively shallow, frost occurred in the upper 10 centimeters of the soil. This was the only year that frost occurred in the soil beneath the snow cover.

The greatest water-equivalent during the 6 years was 373 millimeters measured on April 2 and 3, 1969. The greatest depth was 141 centimeters observed on March 8, 1971.

PARAMETER VALUES USED IN MODEL TESTING

Many of the equations used to compute the energy and mass balance of a snow cover contain parameters and coefficients to which a specific value must be assigned. In some cases experimental results indicate reasonably well-defined limits for a parameter value. In other cases the limits are not as well defined, thus the parameter value must be determined by calibration.

Coefficients Controlling Heat Transfer Within the Snow Cover

The values of most of these coefficients have been reasonably well defined by experimenal results.

1. Coefficient of effective thermal conductivity (k_e). Eq. (4.24) is the expression used for k_e in the model. C_k is assigned a value of 0.006. This value gives a k_e versus density curve which is close to an average of the experimental determinations shown in Fig. 3-1. In addition, the upper limit compares very closely to the thermal conductivity of ice.

2. Effective diffusion coefficient for water vapor in snow (D_e). D_e is computed from Eq. (3.13). For the NOAA-ARS snow research station the mean station pressure of 950 mb is used for the atmospheric pressure (P_a). D_{eo} is assigned a value of 0.9 $cm^2 \cdot sec^{-1} \cdot mb \cdot K^{-n_d}$ and the exponent, n_d, is set equal to 14.0. These values are based on the experimental determinations of D_e versus temperature shown in Fig. 3.2.

3. Extinction coefficient (ν). Eq. (4.26) is used to determine the extinction coefficient. Since only density (ρ_s) is computed by the model, a relationship between grain size (d_s) and ρ_s is needed in order to use Eq. (4.26). The form of the empirical relationship which is used in the program is

$$d_s = G_1 + G_2 \cdot \rho_s^2 + G_3 \cdot \rho_s^4 \qquad (5.1)$$

where G_1, G_2, and G_3 are parameters which need to be determined for a particular location, d_s is in millimeters, and ρ_s is in $gm \cdot cm^{-3}$.

At the NOAA-ARS snow research station the size of aggregate particles was measured, but not the size of individual grains. Thus the parameters could not be determined directly from a plot of d_s versus ρ_s.

In addition to Eq. (3.17), Bohren and Barkstrom (1974) give an expression relating albedo under diffuse illumination to grain size. This expression is

$$A_s = 1.0 - 0.1885 \cdot (\nu_i \cdot d_s)^{\frac{1}{2}} \tag{5.2}$$

where: A_s = albedo of snow expressed as a decimal fraction, and
ν_i = the extinction coefficient for clear ice (mm^{-1}).

An expression for albedo under diffuse illumination as a function of grain size can be obtained by combining Eqs. (3.17), (4.26), and (5.2). The resulting expression is

$$A_s = 1.0 - 0.206 \cdot C_\nu \cdot d_s^{\frac{1}{2}}. \tag{5.3}$$

If the form of Eq. (5.3) is assumed to apply to a combination of direct and diffuse sunlight, Eqs. (5.1) and (5.3) can be used in conjunction with daily measurements of albedo and snow surface density to estimate the parameters C_ν, G_1, G_2, and G_3 for a given location. By trial and error, values of these parameters were determined for the NOAA-ARS snow research station which give reasonable estimates of d_s as a function of ρ_s, and albedo as a function of snow surface density. The values arrived at are $C_\nu = 1.2$, $G_1 = 0.16$ mm, $G_2 = 0.0$, and $G_3 = 110$ $mm \cdot gm^{-4} \cdot cm^{12}$. Fig. 5.2 shows the plot of albedo versus snow surface density. Measured albedo values above 0.9 are generally caused by snow capping the upright pyranometer. Thus all measured values above 0.9 are set equal to 0.9. Snow surface density, rather than total snow cover density, is used because only the properties of the surface layers have a significant effect on albedo. This is evident from the reported values of the extinction coefficient for snow and from the measurements of O'Neill and Gray (1973) which show that albedo is independent of snow depth provided the depth is greater than the thickness of the thin "active" surface layer.

With these values of the parameters, the extinction coefficient can be determined as a function of ρ_s by using Eqs. (4.26) and (5.1). This relationship is shown in Fig. 5.3 along with values of ν as a function

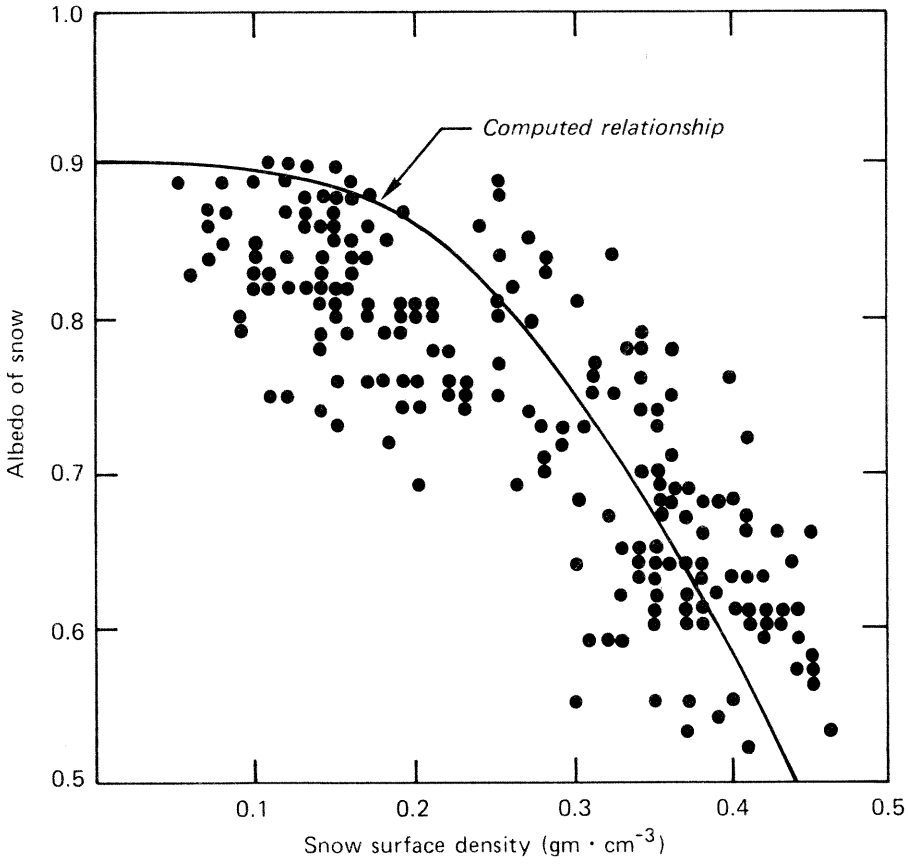

Figure 5.2.--Albedo versus snow surface density.

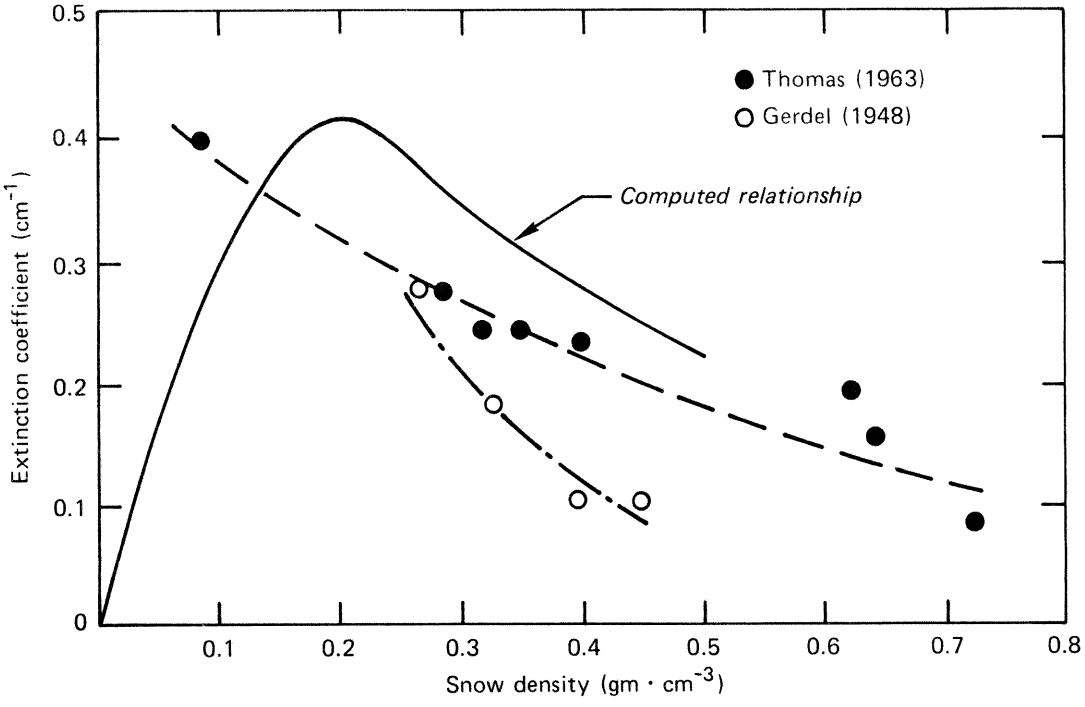

Figure 5.3.--Extinction coefficient versus snow density.

of ρ_s measured by Thomas (1963) and Gerdel (1948). The expression used in the model looks reasonable. As ρ_s goes to zero ν goes to zero as would be expected. For densities above 0.5 $gm \cdot cm^{-3}$ the computed extinction coefficient is probably too high. As density increases ν should approach the value for ice which is about 0.01 cm^{-1} [Weller (1969)].

Liquid-water Retention and Transmission Parameters

The fractional liquid-water-holding capacity (W_e) is computed from Eqs. (4.31) and (4.32). The minimum value of W_e ($W_{e_{min}}$) was determined by calibration and is 0.03. For low densities W_e undoubtedly exceeds this minimum value. However, since no significant rain, melt, or snow cover outflow occurred at low densities, the other parameters could not be determined by calibration. Thus, $W_{e_{max}}$ is arbitrarily set to 0.1 and ρ_e to 0.2 $gm \cdot cm^{-3}$. $W_{e_{min}}$ is used whenever the density of the snow exceeds ρ_e.

Eqs. (4.33), (4.34), and (4.35) are used to estimate snow cover outflow from excess liquid-water. The values of the parameters as determined from Central Sierra Snow Laboratory lysimeter data (CW_1 = 10.0, CW_2 = 1.0, CW_3 = 5.0, and CW_4 = 450.) are used.

Parameters Controlling Compaction and Settling

The change in snow density caused by compaction is computed from Eq. (4.28). The change in density due to settling is computed by Eq. (4.29). The parameters in these equations (C_1, C_2, C_3, C_4, and ρ_d) are based on experiments and calibration.

The 1970-71 accumulation season was used to calibrate the parameters. On the first run the compaction parameters were set equal to values suggested by Kojima (1967), i.e., C_1 = .026 $cm^{-1} \cdot hr^{-1}$ and C_2 = 21 $cm^3 \cdot gm^{-1}$. Settling was neglected on the first run. The results of this run indicated C_1 was too high. The results also showed that settling must be included in order to simulate the increase in snow surface density during periods with no precipitation.

Prior to any further runs, C_3 was set equal to 0.01 and ρ_d to 0.15 $gm \cdot cm^{-3}$ as suggested by experimental results reported by Gunn (1965). C_4 was set to 0.04 $°K^{-1}$. This value is based on the plot of the increase in grain diameter with time for different temperatures given by Yosida (1955). The assumption is made that temperature affects density changes to the same degree as it affects grain diameter changes. These values

gave satisfactory results on subsequent runs and thus were adopted for use during the other years.

Two runs were needed to reach a satisfactory value for the compaction parameter C_1. The value of C_1 is 0.01 $cm^{-1} \cdot hr^{-1}$.

The effect of the parameter C_5, which increases the settling rate when liquid-water is present, could not be isolated during calibration. A value of 2.0 is arbitrarily used.

Wind Function, $f(U_a)$

Both an empirical wind function and a theoretically based wind function with adjustments for stability are used.

1. Empirical wind function. Eq. (2.54) is used to determine a value for $f(U_a)$ based on simultaneous observations of the amount of vapor transfer, wind, and the vapor pressure gradient. At the NOAA-ARS snow research station the vapor transfer is measured by inserting a plastic pan filled with snow into the snow cover so that the top of the pan is flush with the surrounding snow. The amount of vapor transfer is determined by carefully weighing the pan before and after exposure on a beam balance. Pans with surface areas of 210, 730, and 1240 square centimeters have been used. There is no indication that the pan area affects the amount of vapor transfer. Fig. 5-4 contains a plot of the amount of vapor transfer per millibar of vapor pressure gradient versus wind speed. The different symbols indicate the bulk Richardson number $(Ri)_B$ computed for each period of exposure by Eq. (2.50). The data shown in Fig. (5.4) give a wind function of

$$f(U_a) = 0.0031 \cdot U_a \tag{5.4}$$

where U_a is wind travel in kilometers and the units of the constant are $mm \cdot mb^{-1} \cdot km^{-1}$.

The value of $(Ri)_B$ for most of the periods shown in Fig. 5-4 is between 0.0 and 0.05. The value of $(Ri)_B$ during most of the hours when net turbulent heat transfer causes significant snowmelt at the NOAA-ARS snow research station is between 0.05 and 0.1. This suggests that a constant less than 0.0031 would give better simulation results due to the decrease in the bulk transfer coefficient as $(Ri)_B$ increases under stable conditions as shown in Fig. 2.1.

2. Theoretically based wind function. Eq. (2.57) is used to compute the theoretically based wind function. The bulk transfer coefficient

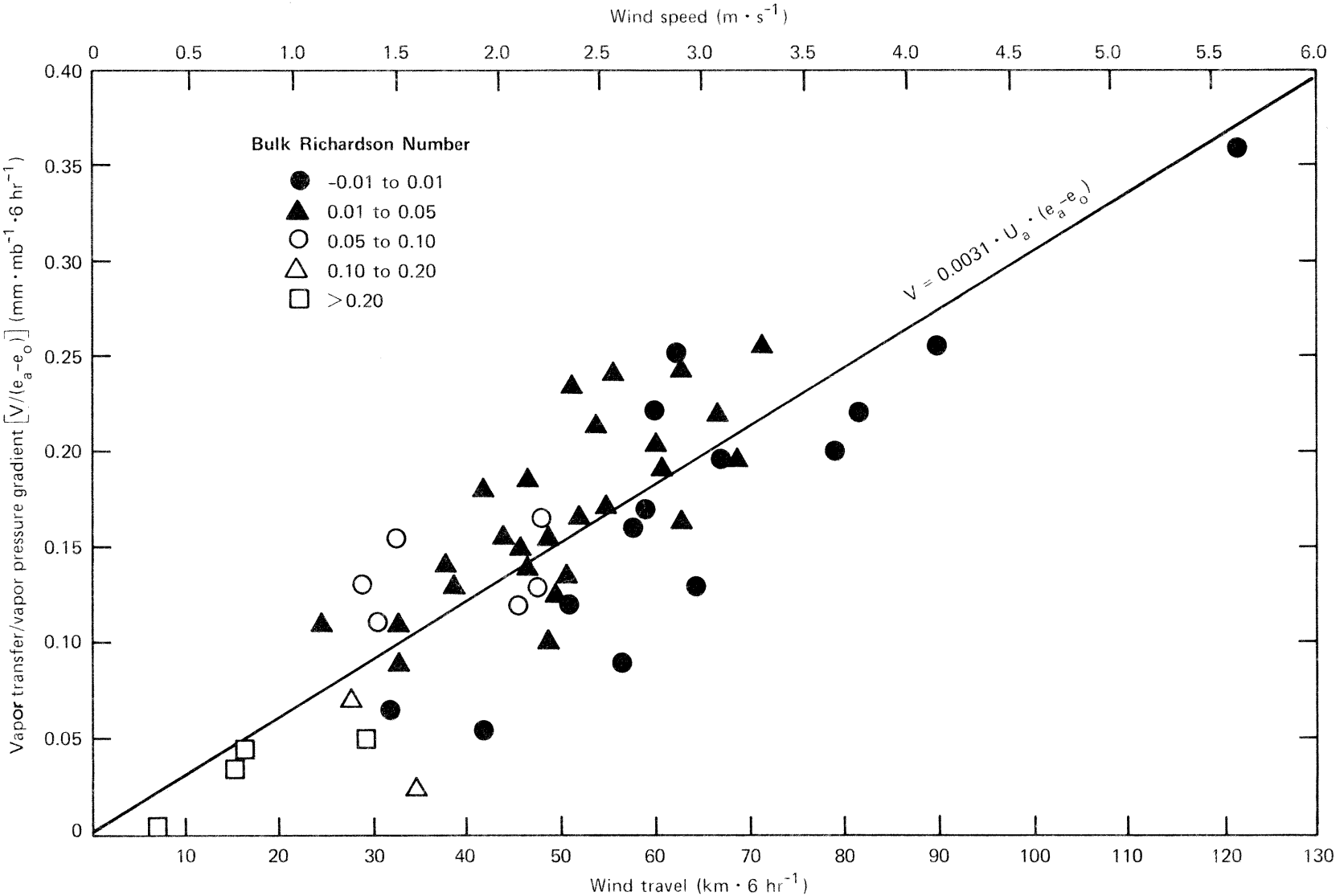

Figure 5.4.--Empirical wind function for the NOAA-ARS snow research station.

varies with stability as shown in Fig. 2-1. In order to apply Eq. (2.57) the bulk transfer coefficient under neutral conditions $(C_W)_N$ must first be determined. In the program $(C_W)_N$ is computed from Eq. (2.46) and is thus based on z_o, the roughness height. The measurement height (z_a) at the NOAA-ARS snow research station is one meter.

No real wind profile measurements have been made at the NOAA-ARS snow research station in order to determine z_o. However, measurements of wind were made at two levels (0.5 and one meter) during the 1970-71 snow season. Table 5-2 gives the ratio of wind speed measured at one meter to that at 0.5 meters, plus the corresponding computed value of z_o for periods when precipitation is not occurring and $(Ri)_B$ is between -0.01 and 0.01. These data suggest that z_o is variable and tends to decrease as the snowmelt season approaches. During the December 1970 period the station log indicates that there was extensive drifting and rippling of the snow surface. This is a very unusual condition.

The literature also gives different values of z_o for snow. Sverdrup (1936) computed z_o = 0.23 cm for a melting snow surface on West Spitsbergen Island. Liljequist (1957) measured z_o values of 0.01 to 0.1 cm over an Antarctic snow-field. Kuzmin (1961) suggests using z_o = .05 cm for stable snow covers which are deeper than 10-20 cm.

In addition to the bulk transfer coefficient under neutral conditions, the value of the critical Richardson number (Ri_{cr}) is very important for snow. Ri_{cr} (α^{-1}) is the only parameter involved in the stability correction under stable conditions Eq. (2.53).

In computing the bulk transfer coefficient for use in determining $f(U_a)$ two combinations of parameters are used. In one case z_o is set to 0.15 cm and Ri_{cr} is determined by calibration. In the other case Ri_{cr} is set to 0.2 and z_o is determined by calibration.

Miscellaneous Parameters

It is not the purpose of this study to determine the best method of simulating the accumulation of snow from precipitation measurements. However, in order to study energy exchange during periods of melt the computed snow cover water-equivalent needs to be reasonably close to the observed value just prior to snowmelt. Also,in order to properly verify the equations which estimate heat transfer and density changes within the snow cover, computed and observed water-equivalent should be in

Table 5-2.--Ratio of one-meter to 0.5-meter[1] wind speed and the corresponding roughness height (z_o) under neutral conditions.

Period	average wind speed at one meter ($m \cdot sec^{-1}$)	$\frac{u_{1.0}}{u_{0.5}}$	z_o (cm)
12/27/70 to 12/30/70	3.27	1.27	3.8
1/3/71 and 1/6/71	2.45	1.18	1.1
2/14/71 to 2/15/71	2.87	1.16	.66
3/24/71 to 3/25/71	3.96	1.15	.50
4/8/71	3.39	1.13	.24
4/14/71 to 4/15/71	3.67	1.10	.05
4/18/71	4.61	1.08	.01
4/22/71 to 4/23/71	2.26	1.10	.05
4/25/71	2.81	1.12	.16

[1]The anemometers may not have been exactly at these levels due to changes in snow cover depth after they were positioned.

Table 5-3.--Snow correction factors used for the model tests.

Year	Snow correction factor (SCF)	
	Accumulation season	Melt season
1968-69	.76	0.95
1969-70	1.03	0.95
1970-71	.92	0.95
1971-72	.90	1.50
1972-73	.75	0.95
1973-74	.97	0.95

reasonably close agreement. As mentioned previously, snow tends to blow off the site area during a windy period following a snowfall. This fact, along with the fact that the precipitation gage catch deficiency for snow varies with wind, causes the snow correction factor (SCF) to vary from storm to storm. SCF is the factor which relates the increase in the water-equivalent of the snow cover to the catch in the precipitation gage. The program uses a mean snow correction factor. For an accumulation season a value of SCF is selected so that the computed and observed water-equivalent at the end of the season are nearly the same. During a melt season a value of SCF is selected so that the increase in computed and observed water-equivalent is nearly the same when significant snowfalls occur. Table 5-3 gives the value of SCF used for each year.

The coefficient of thermal conductivity for soil is assigned a value of 0.001 $cal \cdot cm^{-1} \cdot sec^{-1} \cdot °K^{-1}$. The diffusion coefficient for water vapor in the soil is set to 0.2 $cm^2 \cdot sec^{-1}$.

The desired thickness of each snow layer is computed from Eq. (4.27) with D_z = 2.5 centimeters and C_d = 0.05. The largest number of computed layers occurring during the 6 years is 42 layers.

ACCUMULATION SEASON SIMULATION RESULTS

As mentioned previously the 1970-71 accumulation season was used to calibrate the compaction and settling parameters. The parameters obtained from this calibration are used for the other 5 years. Figs. 5.5 through 5.10 are plots of computed versus observed water-equivalent, snow cover density, and snow surface density for each accumulation season. The density plots are most important in terms of assessing the validity of the equations used to compute density changes due to compaction and settling. An empirical wind function with the constant $\underline{b}$ equal to 0.002 $mm \cdot mb^{-1} \cdot km^{-1}$ is used during the accumulation seasons. The computational time interval is 3 hours. The computed values in these figures are for snow cover conditions at 2400 hours. The snow courses are generally taken in mid-morning. Thus at times the plots appear 1 day out of phase because the computed values are affected by snow which fell after the snow course was taken.

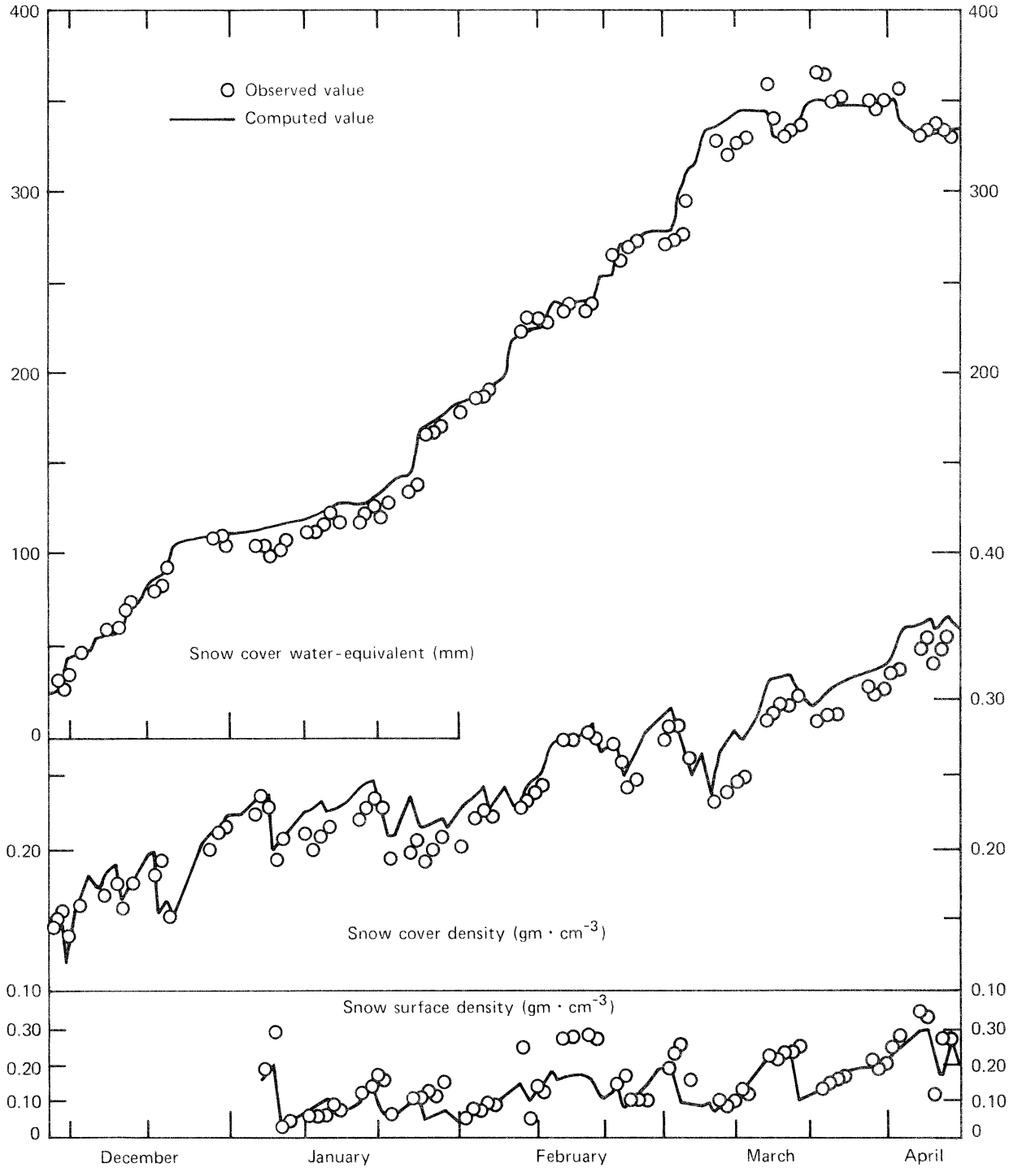

Figure 5.5.--Snow cover density and water-equivalent comparisons during the 1970-71 accumulation season.

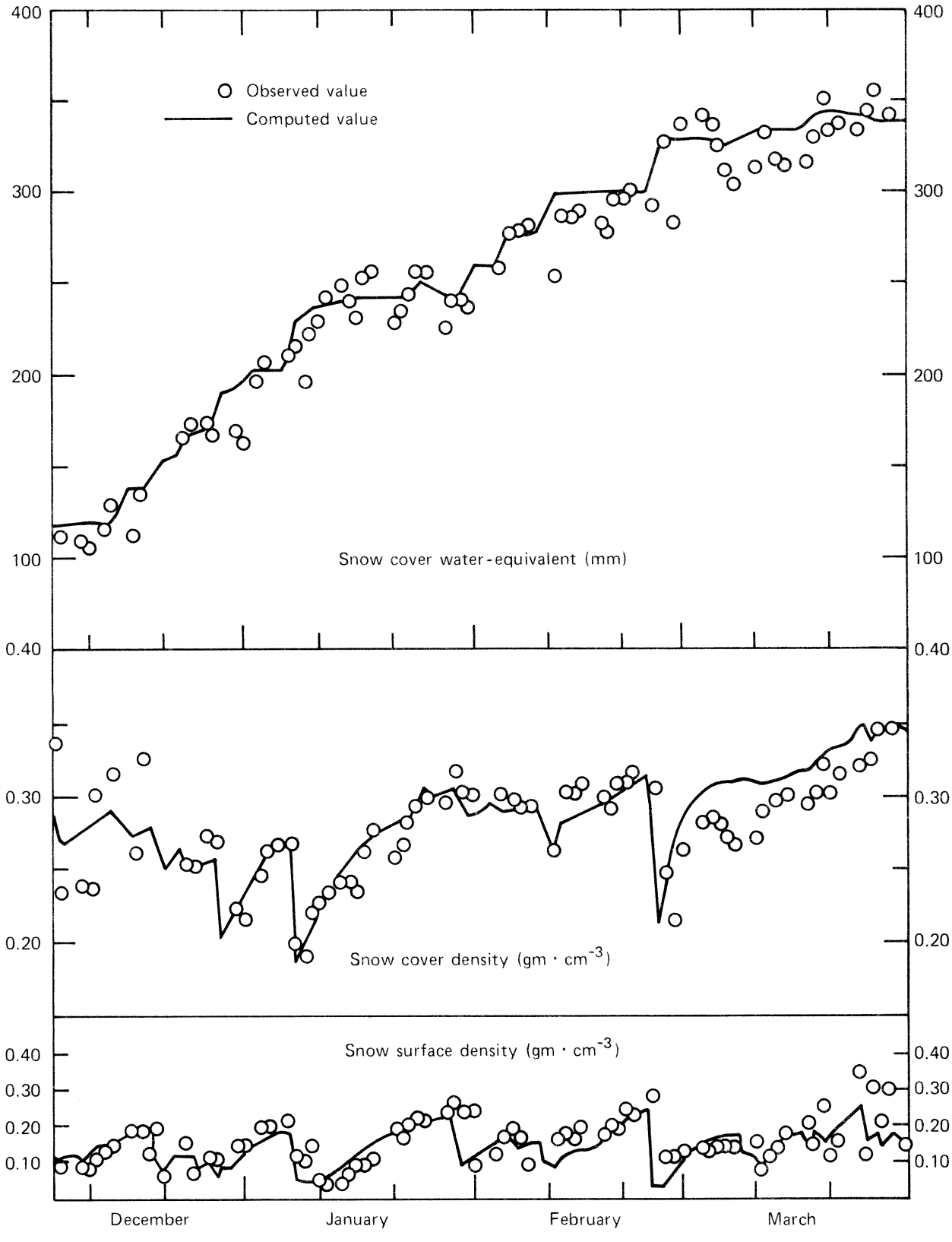

Figure 5.6.--Snow cover density and water-equivalent comparisons for the 1968-69 accumulation season.

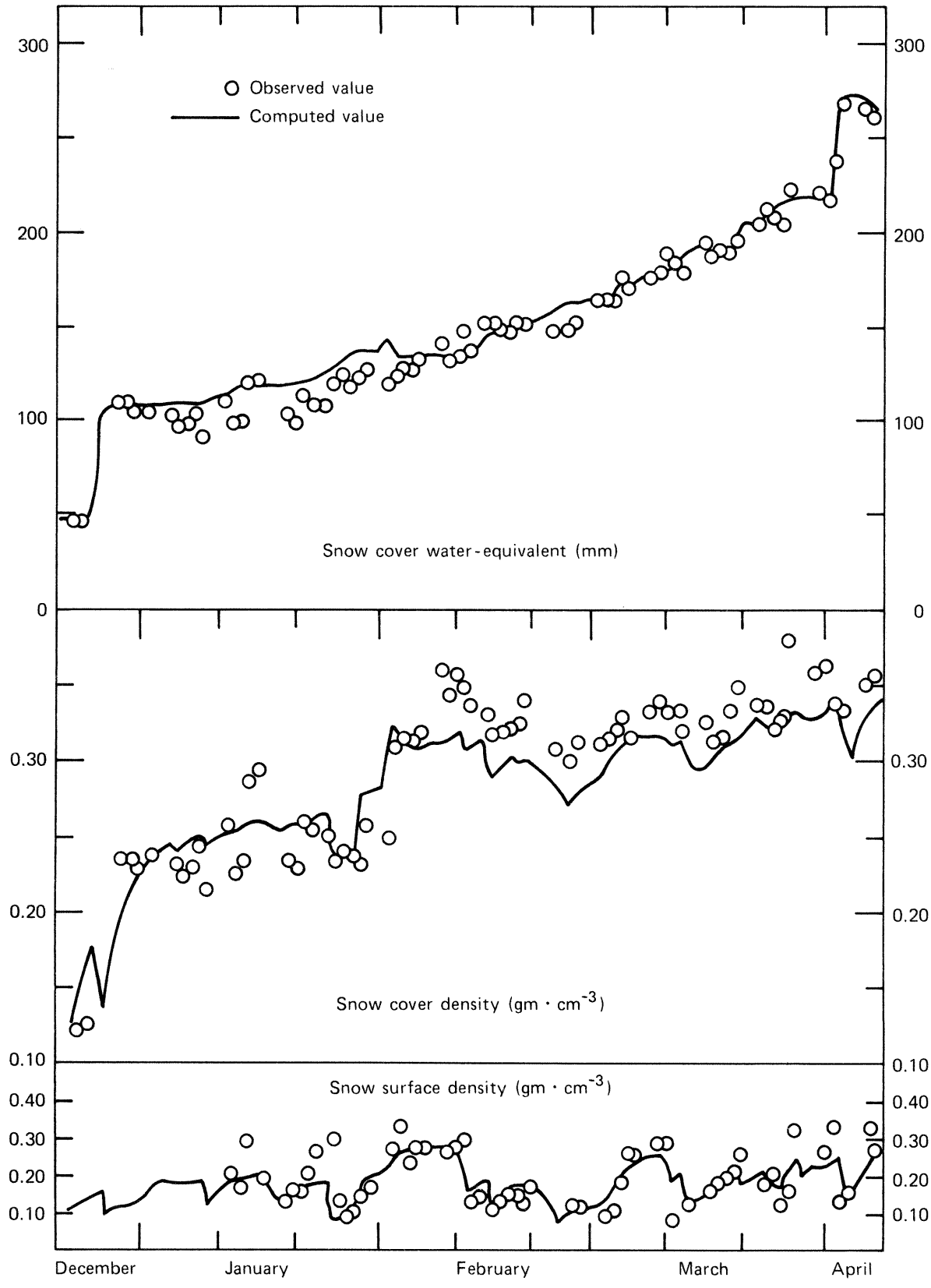

Figure 5.7.--Snow cover density and water-equivalent comparisons for the 1969-70 accumulation season.

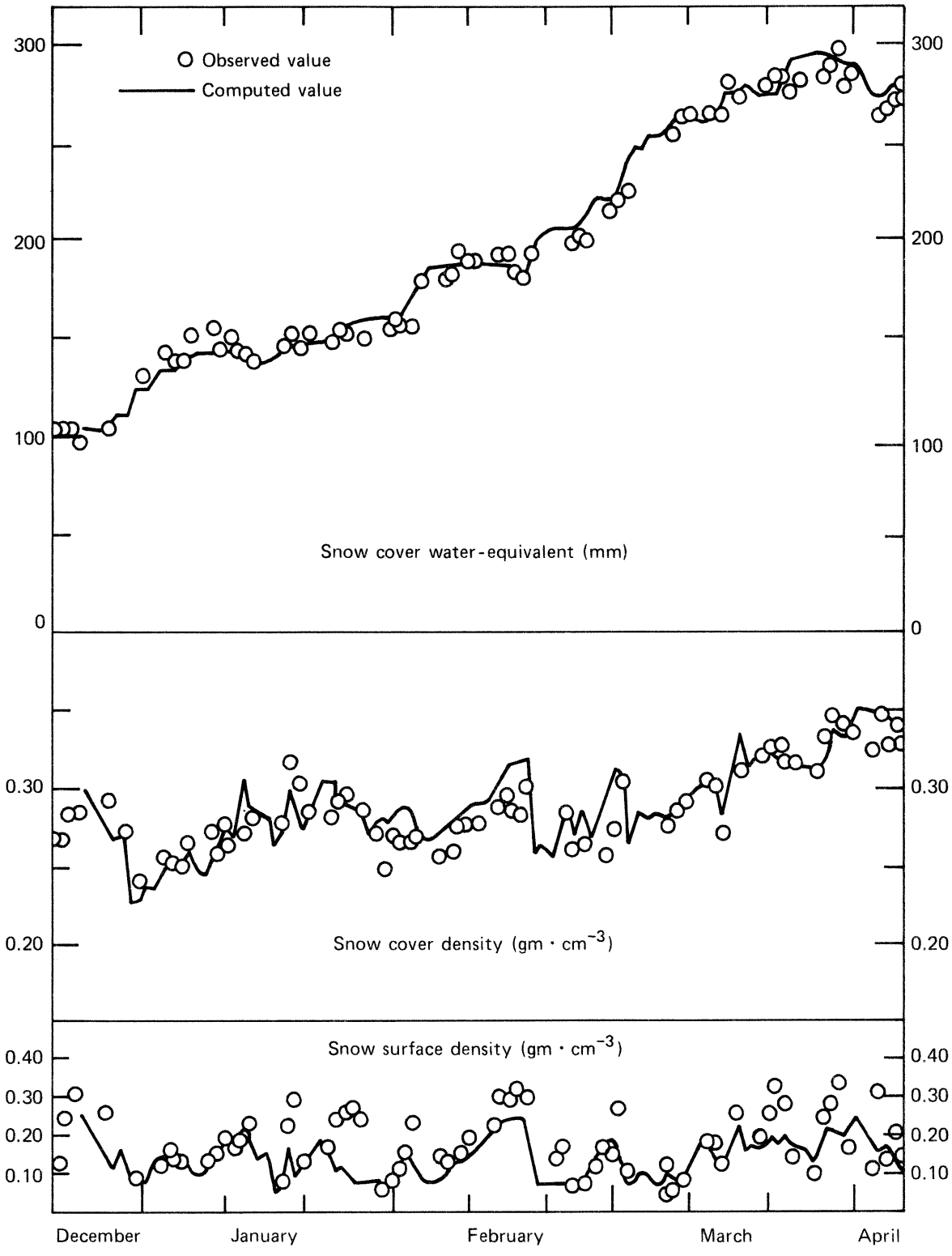

Figure 5.8.--Snow cover density and water-equivalent comparisons for the 1971-72 accumulation season.

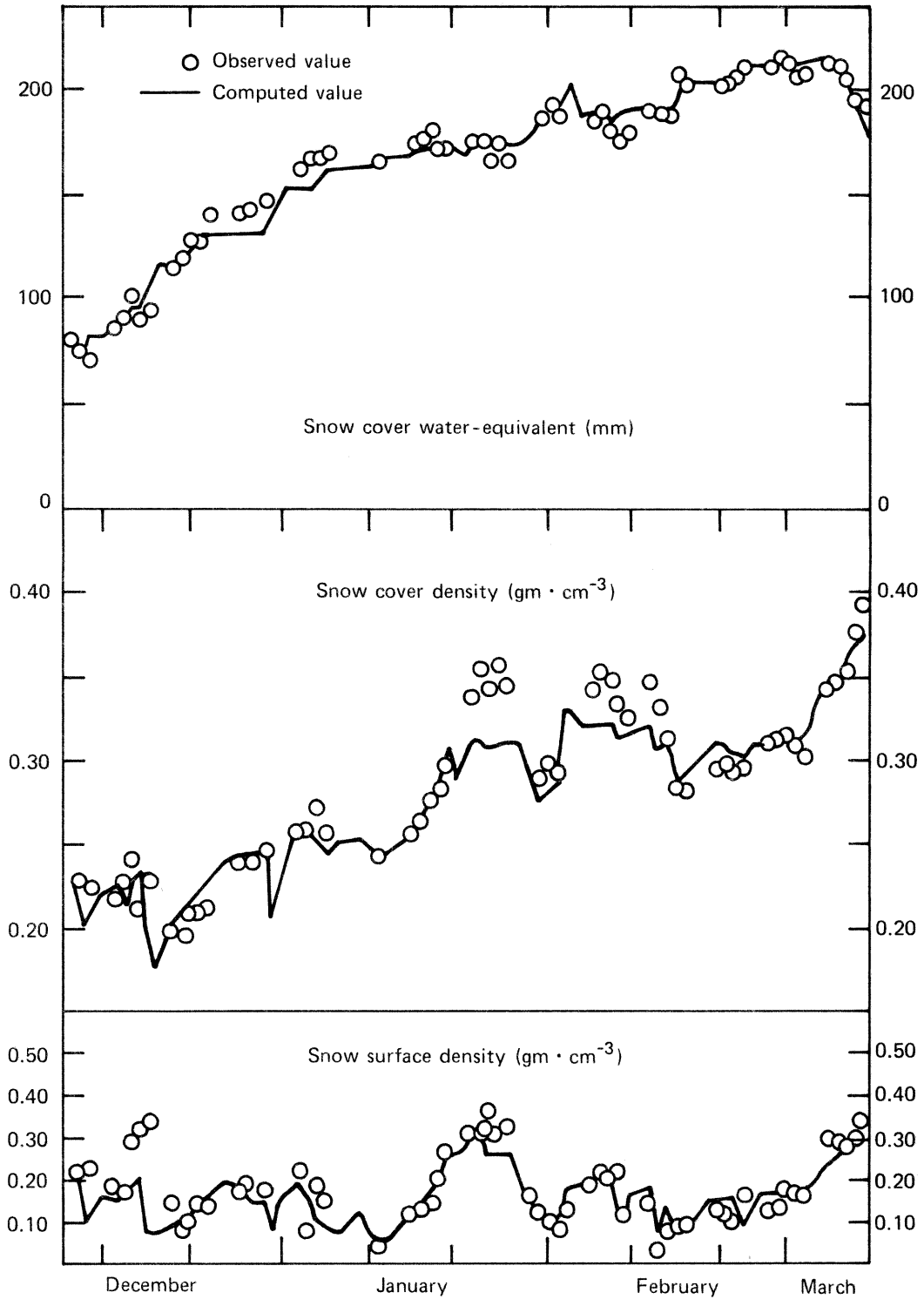

Figure 5.9.--Snow cover density and water-equivalent comparisons for the 1972-73 accumulation season.

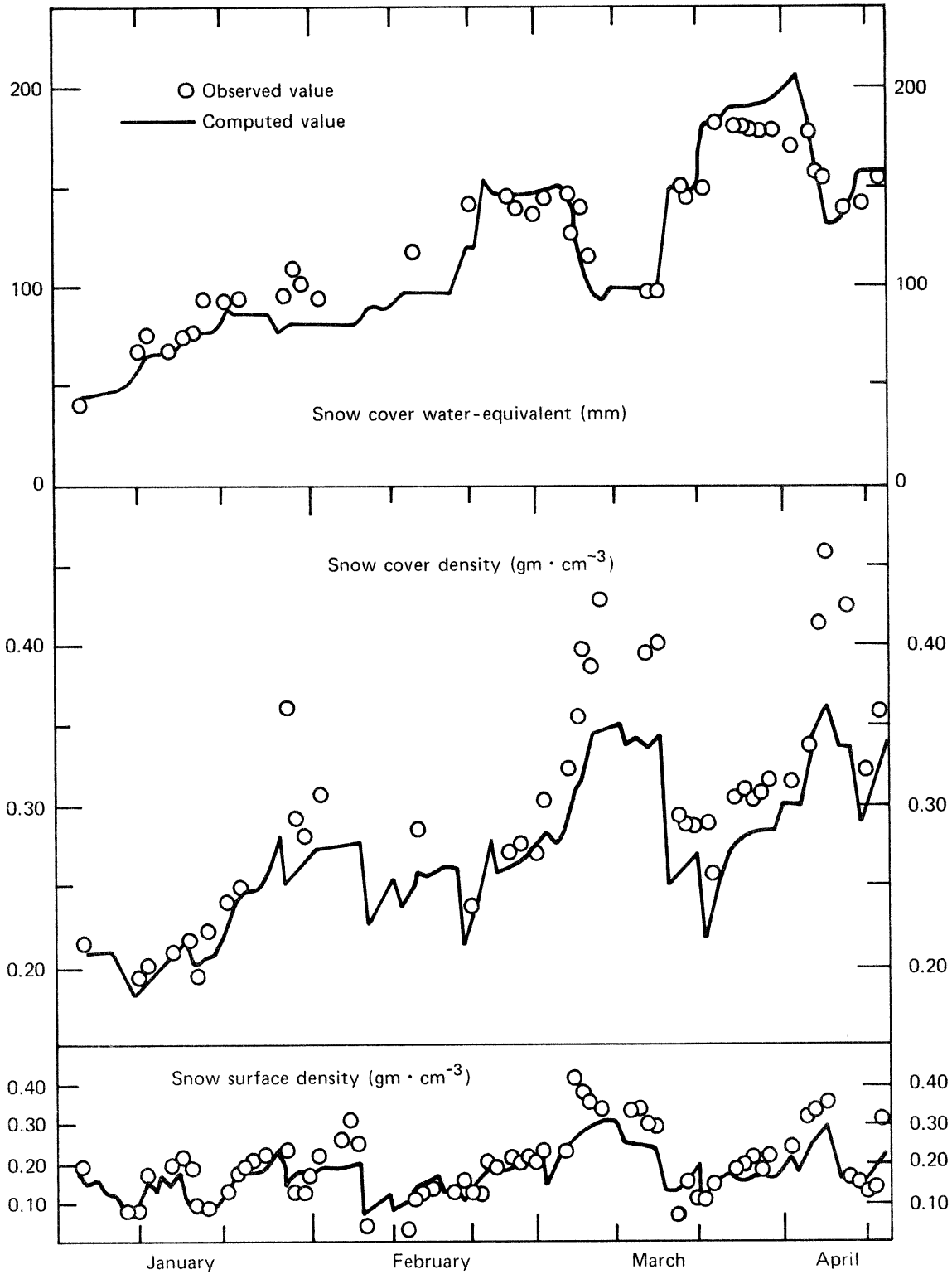

Figure 5.10.--Snow cover density and water-equivalent comparisons for the 1973-74 accumulation season.

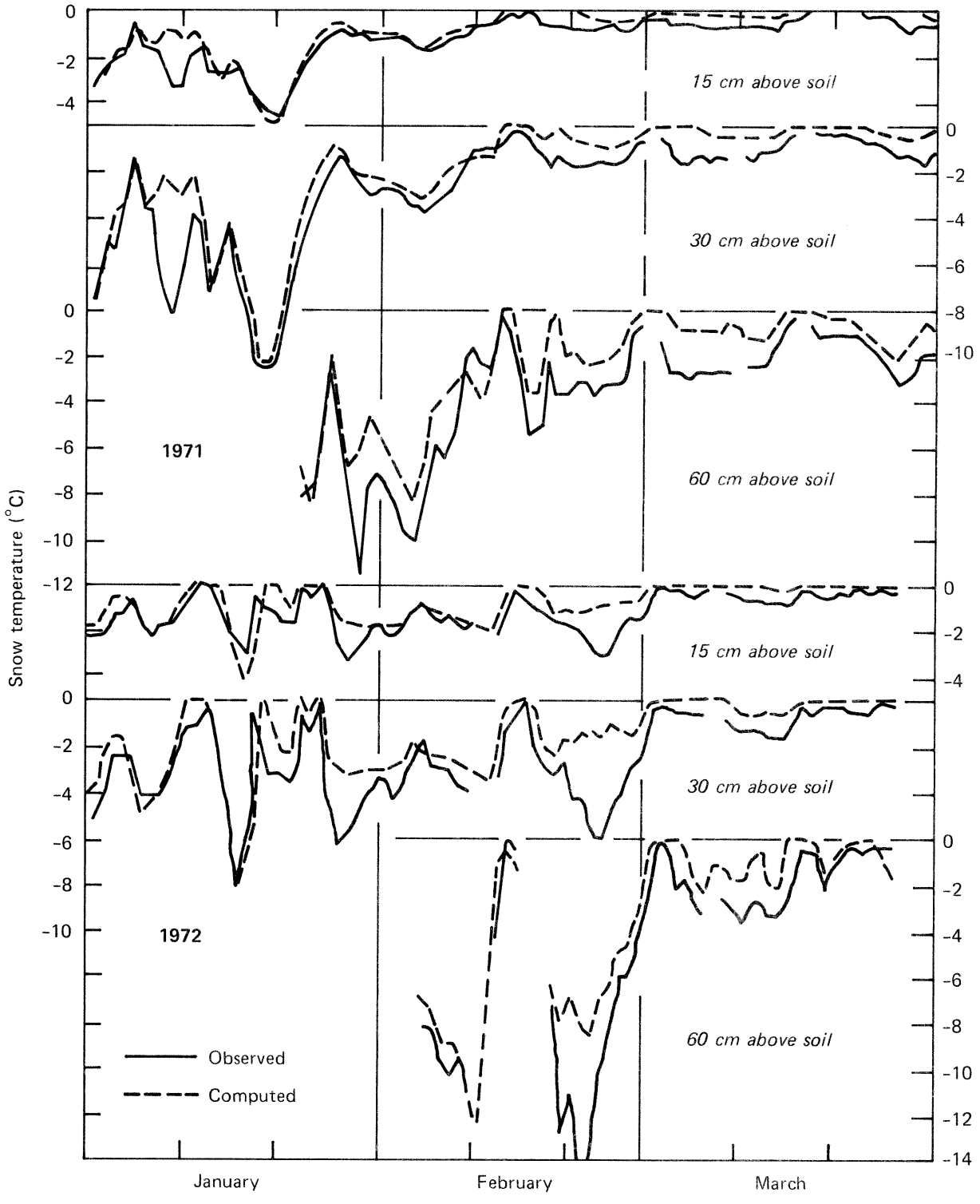

Figure 5.11.--Snow cover temperature comparisons for the 1971 and 1972 accumulation seasons. [Observed values are instantaneous temperatures at midnight.]

The density of new snow is not only a function of the wet-bulb temperature as indicated by Eq. (4.22). Other meteorological variables influence the density of new snow. The wind speed during the snowfall period is especially important. Because of these factors it was necessary to change the new snow density as computed by Eq. (4.22) for about 3 to 5 storms per season. These changes are made because the validity of the compaction and settling equations are being tested and not the validity of Eq. (4.22). Changes are made only when the computed and observed density of the new snow layers is significantly different. These changes do not alter the computed snow cover density beyond about 5 days.

Fig. 5.11 contains plots of computed versus observed temperature at several points within the snow cover during 1970-71 and 1971-72. Temperature within the snow cover was measured only at 15, 30, and 60 centimeters above the snow-soil interface. These heights above the soil are not precise since the thermocouple probe protruded several centimeters beyond the wooden support stake. As the snow cover settled, the thermocouple also had a tendency to be displaced downwards. Thus some of the discrepancy is due to an uncertainty as to the exact position of the thermocouple.

MELT SEASON RESULTS

The melt season simulation runs begin several days prior to the onset of significant melt. The observed and simulated water-equivalent are the same at the beginning of the run. A computational time interval of 1 hour is used during the melt season.

Figs. 5.12, 5.13, and 5.14 are plots of computed versus observed water-equivalent for each of the 6 years using an empirical wind function in the computation of sensible and latent heat transfer. Two computed water-equivalent values are shown. One is computed using $f(U_a) = 0.0031 \cdot U_a$ as determined from the vapor transfer measurements [Fig. 5.4]. The other is computed using $f(U_a) = 0.002 \cdot U_a$. The use of a constant of 0.002 $mm \cdot mb^{-1} \cdot km^{-1}$ was judged to give the best results that could be obtained with an empirical wind function.

Figs. 5.15, 5.16, and 5.17 are plots of computed versus observed water-equivalent using a theoretically based wind function. Again two computed water-equivalent values are shown. One is computed using a roughness

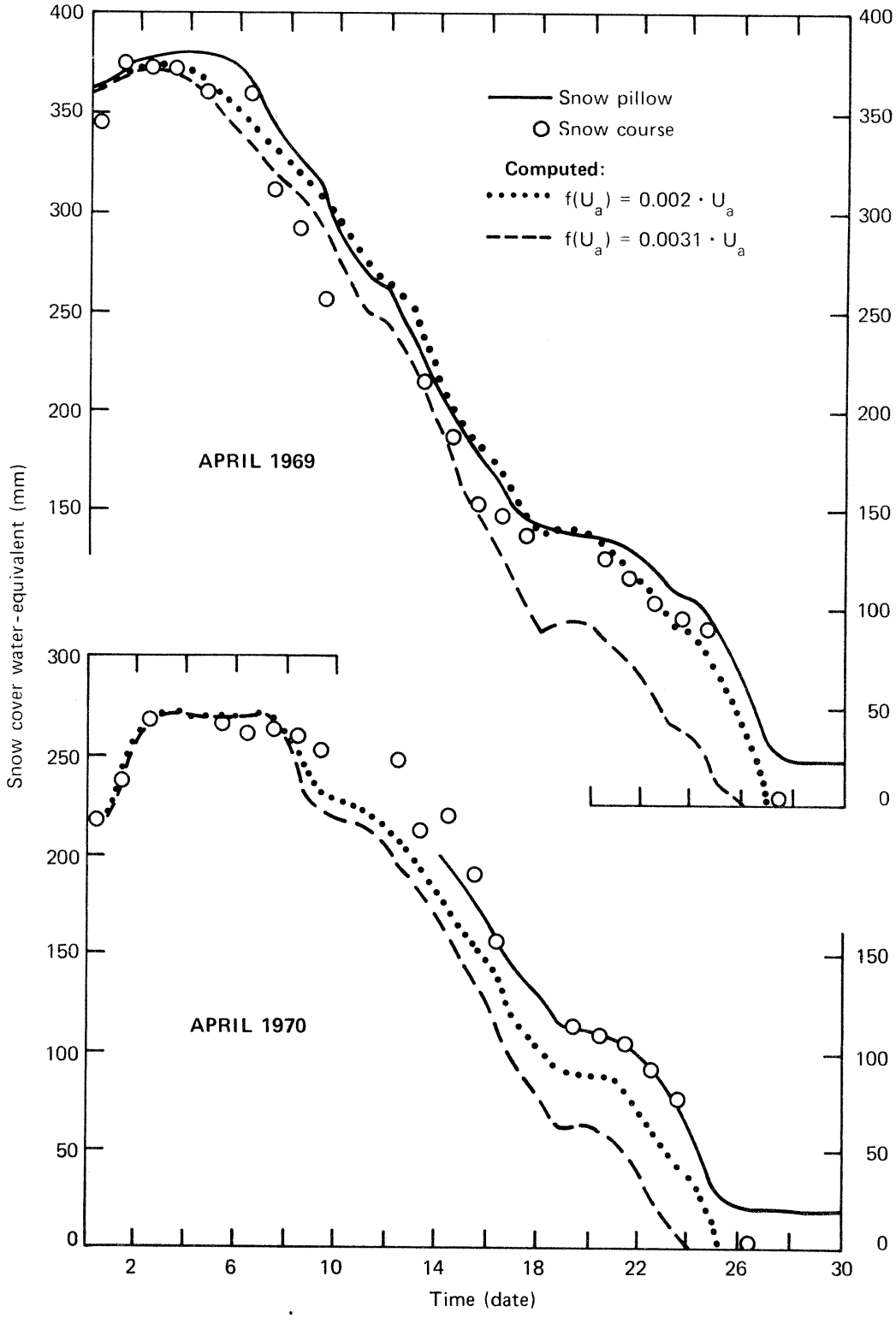

Figure 5.12.--Snow cover water-equivalent comparisons 1969 and 1970. Empirical wind function used to compute sensible and latent heat transfer.

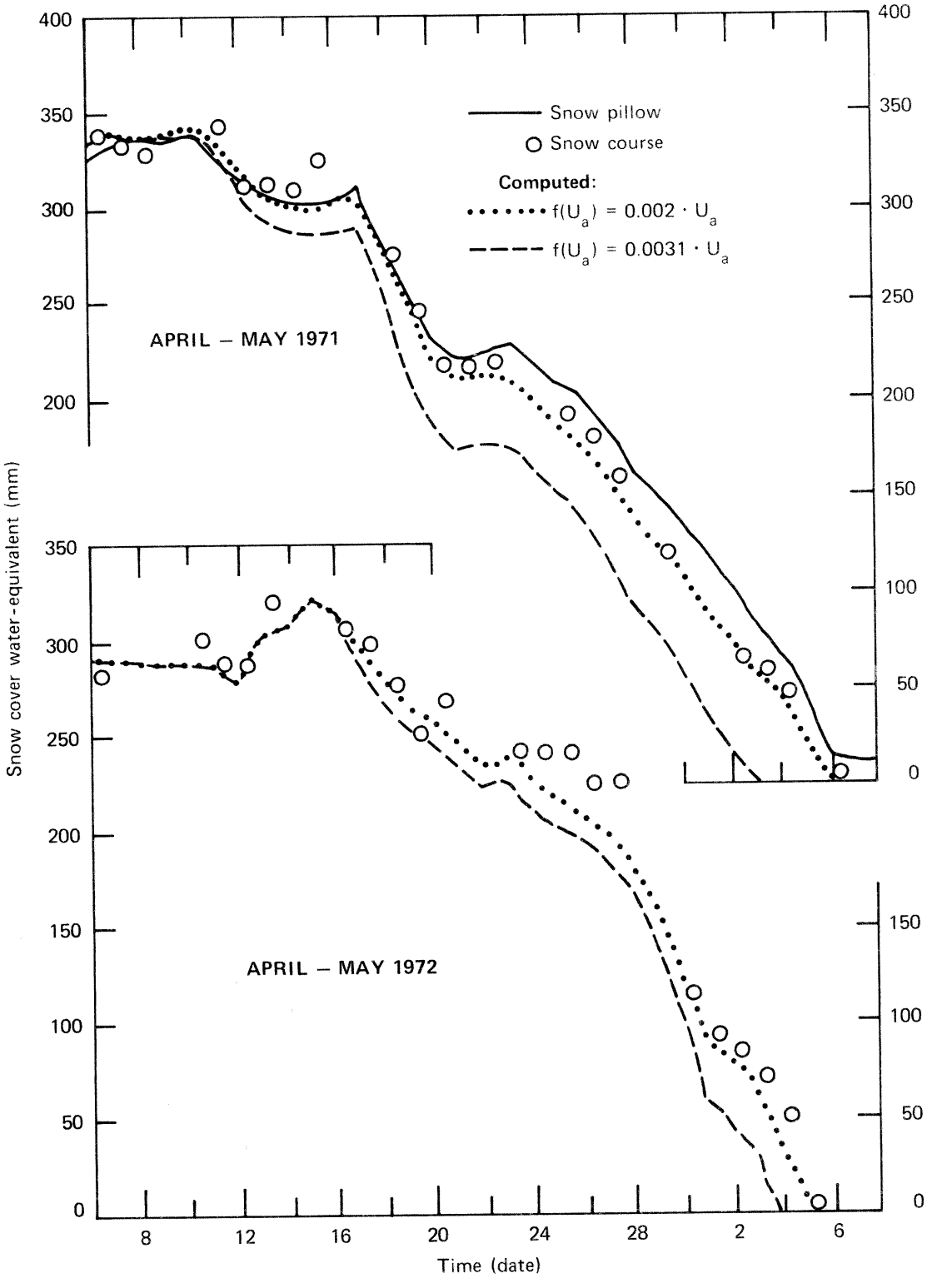

Figure 5.13.--Snow cover water-equivalent comparisons 1971 and 1972. Empirical wind function used to compute sensible and latent heat transfer.

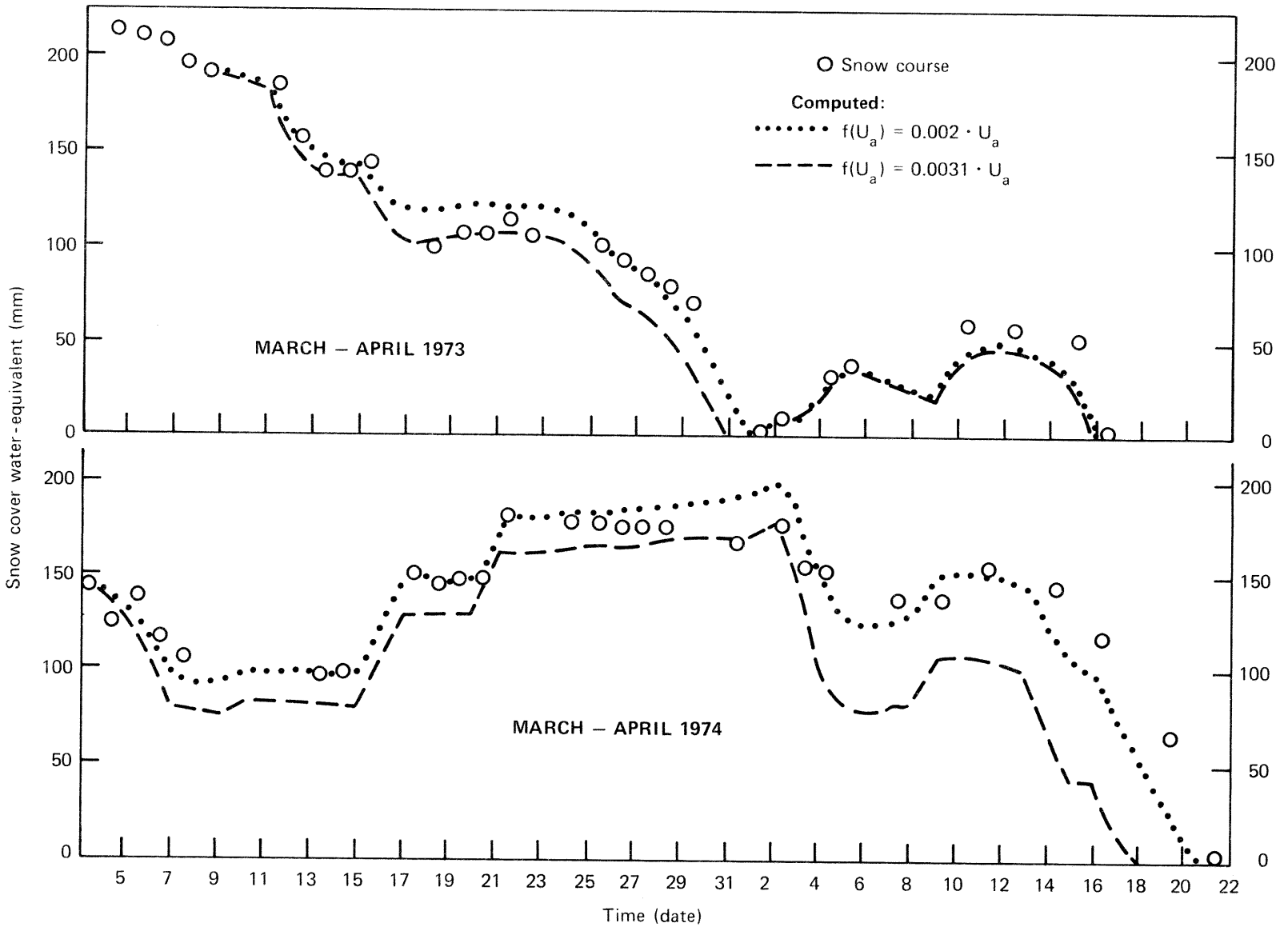

Figure 5.14.--Snow cover water-equivalent comparisons 1973 and 1974. Empirical wind function used to compute sensible and latent heat transfer.

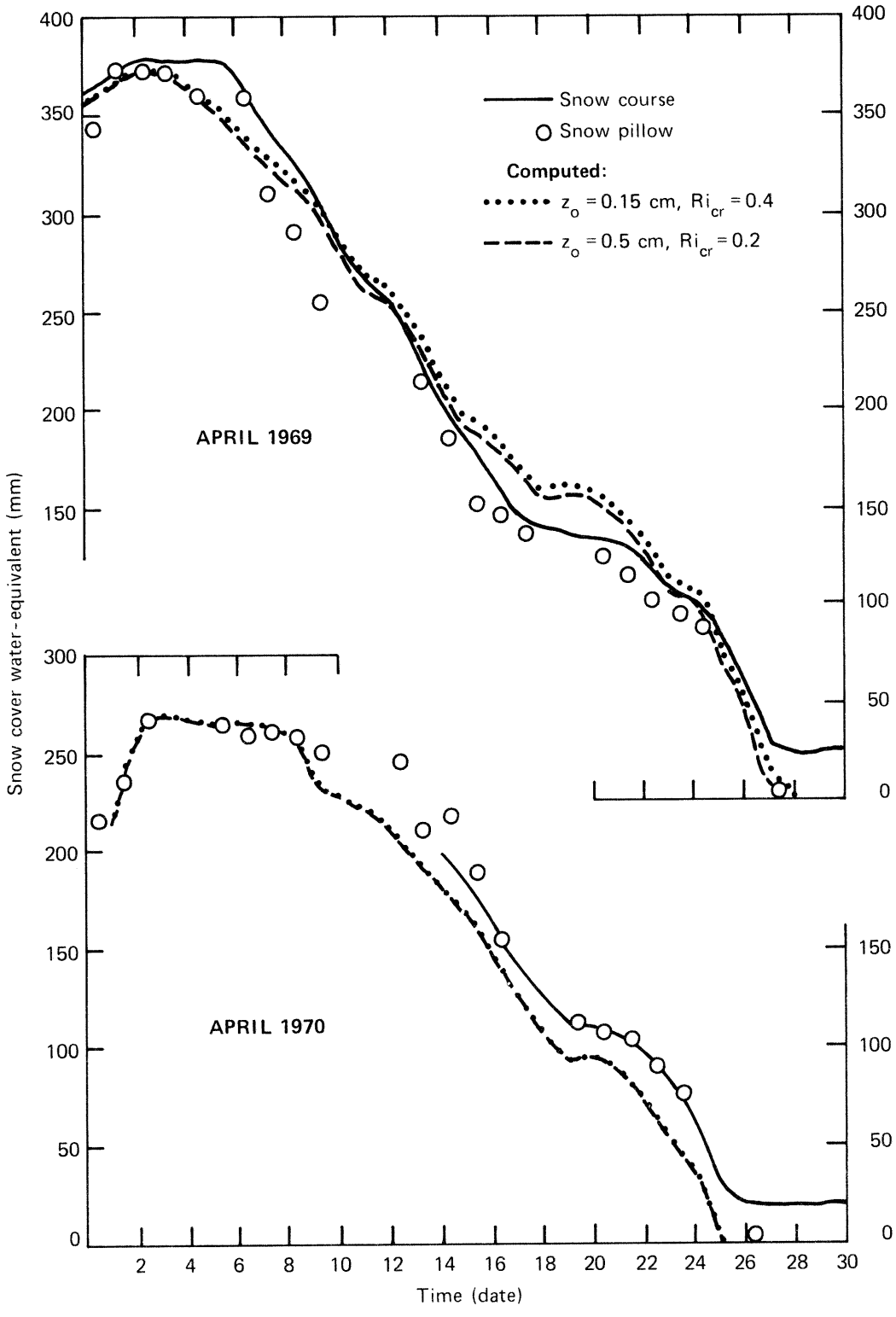

Figure 5.15.--Snow cover water-equivalent comparisons 1969 and 1970. Theoretically based wind function used to compute sensible and latent heat transfer.

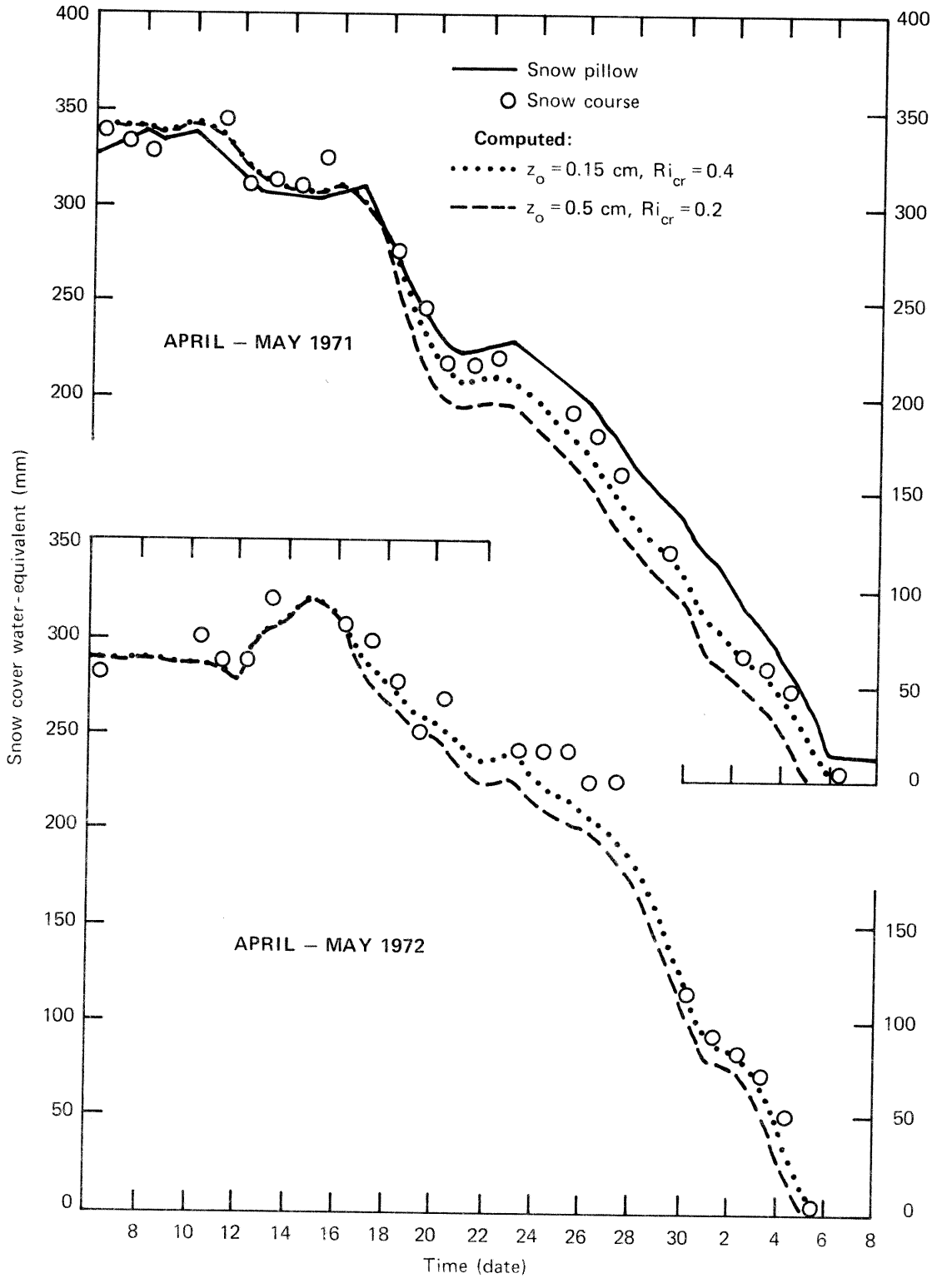

Figure 5.16.--Snow cover water-equivalent comparisons 1971 and 1972. Theoretically based wind function used to compute sensible and latent heat transfer.

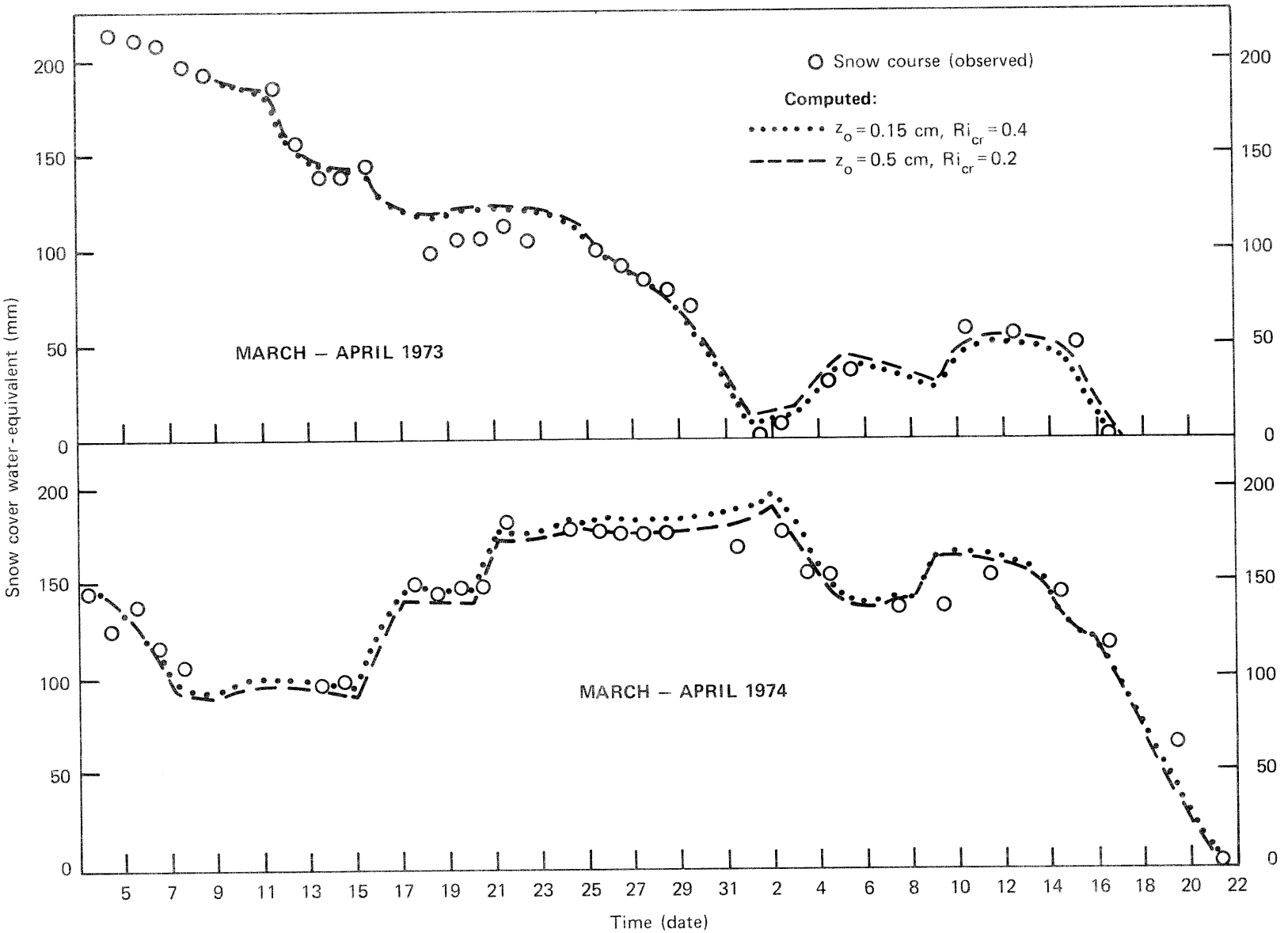

Figure 5.17.--Snow cover water-equivalent comparisons 1973 and 1974. Theoretically based wind function used to compute sensible and latent heat transfer.

height (z_o) of 0.15 cm to calculate the bulk transfer coefficient under neutral conditions and a critical Richardson number (Ri_{cr}) of 0.4 to calculate the stability adjustment under stable conditions. The other computed water-equivalent values are based on z_o = 0.5 cm and Ri_{cr} = 0.2. Values of z_o between 0.15 cm and 0.5 cm, when combined with an appropriate value of Ri_{cr} in the range 0.2 to 0.4, would result in computed water-equivalents somewhere between the two values plotted in these figures.

Fig. 5.18 is a plot of computed daily snow cover outflow versus the amount measured by the lysimeters during 1973. A theoretically based wind function with z_o = 0.15 cm and Ri_{cr} = 0.4 is used in the computations. Unfortunately this is the only year for which lysimeter data are available. Fig. 5.18 also shows plots of hourly computed and observed snow cover outflow for three days when a large amount of outflow occurred. A statistical comparison of computed and observed hourly snow cover outflow yields

1. a root-mean-square (RMS) error (square root of the mean of the sum of the squares of the observed minus computed values) of 0.37 mm,
2. a bias of -6% (observed mean is 0.37 mm),
3. an average absolute error of 0.16 mm, and
4. a correlation coefficient of 0.89.

In all of the previous plots, estimated incoming longwave radiation (Q_a) data are used in the computations. Fig. 5.19 shows the effect on computed water-equivalent of using measured Q_a values. During 1971 and 1972 Q_a was measured with a ventilated total hemispherical radiometer. In 1973 a pyrgeometer with a KRS-5 dome was used. This figure shows the effect of wind and rain on the ventilated radiometer, as well as the tendency of the pyrgeometer to overestimate Q_a, especially during clear sky periods.

SNOW SURFACE TEMPERATURE COMPARISONS

The snow surface temperature (T_o) is an important variable in energy exchange computations. T_o affects sensible and latent heat transfer by its role in determining the size and direction of the air temperature and vapor pressure gradients. The amount of longwave radiation emitted by the snow is solely a function of T_o. In addition, heat transfer

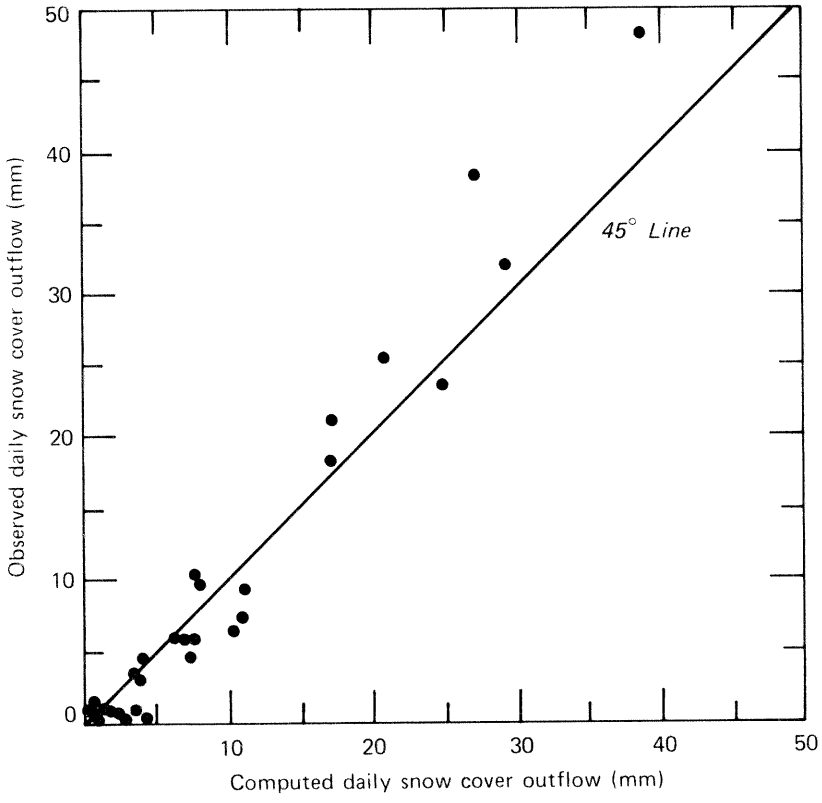

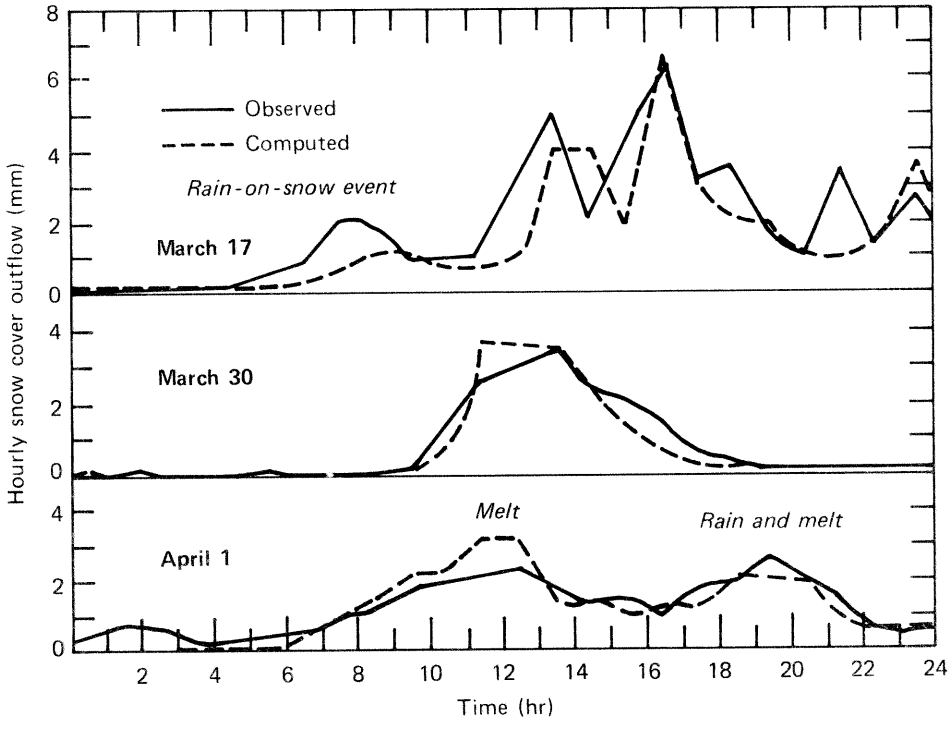

Figure 5.18.--Comparison of computed and observed snow cover outflow during March and April 1973. [Computed using a theoretically based wind function with z_o = 0.15 cm and Ri_{cr} = 0.4.]

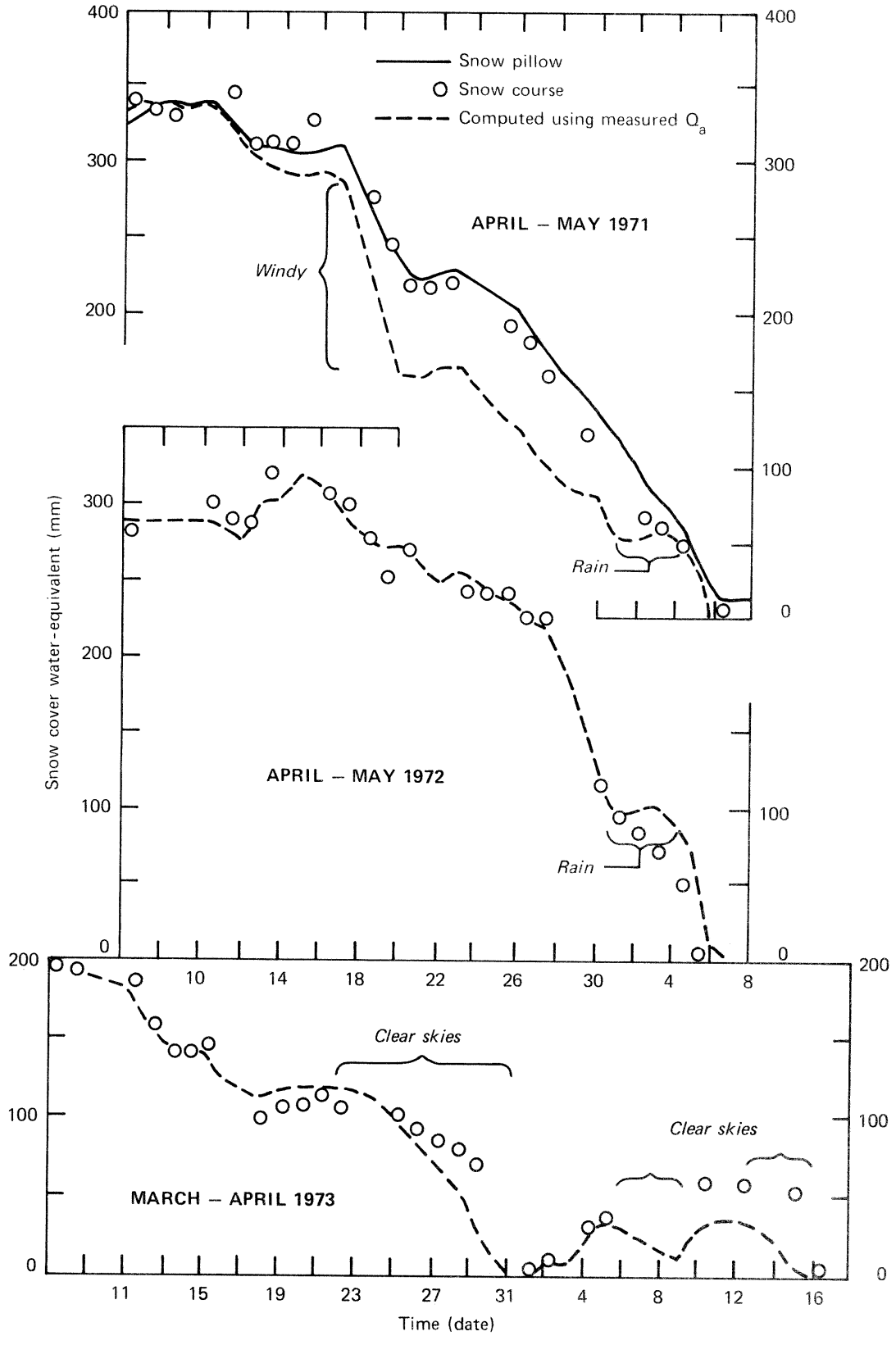

Figure 5.19.--Effect of measured incoming longwave radiation data on the water-equivalent comparisons. [Theoretical $f(U_a)$ with z_o = 0.15 cm and Ri_{cr} = 0.4 is used.]

within the snow cover is very much affected by T_o, since the temperature of the other layers changes primarily as a result of previous changes in T_o.

Table 5.4 contains statistics which summarize the comparison of computed and observed snow surface temperatures. From 1970 through 1973 the measured values of T_o were recorded on a strip chart. Values of T_o below -23°C were not recorded during these years. In 1974 the use of an electronic volt-time integrator eliminated this recording limit. In 1974, snow surface temperatures as low as -41°C were measured.

Fig. 5.20 shows plots of computed versus observed T_o values on several days scattered throughout the data period. These plots are representative of days on which significant diurnal fluctuations in T_o occurred. Large fluctuations in T_o are most likely to occur under clear sky, relatively calm conditions or during air mass changes. Incoming longwave radiation is the most important variable affecting T_o under clear, calm conditions.

In addition to a comparison between computed and observed T_o values, the computed T_o values are used to prepare frequency tables for the bulk Richardson number $(Ri)_B$ and the air temperature gradient (T_a-T_o). Cumulative frequency tables for $(Ri)_B$ and (T_a-T_o) over the entire 6 years are given in Table 5.5. Table 5.5b only includes (T_a-T_o) values for those cases when the air temperature (T_a) is $\leq$ 0°C. Obviously T_a exceeds T_o when T_a is greater than 0°C.

Table 5.5a verifies the statement that stable conditions prevail over a snow cover. An examination of $(Ri)_B$ values during periods when significant net turbulent heat transfer occurs reveals that $(Ri)_B$ values in the range 0.05 to 0.1 predominate. T_a is generally well above 0°C during these periods.

COMPUTED ENERGY BALANCE COMPONENTS

Table 5.6 gives the computed values of the components of the snow cover energy balance for the 6 years. This table shows the relative importance of each energy transfer process at the NOAA-ARS snow research station. At other locations with different physiographic and meteorologic conditions the relative importance of the processes could be quite different.

EFFECT OF THE COMPUTATIONAL TIME INTERVAL AND LAYER THICKNESS ON THE COMPUTED RESULTS

The 1973 snowmelt season is used to show the effect of the computa-

Table 5.4.--Comparison of computed versus observed snow surface temperature.
(All temperatures are in degrees Celsius)

Period	Δt[1]	Number of Cases	Mean T_o		RMS Error	Ave.Abs. Error	Correlation Coefficient	Best fit line	
			Obs.	Comp.				Intercept	Slope
4/1/70 to 4/26/70[2]	1	212	- 2.4	-2.7	2.0	1.3	0.85	0.3	0.98
12/7/70 to 4/10/71	3	762	- 9.0	-8.3	2.7	1.9	0.90	-0.3	1.04
4/1/71 to 5/8/71[2]	1	763	- 2.3	-2.3	1.8	1.0	0.90	0.2	1.07
12/24/71 to 4/7/72	3	697	- 7.4	-8.0	2.7	1.9	0.90	0.3	0.97
4/6/72 to 5/8/72[2]	1	729	- 2.9	-2.5	2.1	1.4	0.87	-0.5	0.96
3/9/73 to 4/15/73[2]	1	743	- 4.0	-4.0	2.1	1.3	0.89	-0.2	0.94
1/3/74 to 4/12/74	3	710	-11.4	-9.8	3.9	2.6	0.93	-0.5	1.11
1/3/74 to 4/12/74	1	2136	-11.4	-9.8	4.0	2.6	0.93	-0.5	1.10
3/1/74 to 4/22/74[2]	1	1150	- 6.7	-5.8	3.4	2.1	0.89	-0.6	1.06

[1] Δt is the computational time interval in hours.

[2] Melt season values were computed using a theoretically based wind function with z_o = 0.15 cm and Ri_{cr} = 0.4.

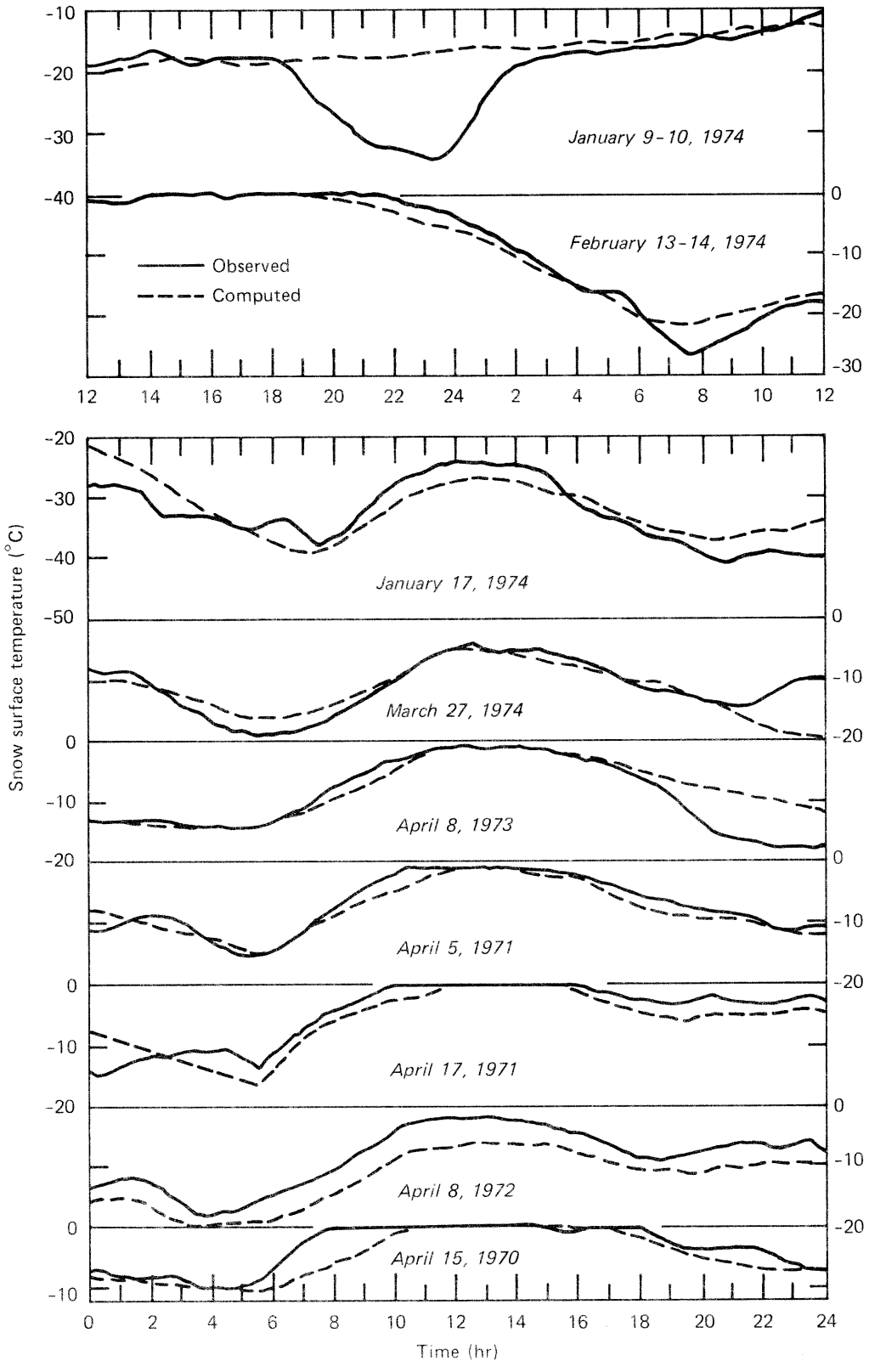

Figure 5.20.--Comparison of hourly computed and observed snow surface temperature on selected days.

Table 5.5.--Cumulative frequency tables for the bulk Richardson number and the air temperature gradient (1969-1974).

a. Bulk Richardson number frequency table.

Interval	Percent of cases in the interval	
	Accumulation season	Melt season
less than -0.2	3	1
-0.2 to -0.02	3	1
-0.02 to 0.0	8	5
0.0 to 0.01	20	18
0.01 to 0.02	11	11
0.02 to 0.05	14	18
0.05 to 0.10	10	12
0.10 to 0.20	8	9
0.20 to 0.40	6	9
greater than 0.4	17	16

b. Air temperature gradient ($T_a - T_o$) frequency table for cases when $T_a \leq 0$ °C.

Interval (°C)	Percent of cases in the interval	
	Accumulation season	Melt season
less than -4	0	0
-4 to -2	1	0
-2 to 0	14	13
0 to 2	39	40
2 to 4	24	22
4 to 6	13	12
6 to 8	5	7
8 to 10	2	3
10 to 12	1	2
greater than 12	1	1

Table 5.6.--Computed energy balance components at the NOAA-ARS snow research station.

Component	Season[1]	1968-69	1969-70	1970-71	1971-72	1972-73	1973-74
1. Net shortwave	A	4011.	4096.	4664.	4053.	2750.	4580.
radiation ($cal.cm^{-2}$)	M	4585.	3081.	3889.	3600.	3575.	4031.
2. Net longwave	A	-6317.	-6201.	-6756.	-5707.	-4165.	-5394.
radiation ($cal.cm^{-2}$)	M	-2415.	-1612.	-1846.	-1786.	-2208.	-2627.
3. Sensible heat	A	2311.	2015.	2697.	2209.	1562.	1955.
transfer ($cal \cdot cm^{-2}$)	M	1590.	1030.	1603.	1573.	1345.	1452.
4. Latent heat	A	-286.	-618.	-648.	-584.	-384.	-487.
transfer ($cal \cdot cm^{-2}$)	M	-677.	-427.	-565.	-689.	-836.	-762.
5. Vapor transfer	A	-4.9	-9.5	-10.3	-9.4	-5.9	-7.1
(millimeters)	M	-10.6	-6.6	-8.7	-10.8	-12.8	-11.5
6. Snow-soil heat	A	735.	1287.	770.	597.	628.	710.
transfer ($cal \cdot cm^{-2}$)	M	125.	85.	121.	102.	228.	222.
7. Heat transferred from	A	2.	20.	6.	9.	17.	24.
rain water ($cal.cm^{-2}$)	M	11.	15.	17.	30.	16.	28.

[1]A = accumulation season, M = melt season. Melt season values are computed using a theoretically based wind function with z_o = 0.15 cm and Ri_{cr} = 0.4.

tional time interval (Δt) on the values computed by the model. Time intervals of 1, 3, and 6 hours are used. Table 5.7 gives the energy balance components, water-equivalent values for various dates, and the mean snow surface temperature as computed using each time interval. This table shows that the computational time interval has only a slight effect on the computed results. There is a tendency for the computed water-equivalents to increase slightly with time as Δt increases.

Under certain meteorological conditions, especially clear, calm nights, very steep temperature gradients occur in the upper few centimeters of a snow cover. In these cases there might be a tendency to suspect that the computed temperature of the surface layer (assumed to occur at the mid-point of the layer) would differ greatly from the temperature right at the interface. It might be suspected that this difference would grow as the thickness of the surface layer increased. However, in the model the temperature of a layer is determined by a balance equation which mathematically represents each heat transfer process that affects the layer. Thus, under a given set of conditions the relative magnitudes of each process determine the temperature of the layer. Under clear, calm conditions at night the expression for net longwave radiation transfer dominates the equation for the surface layer. Thus the computed temperature will be close to the temperature at the interface, which also is basically a function of net longwave radiation. Heat transfer from within the snow cover, plus the change in heat storage of the layer, also have some effect on the computed surface temperature. It is difficult to predict how changes in layer thickness will affect heat transfer within the snow cover. The change in heat storage would increase the computed surface layer temperature since, as the thickness of the surface layer increases, a larger mass of snow must be cooled. However, this increase in the computed temperature should be small because snow has a low heat storage capacity.

Table 5.8 shows the effect of layer thickness on computed model results. Four values of the desired thickness of the upper layers (D_z) are used: 1 cm, 2.5 cm, 5 cm, and 10 cm. The computed energy balance components and the mean snow surface temperature for each D_z value cover the same period (3/1/74 through 4/20/74) for comparative purposes. The computed water-equivalent values increase slightly with time as D_z increases.

Table 5.7.--Effect of the computational time interval on the computed model results for the 1973 snowmelt season.[1]

Value	Δt = 1 hr.	Δt = 3 hrs.	Δt = 6 hrs.
1. Net shortwave radiation ($cal \cdot cm^{-2}$)	3322.	3315.	3312.
2. Net longwave radiation ($cal \cdot cm^{-2}$)	-2109.	-2117.	-2138.
3. Sensible heat transfer ($cal \cdot cm^{-2}$)	1242.	1234.	1222.
4. Latent heat transfer ($cal \cdot cm^{-2}$)	-826.	-796.	-763.
5. Vapor transfer (mm)	-12.6	-12.7	-12.7
6. Snow-soil heat transfer ($cal \cdot cm^{-2}$)	206.	201.	184.
7. Rain water heat transfer ($cal \cdot cm^{-2}$)	16.	16.	16.
8. Water-equivalent (mm) on:			
3/21/73	124.	124.	126.
3/31/73	31.	33.	38.
4/15/73	37.	40.	46.
9. Mean snow surface temperature (°C)	-4.0	-4.0	-4.0

[1] A theoretically based wind function with z_o = 0.15 cm and Ri_{cr} = 0.4 is used. The period of comparison is from 3/9/73 through 4/15/73.

Table 5.8.--Effect of layer thickness on computed model results.[1]

Value	Desired layer thickness (D_z) 1 cm	2.5 cm	5 cm	10 cm
1. Net shortwave radiation ($cal \cdot cm^{-2}$)	3826.	3826.	3826.	3826.
2. Net longwave radiation ($cal \cdot cm^{-2}$)	-2584.	-2608.	-2619.	-2658.
3. Sensible heat transfer ($cal \cdot cm^{-2}$)	1495.	1433.	1368.	1329.
4. Latent heat transfer ($cal \cdot cm^{-2}$)	-715.	-758.	-804.	-838.
5. Vapor transfer (mm)	-10.6	-11.4	-12.2	-12.8
6. Snow-soil heat transfer ($cal \cdot cm^{-2}$)	189.	210.	253.	286.
7. Rain water heat transfer ($cal \cdot cm^{-2}$)	28.	28.	28.	28.
8. Water-equivalent (mm) on:				
3/13/74	97.	98.	99.	100.
4/2/74	196.	200.	203.	204.
4/6/74	135.	139.	142.	145.
4/20/74	14.	27.	35.	46.
9. Time of disappearance of the snow cover:				
day:	21	21	22	22
hour:	11	14	7	11
10. Mean snow surface temperature (°C)	-5.9	-5.8	-5.8	-5.7

[1]A theoretically based wind function with z_o = 0.15 cm and Ri_{cr} = 0.4 is used. The computational time interval is 1 hour.

This increase is basically caused by an increase in the computed heat deficit at night during the snowmelt periods. The computed heat deficit increases as D_z increases because a larger mass of snow must be cooled near the surface. A larger heat deficit at night results in less net melt during the day. Thus, the computed snow cover lasts longer. The computed water-equivalent values for each D_z could be made more nearly similar by applying different turbulent transfer parameters in each case. Thus the D_z value used in the computations does, to a small extent, affect the parameter values.

CHAPTER VI: DISCUSSION

INTRODUCTION

This chapter discusses the results obtained with the snow cover simulation model using the data collected at the NOAA-ARS snow research station near Danville, Vermont. In addition, a comparison is made between melt season water-equivalent simulations as obtained by this model and another snow cover simulation model. The other model [Anderson (1973)] is conceptual in nature, but uses air temperature as the sole index to snow cover energy exchange. Thus it will be referred to as the temperature index model. The model described in this report will be referred to as the energy balance model.

At the end of this chapter suggestions are made regarding the appropriate type of snow cover simulation model to use for various hydrologic applications. These suggestions are based on the results obtained with the energy balance model and the comparisons between snow cover models. The type of model to use is dependent on climatic and physiographic conditions, plus the available data.

DISCUSSION OF ACCUMULATION SEASON RESULTS

Snow surface and snow cover density

In general the agreement between computed and observed snow densities as shown in Figs. 5.5 through 5.10 is quite satisfactory. The computed snow surface density is a function of the density of new snow and the increase in surface layer density due to settling [Eq. (4.29)]. New snow densities estimated from the wet-bulb temperature [Eq. (4.22)] are reasonable for most storms. However, as mentioned previously, during some storms this estimate must be revised due to the influence of other factors on the density of new snow. The meteorological data and remarks in the station log indicate that the major factor necessitating such revisions is high winds during or immediately after the snow storm. The settling equation and the parameter values used in that equation reproduce surface density changes quite adequately. This can be verified by examining periods of little or no precipitation following a significant snowfall. During such periods computed and observed snow surface densities increase at nearly the same rate.

The compaction process, represented by Eq. (4.28) in the model, plays a significant role in determining the total density of the snow cover.

The reproduction of observed snow cover density is very adequate except when rain and/or melt occurs and the snow cover contains relatively impermeable ice layers. Such cases occur in early February 1970 [Fig. 5.7] and late January 1973 [Fig. 5.9]. In these cases the station log indicates that there was a considerable delay in the movement of the liquid-water through the snow cover. Slush layers existed above the ice layers for several days. Studies by Wakahama (1968) and Colbeck (1973) indicate that the rate of compaction can increase significantly when water saturation is high. It is apparent that during these two periods the density of the more saturated portions of the snow cover increased much more rapidly than predicted by Eq. (4.28). This increased densification of portions of the snow cover affects the total snow cover density throughout the remainder of the accululation season. The continued influence of these high density layers is more pronounced in 1970 than in 1973 due to the presence of a thicker and more impermeable ice layer.

In mid-January 1974, the same type of situation occurred [Fig. 5.10]. However, in this case the station log indicates that most of the liquid-water remained in the snow cover long enough to be frozen during a subsequent cold spell. This resulted in the thick ice layer near the base of the snow cover which affected snow cover outflow and water-equivalent measurements throughout the remainder of the snow season.

It can be concluded that the model adequately simulates snow surface and snow cover density except when ice layers significantly retard the movement of liquid-water through the snow cover.

Snow cover temperature

The reproduction of temperatures within the snow cover as shown in Fig. 5.11 is reasonably good except for a few periods. The three periods when the discrepancy is quite large are January 8-11, 1971, January 26-30, 1972, and February 20-28, 1972. In examining these periods in more detail it was noticed that during both of the 1972 periods there is also a discrepancy between computed and observed snow surface density. The basic data shows that high winds accompanied both the snowstorm of January 25-26, 1972, and that of February 19-21, 1972. The density of new snow during these storms had not been previously revised because the effect on total snow cover density did not seem significant. In order to determine the effect of surface density on temperatures within the snow cover, the density of new snow for these two storms was altered and

the 1972 accumulation season rerun. Fig. 6.1 shows the effect of these changes on density and snow cover temperature. The computed and observed snow surface densities as well as the snow cover temperatures are now in good agreement. The low-density surface layers which existed in the earlier simulation run had in effect insulated the snow cover. Thus, the cold temperatures did not penetrate into the snow cover.

During the January 8-11, 1971 period, computed snow surface and snow cover density compares closely with the observed value. At the beginning of this period the model shows a 12-cm thick layer of 0.035 $gm \cdot cm^{-3}$ density snow at the surface. This is the lowest density snow ever observed at the NOAA-ARS snow research station. This density is well below the densities used in the experimental determinations of the heat transfer coefficients [see Table 3.1 and Figs. 3.1 and 3.2]. This suggests that the extrapolated values of these coefficients could be in error at such a low density. It is possible that the rate of heat transfer in very low-density snow is increased since air could move more freely through the snow.

It would be helpful for model verification purposes to measure snow cover temperatures at more frequent depth intervals so that computed and observed snow cover temperature profiles could be compared. Such measurements will be made in the future at the NOAA-ARS snow research station.

Fig. 6.1 shows that an accurate determination of the snow cover density profile is essential in computing temperatures within the snow cover. A correct estimate of the density of the surface layers, where the largest temperature gradients normally occur, is especially critical. Without accurate density profile estimates a reasonable simulation of snow cover temperatures seems impossible except for a very homogeneous snow cover.

DISCUSSION OF SNOW SURFACE TEMPERATURE COMPARISONS

The comparison between computed and observed snow surface temperature (T_o) is summarized by Table 5.4 and Fig. 5.20. The statistical comparison of Table 5.4 shows the model gives relatively unbiased estimates of snow surface temperature. There is a slightly greater tendency to compute T_o values that are too high than to compute too low of a surface temperature. The RMS error is in the range of 1.5 to 2 times as large as the estimated standard error of the infrared thermometer measuring system.

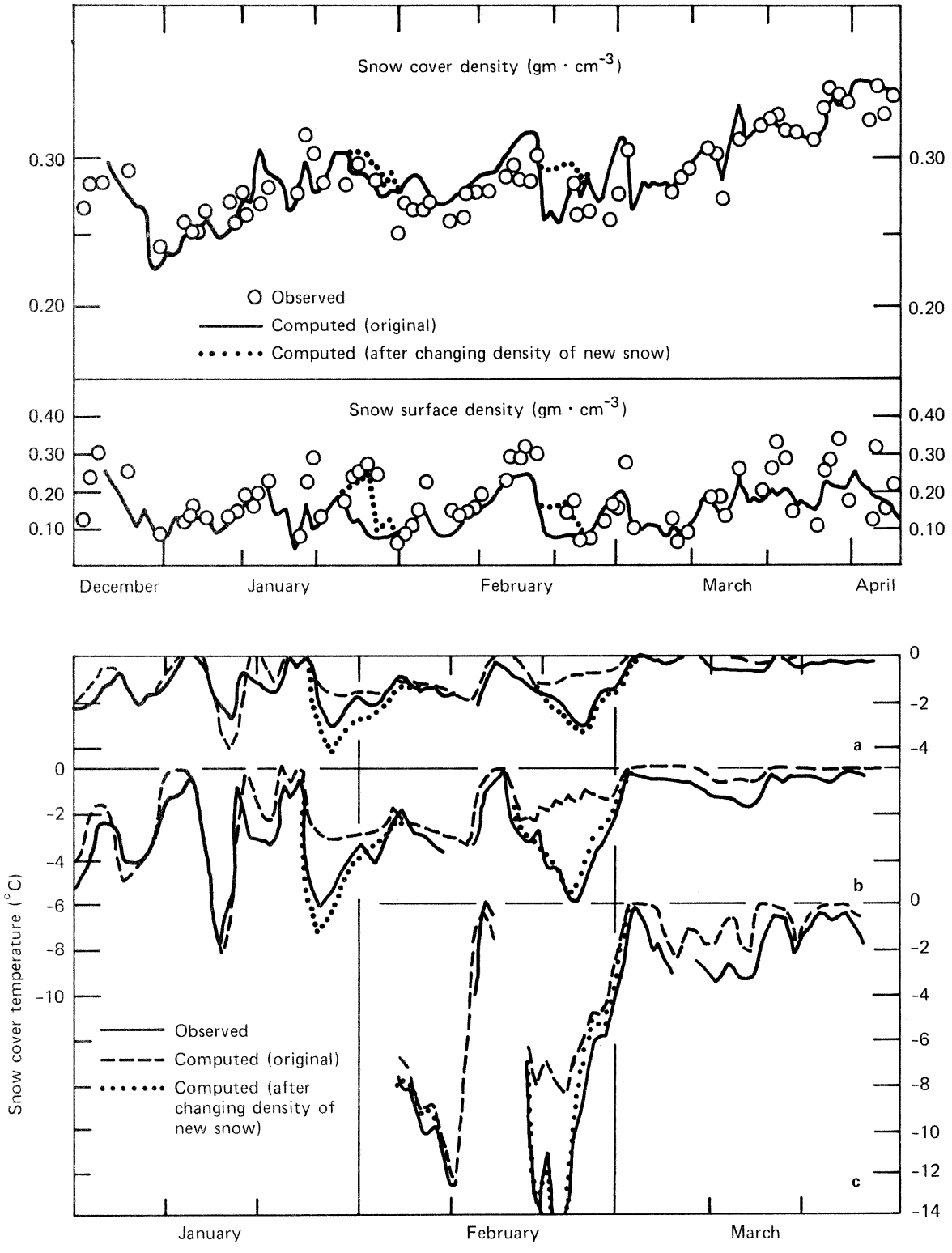

Figure 6.1.--Effect of snow surface density on snow cover temperature during 1972. [(a) 15 cm above soil; (b) 30 cm above; (c) 60 cm above.]

Upon examining the computed and observed T_o values in more detail, it soon becomes obvious that the greatest discrepancies occur under calm conditions and mainly at night. During such periods net longwave radiation dominates the energy balance. As mentioned previously, it has been very difficult to obtain accurate and consistent estimates of incoming longwave radiation (Q_a).

The night of January 9-10, 1974 illustrates the extreme discrepancy that can occur between computed and observed T_o as a result of inaccurate estimates of Q_a. During this night computed T_o is as much as 18°C greater than the observed value [see Fig. 5.20]. During this night the sky was clear and wind movement was near zero. Using the computed T_o values gives large negative bulk Richardson numbers [$(Ri)_B$] for most of the night. Large negative $(Ri)_B$ values are physically impossible under such conditions. For the model to compute such values can only mean that the Q_a values are much too high. The reason for Q_a being much too high on this particular night is because the Q_a estimation procedure uses the ratio of measured solar radiation to clear sky solar radiation as an index to sky conditions. Both January 9 and 10 were overcast. Thus the Q_a estimation procedure also treated the night as overcast when actually the sky was clear for most of the night.

An estimation procedure using a different index to sky conditions or measured Q_a values might easily improve results on the night of January 9-10, 1974. However, most other estimation procedures are probably no more accurate than the method used in this study on a long-term basis. The measurements of Q_a made at the NOAA-ARS snow research station contain inconsistencies, as can be seen from Fig. 5.19. These measurements provide unsuitable continuous estimates of Q_a for use in energy balance model verification. The only solution seems to be to find instruments which are capable of making consistently accurate measurements of Q_a.

Most of the large negative values of $(Ri)_B$ computed by the model occur when computed T_o greatly exceeds the observed surface temperature due to errors in the Q_a data. Removing these periods would result in almost no cases when unstable conditions exist over a snow cover. [In the model computed negative $(Ri)_B$ values occur 7 to 14 percent of the time (see Table 5.5)]. The only periods when truly unstable conditions occur are

when the intensity of the solar radiation is large enough to cause the surface temperature to exceed the air temperature. Such periods are extremely rare over a snow cover because of the high albedo and the high emissivity of snow, the penetration of solar radiation, plus the fact that the surface temperature cannot exceed 0°C. Thus stability corrections for unstable conditions cannot be verified over snow nor are they of any real importance.

Under clear, calm, cool daytime conditions Q_a and absorbed solar radiation dominate the energy balance and thus control T_o. Such cases give some opportunity to evaluate the extinction coefficient (ν). Obviously when the snow cover is isothermal at 0°C, the value of ν is not important except to determine the amount of solar radiation passing through a very shallow snow cover. However, when surface conditions are below 0°C, solar radiation intensity is high, and winds are relatively calm, the computed T_o is significantly influenced by ν. January 17, 1974, April 8, 1973, and April 5, 1971 as shown in Fig. 5.20 are representative of such days. Computed and observed T_o values are generally in good agreement during daytime hours on these days indicating that the values of ν used in the model are reasonable.

DISCUSSION OF MELT SEASON RESULTS

Effect of wind function coefficients on results

It is obvious from Figs. 5.12 through 5.14 that the empirical wind function [$f(U_a)=0.0031 \cdot U_a$] derived from vapor transfer measurements is too high. In order to compare the other wind function coefficients it is first necessary to show how they vary with stability. Fig. 6.2 shows the variation in the theoretically based wind function coefficients [C_t, computed from Eq. (2.58)] as a function of $(Ri)_B$. Also shown is the empirical wind function coefficient of 0.002 $mm \cdot mb^{-1} \cdot km^{-1}$. Only stable conditions are shown in Fig. 6.2 as unstable conditions seldom exist over a snow cover, especially during melt periods. This plot shows that C_t is nearly the same in all three cases over the $(Ri)_B$ range of 0.05 to 0.09. Thus when $(Ri)_B$ is within this range, model results should be similar whether one of the theoretically based wind functions or the empirical wind function coefficient of 0.002 is being used.

Figs. 5.15 through 5.17 show that the two theoretically based wind functions give nearly the same results. This indicates that $(Ri)_B$ is

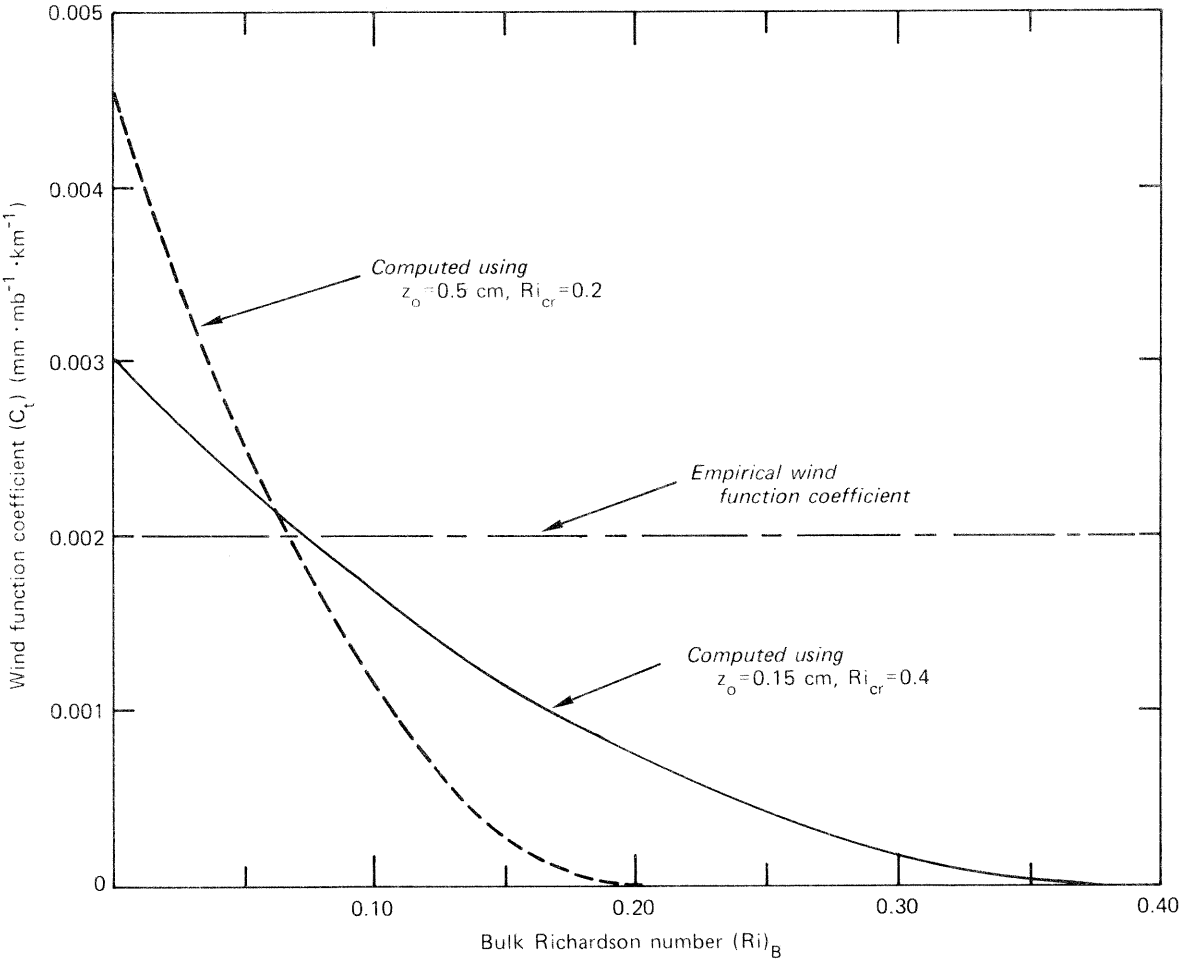

Figure 6.2.--Comparison of wind function coefficients under stable atmospheric conditions.

in the range of 0.05 to 0.09 during most periods when turbulent transfer causes a significant amount of melt. Significant amounts of sensible and latent heat transfer occur under other stability conditions, however, the two terms tend to cancel each other resulting in only a small amount of net turbulent heat transfer. The main deviations between the results obtained with the two theoretically based wind functions occur during April 18-20, 1971 and April 17-19, 1972. During these periods significant net turbulent heat transfer occurs with $(Ri)_B$ less than 0.05. Near neutral conditions occur on April 18, 1971. In general C_t computed using z_o = 0.15 cm and Ri_{cr} = 0.4 gives slightly better results and is thus used in further comparisons.

Stable conditions [$(Ri)_B$ in the range 0.15 to 0.20] cause deviations to occur between C_t computed using z_o = 0.15 cm and Ri_{cr} = 0.4, and the empirical wind function coefficient of 0.002. These deviations occur on April 14-17, 1969, March 28 to April 1, 1973, and April 4-5 and 14-15, 1974. The use of the theoretically based wind function gives results closer to observed conditions in 1973 and 1974, while the use of the empirical function improves results in 1969. In 1971 a very stable period on April 11-13 balances the near neutral period occurring on April 18-20.

The term "empirical wind function" is somewhat of a misnomer, at least in the case of the 0.002-mm·mb^{-1}·km^{-1} coefficient which is not based on vapor transfer measurements. In many investigations a single-valued wind function coefficient is commonly computed from a measured or assumed roughness height parameter (z_o) by an equation of the form

$$C_{t'} = \frac{\rho_a \cdot 0.622}{P_a \cdot \rho_w} \cdot 10^6 \cdot \frac{k^2}{(\ln \frac{z_a}{z_o})^2} \quad , \qquad (6.1)$$

where $C_{t'}$ is a theoretically based wind function coefficient that does not include a stability adjustment term (mm·mb^{-1}·km^{-1}). In order to obtain the value of $C_{t'}$ of 0.002 as used in this study, Eq. (6.1) would require a z_o of 0.034 cm. This is close to the 0.05-cm value of z_o recommended by Kuzmin (1961) to compute $C_{t'}$. Kuzmin also recommends a z_o of 0.25 cm for snow lying in patches and a z_o of 0.6 cm when stubble and grass protrude above the snow.

Overall there is not a great difference in model results as obtained

by using any of the three wind function coefficients shown in Fig. 6.2. This is because of two factors. First, $(Ri)_B$ values do not vary greatly during most periods when net turbulent heat transfer makes up a significant portion of the heat causing snowmelt. Second, winds are generally about 2 $m \cdot sec^{-1}$ and seldom exceed 5 $m \cdot sec^{-1}$ on days when significant melt occurs at the NOAA-ARS snow research station. A stability adjustment to the wind function is probably only necessary when a greater variation in stability conditions, as well as higher winds, occur when net turbulent heat transfer causes a significant amount of snowmelt.

Water-equivalent comparisons

In general the comparison between computed and observed water-equivalent as shown in Figs. 5.12 through 5.17 is quite good. Deviations occur at certain times though it is difficult and probably dangerous to try to pin down the exact days on which the largest errors occur based solely on total snow cover water-equivalent measurements. Snow tube and snow pillow measurements are just not accurate enough to determine the daily change in water-equivalent.

In addition to errors in the water-equivalent measurements, two other uncertainties probably have a significant effect on the discrepancies between computed and observed water-equivalent. These are errors in incoming longwave radiation data and possible variations in the wind function coefficient due to variations in z_o. The measurement errors associated with the other variables are small and probably account for only a small portion of the total discrepancy.

Incoming longwave radiation (Q_a) is a very important part of the energy balance of a snow cover. During heavy melt periods there is nearly a one to one relationship between changes in Q_a and changes in melt because of the high emissivity of snow and the fact that the surface temperature of snow cannot exceed 0°C. In addition, the heat deficit created at night, especially during calm, clear sky periods, is dominated by Q_a. An incorrect determination of this nighttime heat deficit can result in a sizable error in determining the net daytime melt.

The considerable variation in the z_o values reported for snow, plus the dynamic nature of snow surface properties suggest that the roughness height and thus the neutral stability turbulent transfer coefficient can vary with time. Much more detailed wind profile measurements would be needed to determine how much z_o does change during the melt season.

Snow cover outflow comparisons

The lysimeter provides a much more reliable estimate of the short term water-equivalent changes occurring in a snow cover. Unfortunately only one year of lysimeter data are available for analysis. Fig. 5.18 summarizes the comparison between computed and observed snow cover outflow during the 1973 melt season. A statistical comparison of computed and observed daily snow cover outflow results in an intercept of -1.4 mm, a slope of 1.21, a correlation coefficient of 0.979, and a standard error of estimate of 2.4 mm (observed mean is 8.6 mm). If the 2 days with the greatest outflow are removed, the intercept becomes -0.9 mm, the slope is 1.09, the correlation coefficient is 0.973, and the standard error of estimte is 1.9 mm (observed mean is 6.4 mm). The comparison on these remaining days gives a best fit line which is sufficiently close to 45° and a reasonable standard error considering the errors in the input variables and the measured snow cover outflow. The 2 days on which the largest errors occur are March 12 (observed = 38.0 mm, computed = 27.1 mm) and March 17 (observed = 48.4 mm, computed = 38.8). Overcast skies, high humidities, and light winds (1.7 and 1.0 $m \cdot sec^{-1}$, respectively) prevail on these 2 days as they do throughout the early portion of the 1973 melt season. Rain fell on both days with 4 mm on the 12th and 32 mm on the 17th [hourly outflow for the 17th is shown in Fig. 5.18]. Net longwave radiation, sensible and latent heat exchange dominate the energy balance. Q_a estimates during heavily overcast periods are normally quite reliable since Q_a is usually close to black-body radiation at the air temperature. Also, the pyrgeometer should be quite reliable under such conditions. Thus, the fact that there is not much difference between estimated and measured Q_a on these days, would indicate that any errors in the Q_a data are probably small. The use of the empirical wind function derived from vapor transfer measurements [$f(U_a)=0.0031 \cdot U_a$] gave much improved results on these 2 days (computed outflow of 35.7 mm on the 12th and 44.3 mm on the 17th) as it did throughout the early part of the 1973 melt season [see Fig. 5.14]. This evidence suggests that the wind function coefficient might have changed during the 1973 melt season.

The lysimeter measurements of snow cover outflow also make it possible to verify the equations used to account for the movement of excess liquid-water through the snow cover [Eqs. (4.34) and (4.35)]. The hourly

outflow comparisons shown on Fig. 5.18 are reasonable, but indicate improvement is possible. The addition of snow density to these equations seems to change lag and attenuation in the right direction; however, there is not enough density variation nor events during the 1973 melt season to verify the addition of density any further. More theoretically based liquid-water transmission equations should probably be added to the model in the future.

COMPARISON OF ENERGY BALANCE AND TEMPERATURE INDEX MODELS

Introduction

When developing a more complex model of a given process it is important to compare the new model with a more established simpler model. The comparison should assist in showing under what conditions the new model will give improved results. A reasonably long period of record is usually necessary in making the comparison. One or two years is seldom enough. In many cases the advantages of a more physically based and theoretically correct procedure only show up during a few periods. However, these few periods are likely to include the extremes. This is because a more physically based model can usually be extrapolated to fit the extremes more reliably. The extremes are usually most important in terms of public safety and economic benefits. Thus it is important when making comparisons not only to examine the mean error statistics, but to examine the errors under extreme conditions.

The temperature index model

The temperature index model used for the comparison is a conceptual snow accumulation and ablation model [Anderson (1973)]. The model is conceptual in that each of the major components of the snow accumulation and ablation process are mathematically represented. Thus the model differs significantly from degree-day procedures which estimate snow cover outflow without explicitly accounting for heat deficits, liquid-water retention and transmission, and the areal extent of snow cover.

Many of the features incorporated in this temperature index model are based on the results of an earlier snow cover energy balance study [Anderson (1968)]. These include the method of estimating energy exchange during non-melt periods, the functional form of the seasonal melt-factor variation, and the use of different equations to compute melt during rain and non-rain periods. The need for different melt-factors

during rain and non-rain periods is also discussed by Obled (1973).

The final parameter values determined by fitting the temperature index model to the melt season water-equivalent measurements are given in Table 6.1. The reader should refer to the report which describes this model [Anderson (1973)] for a more complete description of the parameters.

Table 6.1.--Final parameter values for the temperature index model for the 1969-74 snowmelt seasons at the NOAA-ARS snow research station.

Identifier	Brief description	Value
SCF	ratio of the increase in water-equivalent of the snow cover to the catch in the precipitation gage	1.5, 1972 0.9 other years.
MFMAX	maximum non-rain melt-factor, occurs on June 21 ($mm \cdot °C^{-1} \cdot 6\ hr^{-1}$)	1.4
MFMIN	minimum non-rain melt-factor, occurs on Dec. 21 ($mm \cdot °C^{-1} \cdot 6\ hr^{-1}$)	0.5
NMF	negative melt-factor ($mm \cdot °C^{-1} \cdot 6\ hr^{-1}$	0.5
UADJ	average wind function during rain-on-snow periods ($mm \cdot mb^{-1}$)	0.125
SI	water-equivalent above which 100 percent areal snow cover always exists (mm)	10.
DAYGM	daily melt at the snow-soil interface (mm)	0.2
MBASE	base temperature for non-rain melt-factor (°C)	0.0
PLWHC	percent liquid-water holding capacity (decimal fraction)	0.03
TIPM	antecedent temperature index parameter	0.1

Comparison of models

The comparison of melt season water-equivalents as computed by the temperature index and the energy balance models with the observed values is shown in Figs. 6.3 through 6.5. The energy balance model results were computed using a theoretically based wind function with z_o = 0.15 cm and Ri_{cr} = 0.4.

During 1972 and 1973 the reproduction of observed water-equivalent

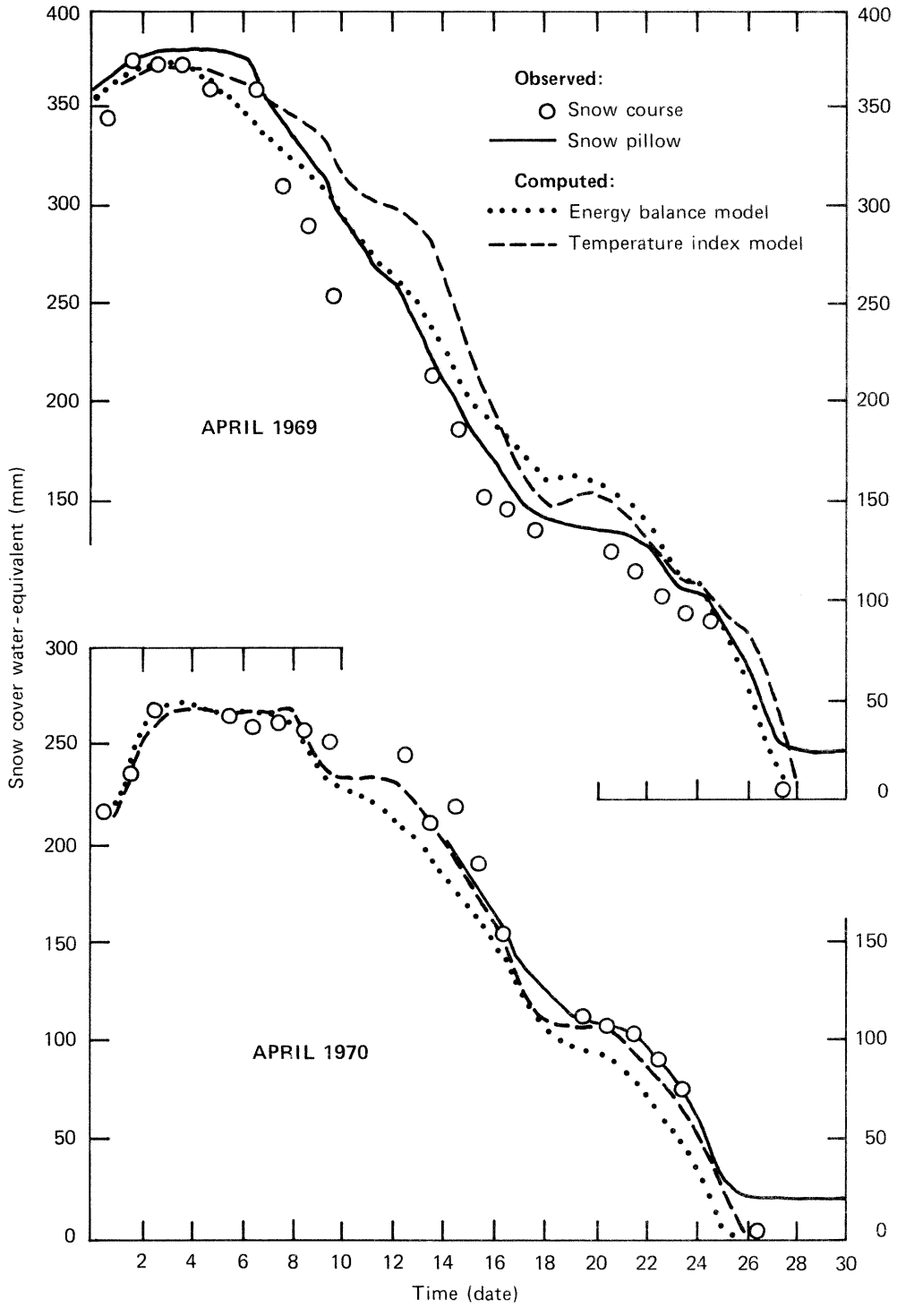

Figure 6.3.--Comparison of energy balance and temperature index models during the 1969 and 1970 melt seasons.

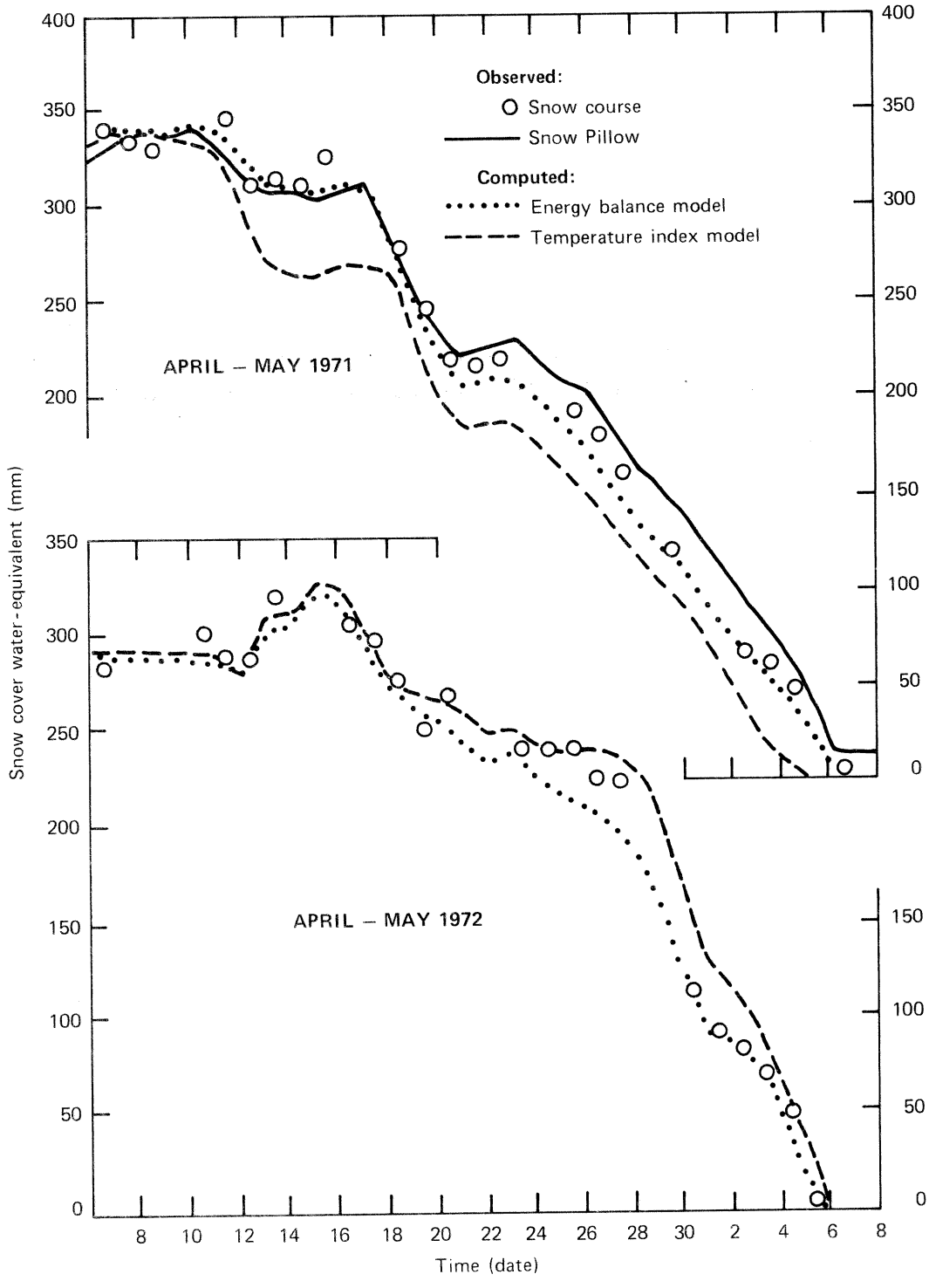

Figure 6.4.--Comparison of energy balance and temperature index models during the 1971 and 1972 melt seasons.

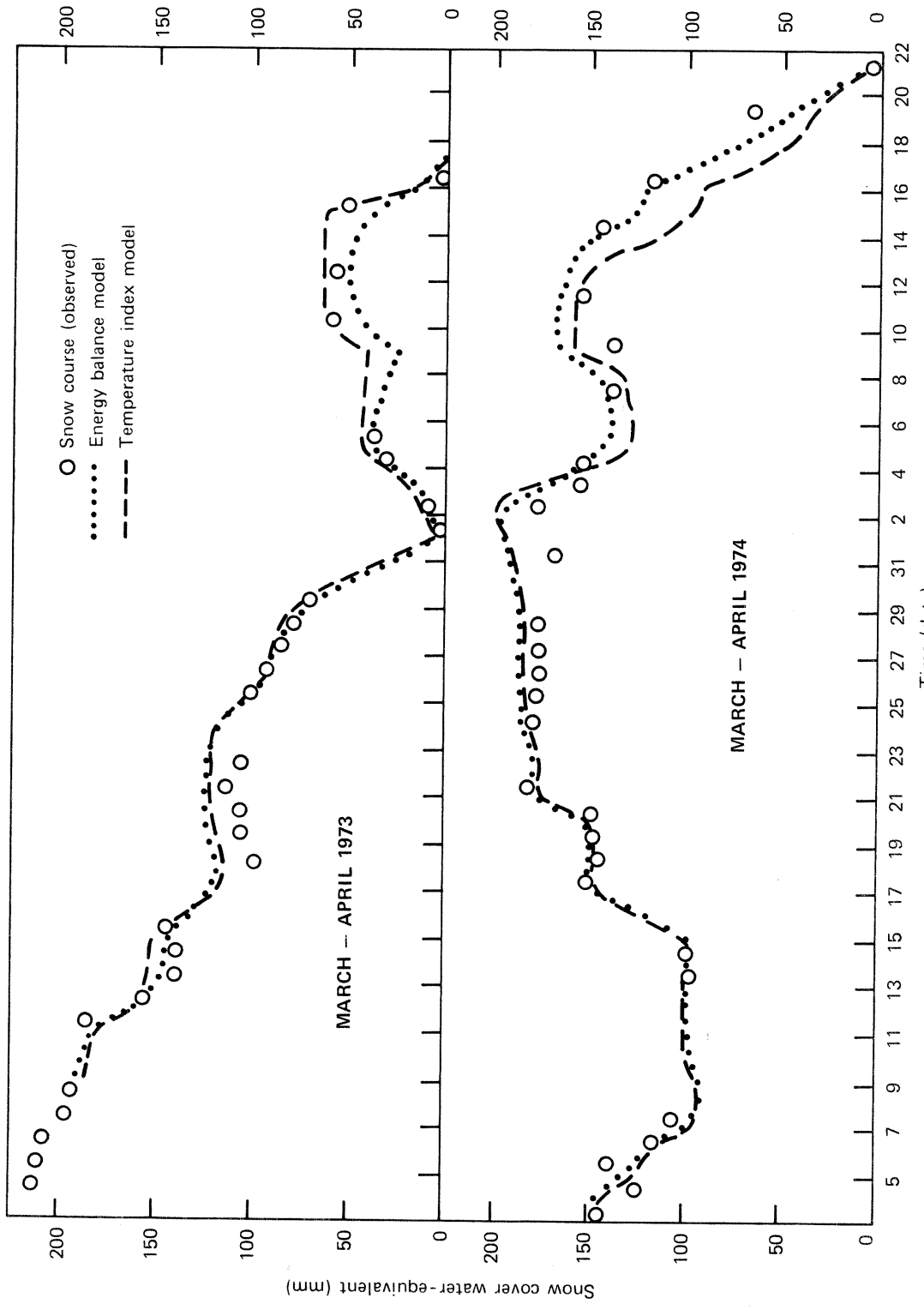

Figure 6.5.--Comparison of energy balance and temperature index models during the 1973 and 1974 melt seasons.

values is judged to be nearly the same for each model. On some days during these two years the temperature index model gives results which are closer to observed conditions while on other days the energy balance model is closer to the measured water-equivalent.

During 1970 the temperature index model reproduces observed conditions better than the energy balance model. The improvement occurs mainly on April 10-12 and April 19-20. These are all days on which the air temperature remained quite close to 0°C. Sensible heat transfer is small because there is only a slight temperature gradient. Latent heat transfer is negative. Therefore the apparent slight overestimation of melt on these days by the energy balance model is most likely caused by an error in the radiation balance. Such conditions also occur on April 25-27, 1972.

During the remaining three years (1969, 1971, and 1974) the energy balance model gives the best results. The improvement is mainly a result of the temperature index model being unable to account for significant deviations from mean conditions. Two types of deviations occur during these years. In 1969 a very long, clear, cool period occurs from April 6 to the 13th. During this period, even though the maximum air temperatures are only slightly above 0°C, there is an abundance of solar radiation to melt the snow. April 12-13, 1971 and April 4-5 and 14-15, 1974 are very warm days, however, winds are light resulting in very stable conditions. Thus sensible and latent heat transfer are near zero. On these days the temperature index model significantly overestimates melt because the melt factors are based on the mean wind speed and stability conditions. Warm stable conditions also prevail on April 15-17, 1969. The overestimation of melt by the temperature index model during this period partly compensates for the underestimation on April 6-13.

The conclusion resulting from this comparison is that, in general, air temperature (T_a) is a good index to snow cover energy exchange. However, when large deviations from normal occur in one or more of the relationships between T_a and the other variables which have a significant effect on the energy balance, T_a is no longer a good index to snowmelt. The frequency and severity of such deviations is a very important consideration in determining the type of snow cover energy exchange model to use for a given hydrologic application.

SUGGESTIONS CONCERNING THE APPROPRIATE TYPE OF SNOW COVER MODEL TO USE FOR VARIOUS HYDROLOGIC APPLICATIONS

Introduction

Based on the previous comparison of snow cover models and the background on snow cover energy exchange developed in Chapters II and III of this report, it seems appropriate to make a few suggestions concerning the appropriate type of snow cover model to use for various hydrologic applications. The main differentiating feature of snow cover models is the method used to estimate energy exchange. The other features of conceptual snow cover simulation models are either similar or could be made similar. For example, the temperature index model used in the previous comparisons [Anderson (1973)] does not simulate snow cover depth and density. However, the equations developed in this report to compute density could be added to the temperature index model.

Snow cover models can be divided into two general types for the purpose of classifying the models for their applicability in solving various hydrologic problems. The basic types are index models and energy balance models. Index models use one or more variables in an empirical expression to estimate snow cover energy exchange. Air temperature is the most commonly used index, but other variables such as net radiation, wind speed, vapor pressure, and solar radiation are also used. It is probably a good idea not to include too many variables in an index model. When a large number of variables are included, it becomes difficult to correctly account for the interdependency between the variables. If a large number of variables are available for use, it is probably much more logical to use a theoretically based energy balance model to insure that the variables are combined in a reasonable manner.

The energy balance model described in this report is probably too complex and too time-consuming from the standpoint of computer usage to be used directly in a practical application. However, with a few simplifications to some of the equations, the use of a 6-hour computational time interval, and some changes to the algorithm which subdivides the snow cover into layers, the model could be reduced to a practical level without sacrificing much in terms of accuracy. In addition, if the model were to be used for an areal application, which would most likely be the case, techniques would need to be devised to account for the

effect of such factors as slope, aspect, elevation, and forest cover on the input variables.

Factors to consider in model selection

There are several factors to consider in selecting a snow cover model for a given hydrologic application.

1. Climatic conditions. The NOAA-ARS snow research station, though not having extreme variations in meteorological conditions, has more variability than most areas. No single weather pattern predominates during snowmelt. During melt, clear, partly cloudy, and overcast sky conditions occur with a similar frequency. Rain occurs frequently during melt, as well as extended non-rain periods. Both high and low humidities are common. The only factor missing is extreme variations in wind speed.

Index snow cover models tend to work best when the amount of climatic variability, especially during snowmelt periods, is slight. When meteorological conditions vary widely during a melt season or from year to year, an energy balance model is more suitable for estimating snowmelt.

2. Physiographic factors. The most important physiographic factors affecting snow cover energy exchange are slope, aspect, elevation, and forest cover. Considerable variation in these factors over a watershed affects the areal and time distribution of melt. This could lead to the need to subdivide the watershed into more homogeneous subareas. However, the main effect of physiographic factors on the selection of an index or energy balance snow cover model is to what degree these factors affect the variation in meteorological conditions.

A thick conifer forest restricts wind movement and the penetration of solar radiation through the forest canopy to the snow cover below. Thus the terms involving wind speed and solar radiation have a small effect on the energy balance. Net longwave radiation would be the dominant method of energy transfer. Incoming longwave radiation is closely related to the forest canopy temperature which in turn is closely related to the air temperature. Thus index models should give good results when applied to heavily forested watersheds.

In open areas there is a much greater chance for variability in meteorological conditions during snowmelt. All of the terms in the energy balance are likely to be important, plus the relative importance can vary from day to day.

3. Available data. An energy balance model obviously requires much more data than an index model. The basic question that needs to be answered is what amount and quality of data are needed to insure that an energy balance model will give improved results as compared to an index model?

In many cases simulation models are used to predict behavior under extreme situations. During extreme events, conditions are likely to be much different from those used in model calibration. An energy balance model offers a much more reliable means of extrapolating to determine behavior under extreme conditions. It might be possible to get improved results by using an energy balance model under extreme conditions even with a minimal amount of data. Whereas, under normal conditions a considerable amount of high-quality data might be needed to improve results over those that could be obtained with an index model.

With extreme events in mind, Franz (1974) explored predictive relationships for solar radiation, dew-point, and wind speed in which daily maximum and minimum air temperature served as the predictor variables. Franz found a strong relationship between dew-point and minimum air temperature, a weak relationship between solar radiation and the daily range in air temperature, and no relationship between wind and air temperature. This would seem to indicate that more than just air temperature data are needed to get improved results by using an energy balance model even under extreme conditions.

Another argument for using an energy balance model, even though only minimal data, such as air temperature, exist, is that as the additional data become available they could be substituted directly into the model without recalibration. This would require extreme care to insure that the relationship between air temperature and each of the other variables is unbiased. It would be especially difficult to establish unbiased relationships when working with areal estimates of the variables. For example, it would be most difficult during calibration to separate the relationship between the wind speed predictor and the mean areal wind speed from the determination of the wind function coefficient. It is very likely that such a procedure would require recalibration of the model whenever additional data become available.

A logical minimum data requirement for using an energy balance model

would be measurements of solar radiation, wind, and vapor pressure in addition to air temperature. A reasonable estimate of solar radiation based on cloud cover or percent of possible sunshine might suffice in place of solar radiation measurements. Whether measurements of these variables at a low elevation station would be adequate for use in a high elevation mountain watershed is uncertain. The extrapolation technique would have to account for the climatic variability between the two locations. If estimates of air temperature, vapor pressure, wind, and solar radiation are available, it is still necessary to estimate incoming longwave radiation and albedo before using an energy balance model.

4. Other considerations. The type of application is an important consideration in model selection. For design applications where only extreme conditions are of interest, an energy balance model is probably needed. Even if the needed data are not available, likely extreme conditions could probably be generated with the aid of meteorological and statistical techniques. When all types of conditions are of interest, as in river and water supply forecasting, the selection of a snow cover model should be based on the other factors affecting model performance (climatic conditions, physiographic factors, and available data).

Economic considerations should also influence the selection of a snow cover model. The question that needs to be asked is how much improvements in accuracy are worth? For a given application it needs to be determined if the benefits will exceed the costs of obtaining the improvements in accuracy.

Conclusions regarding model selection

The discussion of the factors affecting the selection of a snow cover simulation model for various hydrologic applications can be summarized with the following conclusions.

1. The minimal recommended data needed to apply an energy balance model are a good estimate of incoming solar radiation, plus measurements of air temperature, vapor pressure, and wind speed.

2. An energy balance model should give improved results, as compared to an index snow cover model, when applied to a relatively open area where there is considerable variability in meteorological conditions during snowmelt.

In large relatively uniform open areas like those which encompass a

large part of the upper midwest portion of the United States, an energy balance model could be used for river forecasting without treating each watershed separately. If the necessary data are available, the snow cover could be simulated for 10 to 20 locations throughout the area. From the energy balance estimate of energy exchange the appropriate melt-factor for the day could be computed for each location. Then the melt-factors for each watershed could be determined by an interpolation scheme. The results should be nearly the same as if an energy balance model were used for each watershed. However, the computer requirements would be much less demanding.

3. In heavily forested watersheds an index snow cover model should give results that are similar to those that can be obtained with an energy balance model.

4. On other watersheds model selection will depend on the degree of climatic and physiographic variability. The more variability the better the chance that an energy balance model will give improved results as compared to an index model.

5. When extreme conditions are the only concern, an energy balance snow cover model should be used.

CHAPTER VII: CONCLUSIONS

The purpose of this study was to expand the understanding of snow cover energy exchange by combining the results of various investigations dealing with specific energy transfer processes and to test the resulting energy and mass balance model on some of the best available data. The model is based on theoretical expressions for energy exchange across the air-snow interface and for heat transfer within the snow cover and across the snow-soil interface. In addition, other processes which affect energy transfer are included in the model. These include the addition of new snow, compaction and settling of the snow cover, and liquid-water retention and transmission. The model is tested on 6 years of data collected at the NOAA-ARS snow research station near Danville, Vermont. The results of the energy balance model are also compared with the results obtained by a simpler conceptual snow cover model [Anderson (1973)]. This model uses air temperature as the sole index to snow cover energy exchange. The conclusions are based on the tests of the energy balance model and the comparison between the energy balance and temperature index snow cover models.

1. The overall results of the energy balance model, based on comparisons between computed and observed values of snow cover variables at the NOAA-ARS snow research station, are quite good. The values of most of the model parameters are based directly on experimental determinations given in the literature. Calibration was only necessary in the case of a compaction parameter (C_1), the minimum fractional liquid-water-holding capacity ($W_{e_{min}}$), and the parameters which define the turbulent transfer coefficients ($\underline{b}$, z_o, and Ri_{cr}). Experimental measurements indicate a range of values for each of these parameters. The calibrated values fell within this range in each case, thus helping to substantiate the validity of the model.

The model, in its present form, probably uses too much computer time and is too complex for use in a practical application. However, by increasing computational time-step and depth intervals, plus making a few simplifications, the model could be reduced to a practical level without significantly reducing the computational accuracy. Techniques to account for the effect of slope, aspect, elevation, and forest cover

on the input variables are also needed before the model can be used for an areal application.

2. The verification of the energy balance model using the NOAA-ARS data resulted in a number of conclusions regarding specific parts of the model.

a. The model adequately simulates snow surface and snow cover density under most conditions. The only exception is that the model does not account for the increased rate of densification when water saturation is high in portions of the snow cover. High saturation levels are rare, but can occur when ice layers significantly retard the movement of liquid-water through the snow cover.

b. The reproduction of temperatures within the snow cover by the model is good. A reasonably accurate determination of the snow cover density profile, especially in the surface layers where the greatest temperature gradients occur, is shown to be essential to the accurate reproduction of snow cover temperature profiles.

c. The model gives reasonably unbiased estimates of snow surface temperature. The RMS error between computed and observed snow surface temperature is 1.5 to 2 times as large as the estimated standard error of the infrared thermometer measuring system. Errors in estimated incoming longwave radiation, primarily affecting nighttime values, are responsible for a significant portion of the discrepancies between computed and observed snow surface temperatures.

d. Stable atmospheric conditions exist nearly all of the time over a snow cover. Unstable conditions are of no real importance, especially during periods of significant snowmelt. Stability adjustments to the turbulent transfer coefficients give only a slight improvement in the reproduction of water-equivalent during the melt season. This is because stability conditions are nearly the same (bulk Richardson numbers from 0.05 to 0.1) during most hours when net turbulent heat transfer causes a significant amount of snowmelt at the NOAA-ARS snow research station.

e. The comparison between computed and observed water-equivalent is good for all years. Accurate measurements of snow cover outflow from a 7.3 m^2 lysimeter are only available during 1973. A statistical comparison of computed and observed daily snow cover outflow yields a standard error of 2.4 mm and a correlation coefficient of 0.98. Discrepancies are primarily caused by errors in the observed water-equivalent data, errors in the determination of incoming longwave radiation, and possible variations in the turbulent transfer coefficients during the snowmelt season due to variations in the roughness height parameter (z_o).

3. The comparison between the energy balance and temperature index snow cover models indicates that the energy balance model gives improved results. Air temperature is a good index to snowmelt during most periods. However, when the relationships between air temperature and the other meteorological variables deviate significantly from normal, the temperature index model does not provide good estimates of snowmelt. The energy balance model gives good estimates of snowmelt under all meteorological conditions.

4. The minimum recommended data requirements for using an energy balance model are measurements of air temperature, vapor pressure, and wind, plus a good estimate of incoming solar radiation. Index models are recommended for use when available data does not meet these requirements and in very heavily forested areas. Energy balance models should give improved results in open and partly forested areas when there is considerable variability in meteorological conditions during the snowmelt period. An energy balance snow cover model offers a much more reliable means of extrapolating to determine behavior under extreme conditions.

BIBLIOGRAPHY

Amorocho, J., and Espildora B., 1966: "Mathematical Simulation of the Snow Melting Processes," Water Science and Engineering Papers No. 3001, University of California, Davis, Calif., 156 pp.

Anderson, Eric A., and Crawford, Norman H., 1964: "The Synthesis of Continuous Snowmelt Runoff Hydrographs on a Digital Computer," Department of Civil Engineering Technical Report No. 36, Stanford University, Stanford, Calif., 103 pp.

Anderson, E. A., and Baker, D. R., 1967: "Estimating Incident Terrestrial Radiation under all Atmospheric Conditions," Water Resources Research, Vol. 3, No. 4, pp. 975-987.

Anderson, E. A., 1968: "Development and Testing of Snow Pack Energy Balance Equations," Water Resources Research, Vol. 4, No. 1, pp. 19-37.

Anderson, Eric A., 1973: "National Weather Service River Forecast System--Snow Accumulation and Ablation Model," NOAA Technical Memorandum NWS HYDRO-17, U.S. Dept. of Commerce, Silver Spring, Md., 217 pp.

Bader, H., Haefeli, R., Bucher, J., Neher, J., Eckel, O., and Thams, Chr., 1939: "Der Schnee und Seine Metamorphose," Beitrage zur Geologie der Schweiz, Geotechnische Serie, Hydrologie, Lieferung 3, Bern [English translation: "Snow and Its Metamorphism," Translation 14, Snow, Ice and Permafrost Research Establishment, 313 pp. (Available from Cold Regions Research and Engineering Laboratory, Hanover, N.H.)].

Bohren, Craig F., and Barkstrom, Bruce R., 1974: "Theory of the Optical Properties of Snow," Journal of Geophysical Research, Vol. 79, No. 30, pp. 4527-4535.

Bowen, I. S., 1926: "The Ratio of Heat Losses by Conduction and Evaporation from any Water Surface," Physical Review, Vol. 27, No. 6, pp. 779-787.

Bradley, E. F., 1968: "A Shearing Stress Meter for Micrometeorological Studies," Quart. Jour. Royal Meteorol. Soc., Vol. 94, London, England, pp. 380-387.

Brutsaert, Wilfried, 1972: "Radiation, Evaporation and the Maintenance of Turbulence under Stable Conditions in the Lower Atmosphere," Boundary-Layer Meteorology, Vol. 2, pp. 309-325.

Businger, J. A., Wyngaard, J. C., Izumi, Y., and Bradley, E. F., 1971: "Flux-Profile Relationships in the Atmospheric Surface Layer," Jour. of the Atmospheric Sciences, Vol. 28, pp. 181-189.

Businger, Joost A., 1973: "Turbulent Transfer in the Atmospheric Surface Layer," Workshop on Micrometeorology, Duane A. Haugen, editor, American Meteorological Society, pp. 67-100.

Carlson, Robert F., Norton, William, and McDougall, James, 1974: "Modeling Snowmelt Runoff in an Arctic Coastal Plain," Institute of Water Resources, University of Alaska (available as PB-232-431), Fairbanks, Alaska 72 pp.

Colbeck, S. C., 1972: "A Theory of Water Percolation in Snow," Journal of Glaciology, Vol. 11, No. 63, pp. 369-385.

Colbeck, S. C., 1973: "Theory of Metamorphism of Wet Snow," Cold Regions Research and Engineering Laboratory Research Report 313, Hanover, N.H., 11 pp.

Colbeck, S. C., and Davidson, G., 1973: "Water Percolation through Homogeneous Snow," Proceedings of Banff Symposium: The Role of Snow and Ice in Hydrology, Intern. Assoc. Hydrologic Sci. Publ. No. 107, Vol. 1, pp. 242-257. (Available from Atm. Sci. Library, NOAA, Silver Spring, Md.)

Colbeck, S. C., 1974: "The Capillary Effects on Water Percolation in Homogeneous Snow," Journal of Glaciology, Vol. 13, No. 67, pp. 85-97.

Colbeck, S. C., 1975a: "A Theory for Water Flow through a Layered Snowpack," Water Resources Research, Vol. 11, No. 2, pp. 261-266.

Colbeck, S. C., 1975b: "Analysis of Hydrologic Response to Rain-on-Snow," Cold Regions Research and Engineering Laboratory Research Report 340, Hanover, N.H., 13 pp.

Deardorf, James W., 1968: "Dependence of Air-Sea Transfer Coefficients on Bulk Stability," Jour. of Geophysical Research, Vol. 73, No. 8, pp. 2549-2557.

deQuervain, M. R., 1963: "On the Metamorphism of Snow," Ice and Snow, W. D. Kingery, editor, the M.I.T. Press, Cambridge, Mass., pp. 377-390.

deQuervain, M. R., 1973: "Snow Structure, Heat and Mass Flux through Snow," Proceedings of Banff Symposium: The Role of Snow and Ice in Hydrology, Intern. Assoc. Hydrologic Sci. Publ. No. 107, Vol. 1, pp. 203-226. (Available from Atm. Sci. Library, NOAA, Silver Spring, Md.)

Dyer, A. J., 1961: "Measurements of Evaporation and Heat Transfer in the Lower Atmosphere by an Automatic Eddy-correlation Technique," Quart. Jour. Royal Meteorol. Soc., Vol. 87, London, England, p. 401.

Dyer, A. J., 1967: "The Turbulent Transport of Heat and Water Vapor in an Unstable Atmosphere," Quart. Jour. Royal Meteorol. Soc., Vol. 93, London, England, pp. 501-508.

Dyer, A. J., and Hicks, B. B., 1970: "Flux-Gradient Relationships in the Constant Flux Layer," Quart. Jour. Royal Meteorol. Soc., Vol. 96, London, England, pp. 715-721.

Dyer, A. J., and Maher, F. J., 1965: "Automatic Eddy-Flux Measurement with the Evapotron," Jour. of Applied Meteorology, Vol. 4, No. 5, p. 622.

Eggleston, Keith O., Israelsen, Eugene K., and Riley, J. Paul, 1971: "Hybrid Computer Simulation of the Accumulation and Melt Processes in a Snowpack," PRWG65-1, Utah Water Research Laboratory, Utah State University, Logan, Utah, 77 pp.

Franz, Delbert D., 1974: "Prediction of Dew Point Temperature, Solar Radiation and Wind Movement Data for Simulation and Operations Research Models," (OWRR contract 14-31-0001-3736), Hydrocomp, Inc., Palo Alto, Calif., 53 pp.

Gerdel, R. W., 1948: "Penetration of Radiation into the Snow Pack," Transactions, American Geophysical Union, Vol. 29, No. 3, pp. 366-374.

Giddings, J. C., and LaChapelle, E., 1961: "Diffusion Theory Applied to Radiant Energy Distribution and Albedo of Snow," Jour. of Geophysical Research, Vol. 66, No. 1, pp. 181-189.

Gunn, K. L. S., 1965: "Measurements on New-Fallen Snow," Stormy Weather Group Scientific Report MW-44 (available from NTIS, report No. AFCRL-65-554), McGill University, Montreal, Canada, 62 pp.

Humphrey, John H., and Skau, Clarence M., 1974: "Variation of Snowpack Density and Structure with Environmental Conditions," Center for Water Resources Research, Desert Research Institute (available as PB-238-000), University of Nevada System, Reno, Nevada, 15 pp.

Jakob, M., and Hawkins, G. A., 1942: Elements of Heat Transfer and Insulation, John Wiley and Sons, New York, pp. 46-53.

Johnson, Martin L., and Anderson, Eric, 1968: "The Cooperative Snow Hydrology Project--ESSA Weather Bureau and ARS Sleepers River Watershed," Proceedings of the Eastern Snow Conference, pp. 13-23. (Available from Atm. Sci. Library, NOAA, Silver Spring, Md.)

Kohler H., 1950: "On Evaporation from Snow Surfaces," Arkiv fur Geofysik, B. 1, No. 8, Uppsala, Sweden, pp. 159-185.

Kojima, Kenji, 1967: "Densification of Seasonal Snow Cover," Physics of Snow and Ice, Proceedings of International Conf. on Low Temperature Science--Sapporo, Vol. I, Part 2, The Institute of Low Temperature Science, Hokkaido University, Sapporo, Japan, pp. 929-952.

Kondrat'eva, A. S., 1945: "Teploprovodnost Snegovogo pokrova i fizicheskie protsessy, proiskhodiaschie v nem pod vlianiem temperaturnogo gradienta," Izvest. Akad. Nauk SSSR, Moscow-Leningrad [English translation: "Thermal Conductivity of the Snow Cover and Physical Processes Caused by the Temperature Gradient," Translation 22, Snow, Ice and Permafrost Research Establishment, 13 pp. (Available from Cold Regions Research and Engineering Laboratory, Hanover, N.H.)]

Kraus, H., 1973: "Energy Exchange at Air-Ice Interface," Proceedings of Banff Symposium: The Role of Snow and Ice in Hydrology, Intern. Assoc. Hydrologic Sci. Publ. No. 107, Vol. 1, pp. 128-164. (Available from Atm. Sci. Library, NOAA, Silver Spring, Md.)

Kuzmin, P. P., 1961: Protsess tayaniya shezhnogo pokrova, Gidrometeorologicheskoe Izdatel'stvo, Leningrad [English translation: "Melting of Snow Cover," Israel Program for Scientific Translations (TT 71-50095), 290 pp.].

LaChapelle, E. R., 1969: "Properties of Snow," prepared for Hydrologic Systems course presented by College of Forest Resources, Nov. 17-18, University of Washington, Seattle, 21 pp.

Larson, Lee W., 1972: "Approaches to Measuring 'True' Snowfall," Proceedings of the Eastern Snow Conference, pp. 65-76. (Available from Atm. Sci. Library, NOAA, Silver Spring, Md.).

Leaf, Charles F., and Brink, Glen E., 1973: "Computer Simulation of Snowmelt within a Colorado Subalpine Watershed," USDA Forest Service Research Paper RM-99, Rocky Mountain Forest and Range Experiment Station, U.S. Forest Service, Ft. Collins, Colo., 22 pp.

Liljequist, G. H., 1957: "Wind Structure in the Lower Layer," Norwegian-British-Swedish Antarctic Expedition 1949-52, Scientific Results, Vol. II, Part 1, Energy Exchange of an Antractic Snow-Field, Norsk Polarinstitutt, Olso, Norway, pp. 193-206.

Lumley, J. L., and Panofsky, H. A., 1964: The Structure of Atmospheric Turbulence, Interscience Publishers, John Wiley and Sons, New York, pp. 99-118.

Mantis, Homer T. (editor), 1951: "Review of the Properties of Snow and Ice," SIPRE Report 4, Snow, Ice and Permafrost Research Establishment, pp. 64-70. (Available from Cold Regions Research and Engineering Laboratory, Hanover, N.H.)

McVehil, G. E., 1964: "Wind and Temperature Profiles near the Ground in Stable Conditions," Quart. Jour. Royal Meteorol. Soc., Vol. 90, London, England, pp. 136-146.

Meiman, J. R., and Grant, L. O., 1974: "Snow-Air Interactions and Management of Mountain Watershed Snowpack," Environmental Resources Center Completion Report Series No. 57, Colorado State University (available as PB-235-825), Ft. Collins, Colo., 36 pp.

Mellor, Malcolm, 1964: "Properties of Snow," Cold Regions Science and Engineering Monograph III-A1, Cold Regions Research and Engineering Laboratory, Hanover, N.H., 105 pp.

Mellor, M., 1966: "Some Optical Properties of Snow," International Symposium on Scientific Aspects of Snow and Ice Avalanches--Davos, Intern. Assoc. Sci. Hydrology Publ. No. 69, pp. 128-140. (Available from Atm. Sci. Library, NOAA, Silver Spring, Md.)

Monin, A. S., and Obukhov, A. M., 1954: "Basic Laws of Turbulent Mixing in the Surface Layer of the Atmosphere," Akad. Nauk, SSSR Trudy Geofizicheskii Institut, No. 24 (151), pp. 163-187. (Available from Atm. Sci. Library, NOAA, Silver Spring, Md.)

Morozov, G. A., 1967: "Computation of the Change in the Density of Snow Cover under the Influence of Water Vapor Diffusion, Convection, Sublimation and Condensation in It," Meteorologiya i gidrologiya, No. 6, pp. 98-103 [English translation: Soviet Hydrology: Selected Papers, No. 3, pp. 314-319.]

Obled, Charles, 1973: "Modeles Mathematiques de la Fusion Nivale Etude des Risques D'Avalanches," Laboratories de Mecanique des Fluides, Institut National Polytechnique de Grenoble, Grenoble, France, 47 pp. [English translation: "Mathematical Models of Snowmelt Study of Avalanche Risks," Translated for NOAA, available on loan from Language Services Division, F43, National Marine Fisheries Service, NOAA, Washington, D.C., 20235, 73 pp.]

Oke, T. R., 1970: "Turbulent Transport near the Ground in Stable Conditions," Jour. of Applied Meteorology, Vol. 9, pp. 778-786.

O'Neill, A. D. J., and Gray, D. M., 1973: "Solar Radiation Penetration through Snow," Proceedings of Banff Symposium: The Role of Snow and Ice in Hydrology, Intern. Assoc. Hydrologic Sci. Publ. No. 107, Vol. 1, pp. 227-241. (Available from Atm. Sci. Library, NOAA, Silver Spring, Md.)

Outcalt, S. I., Goodwin, C., Weller, G., and Brown, J., 1975: "A Digital Computer Simulation of the Annual Snow and Soil Thermal Regimes at Barrow, Alaska," Cold Regions Research and Engineering Laboratory Research Report 331, Hanover, N.H., 18 pp.

Priestly, C. H. B., 1959: Turbulent Transfer in the Lower Atmosphere, University of Chicago Press, Chicago, 130 pp.

Pruitt, W. O., and Angus, D. E., 1960: "Large Weighing Lysimeter for Measuring Evapotranspiration," Transactions Amer. Soc. Agricultural Engineers, Vol. 3, No. 2, pp. 13-18.

Pruitt, W. O., Morgan, D. L., and Lourence, F. J., 1971: "Evaluation of Eddy-Transfer Coefficients and Diabatic-Profile Functions under Turbulent Flow in the Lower Atmosphere," Chapter III, Final Technical Report, ECOM-68-G10-F, University of California, Davis, Calif. (AD 721-301), pp. 15-35.

Quick, M. C., 1967: "A Comparison of Measured and Theoretical Snowpack Temperatures," Jour. of Hydrology, Vol. 5, pp. 1-20.

Richardson, L. F., 1920: "The Supply of Energy from and to Atmospheric Eddies," Proceedings of the Royal Society of London, Series A, Vol. 97, London, England, pp. 354-373.

Rockwood, D. M., 1964: "Streamflow Synthesis and Reservoir Regulation," Technical Bulletin No. 22, U.S. Army Engineer Division, North Pacific, Portland, Oreg., 96 pp.

Rose, C. W., 1966: Agricultural Physics, Pergamon Press, London, 230 pp.

Schwerdtfeger, Peter, 1963: "Theoretical Derivation of the Thermal Conductivity and Diffusivity of Snow," Intern. Assoc. Sci. Hydrology, General Assembly-Berkeley, Intern. Assoc. Sci. Hydrology Publ. No. 61, pp. 75-81. (Available from Atm. Sci. Library, NOAA, Silver Spring, Md.)

Shafer, Benard A., and Super, Arlin B., 1971: "Infrared Temperature Sensing of Snow-Covered Terrain," Contract Number DAHC04-67-C-0058, Montana State University, Bozeman, Mont. (AD732849), 95 pp.

Shimizu, H., 1970: "Air Permeability of Deposited Snow," Contributions from the Institute of Low Temperature Science, Series A, No. 22, Sapporo, Japan, pp. 1-32.

Smithsonian Meteorological Tables, 1968: Sixth Revised Edition, 4th Reprint, Smithsonian Institution Press, Washington, D.C., pp. 343-381.

Snow Hydrology, 1956: Summary Report of the Snow Investigations, Corps of Engineers, North Pacific Division (available as PB-151660), Portland, Oreg., 437 pp.

Snow Investigations, 1955: "Lysimeter Studies of Snow Melt," Snow Investigations Research Note 25, Corps of Engineers, North Pacific Division, Portland, Oreg., 52 pp.

Sommerfield, R. A., and LaChapelle, E., 1970: "The Classification of Snow Metamorphism," Jour. of Glaciology, Vol. 9, No. 55, pp. 3-17.

SSARR Model, 1972: "Program Description and User's Manual, Program 724-K5-G0010, U.S. Army Engineer Division, North Pacific, Portland, Oreg., 201 pp.

Sulakvelidze, G. K., 1959: "Thermoconductivity Equation for Porous Media Containing Saturated Vapor, Water or Ice," Izv. Akad. Nauk SSSR Ser. Geofiz., pp. 284-287 [English translation: Bull. Acad. Sci. USSR Geophys. Ser., pp. 186-188.]

Sutton, O. G., 1953: Micrometeorology, McGraw-Hill, New York, 333 pp.

Sutton, O. G., 1954: Atmospheric Turbulence, 2nd Edition, Methuen, London, 111 pp.

Sverdrup, H. U., 1936: "The Eddy Conductivity of the Air over a Smooth Snow Field," Geofysiske Publikasjoner, Vol. XI, No. 7, Oslo, Norway, pp. 5-69.

Thomas, Charles W., 1963: "On the Transfer of Visible Radiation through Sea Ice and Snow," Jour. of Glaciology, Vol. 4, No. 34, pp. 481-484.

Wakahama, Gorow, 1968: "The Metamorphism of Wet Snow," Commission of Snow and Ice--General Assembly of Bern, Intern. Assoc. Sci. Hydrology Publ. No. 79, pp. 370-379. (Available from Atm. Sci. Library, NOAA, Silver Spring, Md.)

Webb, E. K., 1970: "Profile Relationships: The Log Linear Range, and Extension to Strong Stability," Quart. Jour. Royal Meteorol. Soc., Vol. 96, London, England, pp. 67-90.

Weller, Gunter E., 1969: "Radiation Diffusion in Antarctic Ice Media," Nature, Vol. 221, No. 5178, pp. 355-356.

Woodside, William, 1958: "Calculation of the Thermal Conductivity of Porous Media," Canadian Jour. of Physics, Vol. 36, Toronto, Canada, pp. 815-823.

Yen, Yin-Chao, 1965: "Heat Transfer Characteristics of Naturally Compacted Snow," Cold Regions Research and Engineering Laboratory Research Report 166, Hanover, N.H., 9 pp.

Yen, Yin-Chao, 1967: "The Rate of Temperature Propagation in Moist Porous Mediums with Particular Reference to Snow," Jour. of Geophysical Research, Vol. 72, No. 4, pp. 1283-1288.

Yen, Yin-Chao, 1969: "Recent Studies on Snow Properties," Advances in Hydroscience, Academic Press, New York, pp. 173-214.

Yosida, Zyungo, and Colleagues, 1955: "Physical Studies on Deposited Snow. I. Thermal Properties," Contributions from the Institute of Low Temperature Science, No. 7, Sapporo, Japan, pp. 19-74.

Yosida, Zyungo, 1958: "Quantitative Study of the Metamorphism of Snow Crystals by Sublimation," Translation 57, Snow, Ice and Permafrost Research Establishment, 10 pp. (Available from Cold Regions Research and Engineering Laboratory, Hanover, N.H.)

Yosida, Zyungo, 1963: "Physical Properties of Snow," Ice and Snow, W. D. Kingery, editor, the M.I.T. Press, Cambridge, Mass., pp. 485-527.

APPENDIX A

PARTIAL DERIVATIVES OF BASIC EQUATIONS WITH RESPECT TO THE UNKNOWN QUANTITIES

This appendix lists the partial derivatives for each of the basic finite-difference equations [Eqs. (4.4), (4.9), and (4.12)] with respect to the unknown quantities included in the equations. These partial derivatives are needed in order to solve the equations by use of the Newton-Raphson iteration technique.

Symbols which were defined in Chapter IV are not redefined. Eq. (3.18) is used for the specific heat of ice with C_{H1} representing the constant 0.0222, and C_{H2} representing 0.00176, the other constant in Eq. (3.18). Eq. (3.19) is used for the saturation vapor pressure at the snow surface (e_o). The finite-difference expression for $\partial T/\partial z$ is written as

$$\left(\frac{\partial T}{\partial z}\right)_n = \frac{F6_n}{2 \cdot DL_1 \cdot DL_2} \quad , \tag{A.1}$$

where:

$$DL_1 = z^t_n - z^t_{n-1} \quad ,$$

$$DL_2 = z^t_{n+1} - z^t_n \quad , \text{ and}$$

$$F6_n = DL_1 \cdot T_{n+1} + (DL_2 - DL_1) \cdot T_n - DL_2 \cdot T_{n-1} \quad .$$

The finite-difference expression for $\partial^2 T/\partial z^2$ is written as

$$\left(\frac{\partial^2 T}{\partial z^2}\right)_n = \frac{2 \cdot F7_n}{DL_1 \cdot DL_2 \cdot (DL_1 + DL_2)} \quad , \tag{A.2}$$

where $F7_n = DL_1 \cdot T_{n+1} - (DL_1 + DL_2) \cdot T_n + DL_2 \cdot T_{n-1}$.

Derivatives of the Surface Layer Equation (E_o)

The partial derivatives of the surface layer equation are: with respect to the surface layer temperature at time $t + \Delta t$

$$\frac{\partial E_o}{\partial T_o}_{t+\Delta t} = (d \cdot \rho_s)^t_o \cdot C_{H1} + 2 \cdot (d \cdot \rho_s)^t_o \cdot C_{H2} \cdot T_o^{t+\Delta t} \tag{A.3}$$

$$+ 4\cdot\theta\cdot\Delta t\cdot\varepsilon\cdot\sigma\cdot(T_o^{t+\Delta t})^3 + \theta\cdot(L_s\cdot\rho_w/10)\cdot f(U_a)\cdot\gamma$$

$$+ [\theta\cdot L_s^2\cdot\rho_w\cdot f(U_a)\cdot e_o^{t+\Delta t}]/[10\cdot R_w\cdot(T_o^{t+\Delta t})^2] \quad ,$$

with respect to intermediate layer temperatures at time t + Δt (n varies from 1 to N-1)

$$\frac{\partial E_o}{\partial T_n^{t+\Delta t}} = (d\cdot\rho_s)_n^t\cdot C_{H1} + 2\cdot(d\cdot\rho_s)_n^t\cdot C_{H2}\cdot T_n^{t+\Delta t} \quad , \tag{A.4}$$

with respect to the bottom layer temperature at time t + Δt (bottom layer not at 0°C)

$$\frac{\partial E_o}{\partial T_N^{t+\Delta t}} = \frac{\theta\cdot\Delta t\cdot Fl_g^{t+\Delta t}}{0.5\cdot d_N^t\cdot Fl_g^{t+\Delta t} + d_g\cdot Fl_N^{t+\Delta t}}\cdot\left\{Fl_N^{t+\Delta t} - L_s\cdot C_D\cdot F3_N^{t+\Delta t}\cdot(T_g^{t+\Delta t} - T_N^{t+\Delta t})\right.$$
$$\left. + \frac{d_g\cdot L_s\cdot C_D\cdot Fl_N^{t+\Delta t}\cdot F3_N^{t+\Delta t}\cdot(T_g^{t+\Delta t} - T_N^{t+\Delta t})}{0.5\cdot d_N^t\cdot Fl_g^{t+\Delta t} + d_g\cdot Fl_N^{t+\Delta t}}\right\} \quad , \tag{A.5}$$

with respect to the bottom layer temperature at time t + Δt (bottom layer at 0°C)

$$\frac{\partial E_o}{\partial T_N^{t+\Delta t}} = \frac{\theta\cdot\Delta t\cdot Fl_g^{t+\Delta t}}{d_g} \quad , \tag{A.6}$$

and with respect to the amount of liquid-water in each layer at time T + Δt (n varies from zero to N)

$$\frac{\partial E_o}{\partial W_n^{t+\Delta t}} = \frac{L_f\cdot\rho_w}{10} \quad . \tag{A.7}$$

R_w is the gas constant for water vapor and F3 is defined as

$$F3 = \frac{\partial F2}{\partial T} = T^{n_d}\cdot f'' + n_d\cdot f'\cdot T^{(n_d-1)} \quad . \tag{A.8}$$

Derivatives of the Intermediate Layer Equations (E_n)

The partial derivatives of the intermediate layer equation (n varies from 1 to N-1) are:

with respect to the temperature of the layer above at time t + Δt

$$\frac{\partial E_n}{\partial T_{n-1}^{t+\Delta t}} = -\frac{2\cdot\theta\cdot\Delta t\cdot Fl_n^{t+\Delta t}}{(\rho_s)_n^t\cdot(c_i)_n^{t+\Delta t}\cdot DL_1\cdot(DL_1+DL_2)} + \frac{\theta\cdot\Delta t\cdot\left[\frac{\partial k_e}{\partial \rho_s}\right]_n^t}{2\cdot(\rho_s)_n^t\cdot(c_i)_n^{t+\Delta t}\cdot DL_1}\cdot\left[\frac{\partial \rho_s}{\partial z}\right]_n^t$$

$$+\frac{\theta\cdot\Delta t\cdot C_D\cdot L_s\cdot F6_n^{t+\Delta t}\cdot\left[\frac{n_d}{T_n^{t+\Delta t}}\cdot F2_n^{t+\Delta t}+F4_n^{t+\Delta t}\right]}{2\cdot(\rho_s)_n^t\cdot(c_i)_n^{t+\Delta t}\cdot(DL_1)^2\cdot DL_2}, \qquad (A.9)$$

with respect to the temperature of the given layer at time t + Δt

$$\frac{\partial E_n}{\partial T_n^{t+\Delta t}} = 1.0 + \frac{\theta\cdot C_{H2}\cdot I_n}{(d\cdot\rho_s)_n^t\cdot\left[(c_i)_n^{t+\Delta t}\right]^2} + \frac{2\cdot\theta\cdot\Delta t}{(\rho_s)_n^t\cdot DL_1\cdot DL_2\cdot(DL_1+DL_2)\cdot(c_i)_n^{t+\Delta t}}$$

$$\cdot\left[\frac{C_{H2}\cdot(F1\cdot F7)_n^{t+\Delta t}}{(c_i)_n^{t+\Delta t}} - L_s\cdot C_D\cdot(F3\cdot F7)_n^{t+\Delta t} + (DL_1+DL_2)\cdot Fl_n^{t+\Delta t}\right] \qquad (A.10)$$

$$+\frac{\theta\cdot\Delta t\cdot\left[\frac{\partial k_e}{\partial \rho_s}\right]_n^t\cdot\left[\frac{\partial \rho_s}{\partial z}\right]_n^t}{2\cdot(\rho_s)_n^t\cdot DL_1\cdot DL_2\cdot(c_i)_n^{t+\Delta t}}\cdot\left[\frac{C_{H2}\cdot F6_n^{t+\Delta t}}{(c_i)_n^{t+\Delta t}} - (DL_2-DL_1)\right]$$

$$+\frac{\theta\cdot\Delta t\cdot C_D\cdot L_s}{4\cdot(\rho_s)_n^t\cdot(DL_1\cdot DL_2)^2\cdot(c_i)_n^{t+\Delta t}}\cdot\left[\frac{C_{H2}\cdot\left(F6_n^{t+\Delta t}\right)^2\cdot\left[\frac{n_d}{T_n^{t+\Delta t}}\cdot F2_n^{t+\Delta t}+F4_n^{t+\Delta t}\right]}{(c_i)_n^{t+\Delta t}}\right]$$

$$- \left(F6_n^{t+\Delta t}\right)^2 \cdot \left[F5_n^{t+\Delta t} + \frac{n_d}{T_n^{t+\Delta t}} \cdot F3_n^{t+\Delta t} - \frac{n_d \cdot F2_n^{t+\Delta t}}{(T_n^{t+\Delta t})^2}\right.$$

$$\left. - 2 \cdot F6_n^{t+\Delta t} \cdot (DL_2 - DL_1) \cdot \left(\frac{n_d}{T_n^{t+\Delta t}} \cdot F2_n^{t+\Delta t} + F4_n^{t+\Delta t}\right)\right] \quad ,$$

with respect to the temperature of the layer below at time t + Δt

$$\frac{\partial E_n}{\partial T_{n+1}^{t+\Delta t}} = - \frac{2 \cdot \theta \cdot \Delta t \cdot F1_n^{t+\Delta t}}{(\rho_s)_n^t \cdot (c_i)_n^{t+\Delta t} \cdot DL_2 \cdot (DL_1 + DL_2)} - \frac{\theta \cdot \Delta t \cdot \left(\frac{\partial k_e}{\partial \rho_s}\right)_n^t}{2 \cdot (\rho_s)_n^t \cdot (c_i)_n^{t+\Delta t} \cdot DL_2} \cdot \left(\frac{\partial \rho_s}{\partial z}\right)_n^t$$

$$- \frac{\theta \cdot \Delta t \cdot C_D \cdot L_s \cdot F6_n^{t+\Delta t} \cdot \left(\frac{n_d}{T_n^{t+\Delta t}} \cdot F2_n^{t+\Delta t} + F4_n^{t+\Delta t}\right)}{2 \cdot (\rho_s)_n^t \cdot (c_i)_n^{t+\Delta t} \cdot DL_1 \cdot (DL_2)^2} \quad , \tag{A.11}$$

and with respect to the amount of liquid-water in the given layer at time t + Δt

$$\frac{\partial E_n}{\partial W_n^{t+\Delta t}} = \frac{L_f \cdot \rho_w}{10 \cdot (d \cdot \rho_s)_n^t \cdot (c_i)_n^{t+\Delta t}} \quad . \tag{A.12}$$

F5 is defined as

$$F5 = \frac{\partial F4}{\partial T} = T^{n_d} \cdot f''' + n_d \cdot f'' \cdot T^{(n_d - 1)} \quad , \tag{A.13}$$

where f''' is defined by Eq. (3.24).

Derivatives of the Bottom Layer Equation (E_N)

The partial derivatives of the bottom layer equation are:
with respect to the temperature of the layer above at time t + Δt

$$\frac{\partial E_N}{\partial T_{N-1}^{t+\Delta t}} = \frac{2\cdot\theta\cdot\Delta t\cdot Fl_N^{t+\Delta t}}{(d\cdot\rho_s)_N^t\cdot(c_i)_N^{t+\Delta t}\cdot\left(d_{N-1}^t\cdot Fl_N^{t+\Delta t}+d_N^t\cdot Fl_{N-1}^{t+\Delta t}\right)}$$

$$\cdot\left(\frac{d_N^t\cdot L_s\cdot C_D\cdot(Fl\cdot F3)_{N-1}^{t+\Delta t}\cdot\left(T_{N-1}^{t+\Delta t}-T_N^{t+\Delta t}\right)}{d_{N-1}^t\cdot Fl_N^{t+\Delta t}+d_N^t\cdot Fl_{N-1}^{t+\Delta t}}\right. \tag{A.14}$$

$$\left. - L_s\cdot C_D\cdot F3_{N-1}^{t+\Delta t}\cdot\left(T_{N-1}^{t+\Delta t}-T_N^{t+\Delta t}\right) - Fl_{N-1}^{t+\Delta t}\right) \quad ,$$

and with respect to the temperature of the bottom layer at time t + Δt

$$\frac{\partial E_N}{\partial T_N^{t+\Delta t}} = 1.0 + \frac{\theta\cdot C_{H2}\cdot I_N}{(d\cdot\rho_s)_N^t\cdot\left((c_i)_N^{t+\Delta t}\right)^2} + \frac{2\cdot\theta\cdot\Delta t\cdot Fl_{N-1}^{t+\Delta t}}{(d\cdot\rho_s)_N^t\cdot(c_i)_N^{t+\Delta t}\cdot\left(d_{N-1}^t\cdot Fl_N^{t+\Delta t}+d_N^t\cdot Fl_{N-1}^{t+\Delta t}\right)}$$

$$\cdot\left(\frac{d_{N-1}^t\cdot L_s\cdot C_D\cdot(Fl\cdot F3)_N^{t+\Delta t}\cdot\left(T_{N-1}^{t+\Delta t}-T_N^{t+\Delta t}\right)}{d_{N-1}^t\cdot Fl_N^{t+\Delta t}+d_N^t\cdot Fl_{N-1}^{t+\Delta t}}\right. \tag{A.15}$$

$$+\frac{C_{H2}\cdot Fl_N^{t+\Delta t}\cdot\left(T_{N-1}^{t+\Delta t}-T_N^{t+\Delta t}\right)}{(c_i)_N^{t+\Delta t}} - L_s\cdot C_D\cdot F3_N^{t+\Delta t}\cdot\left(T_{N-1}^{t+\Delta t}-T_N^{t+\Delta t}\right)$$

$$\left. + Fl_N^{t+\Delta t}\right) + \frac{\partial T_g}{\partial T_N^{t+\Delta t}} \quad .$$

When the bottom layer is not at 0°C

$$\frac{\partial T_g}{\partial T_N^{t+\Delta t}} = \frac{\theta\cdot\Delta t\cdot Fl_g^{t+\Delta t}}{(d\cdot\rho_s)_N^t\cdot(c_i)_N^{t+\Delta t}\cdot\left(d_g\cdot Fl_N^{t+\Delta t}+0.5\cdot d_N^t\cdot Fl_g^{t+\Delta t}\right)}$$

$$\cdot \left[\frac{L_s \cdot C_D \cdot d_g \cdot \left[F1 \cdot F3 \right]_N^{t+\Delta t} \cdot \left(T_g^{t+\Delta t} - T_N^{t+\Delta t} \right)}{d_g \cdot Fl_N^{t+\Delta t} + 0.5 \cdot d_N^t \cdot Fl_g^{t+\Delta t}} \right. \tag{A.16}$$

$$+ \frac{C_{H2} \cdot Fl_N^{t+\Delta t} \cdot \left(T_g^{t+\Delta t} - T_N^{t+\Delta t} \right)}{(c_i)_N^{t+\Delta t}}$$

$$\left. - L_s \cdot C_D \cdot F3_N^{t+\Delta t} \cdot \left(T_g^{t+\Delta t} - T_N^{t+\Delta t} \right) + Fl_N^{t+\Delta t} \right] \quad ,$$

and when the bottom layer is at 0°C

$$\frac{\partial T_g}{\partial T_N^{t+\Delta t}} = \frac{\theta \cdot \Delta t \cdot Fl_g^{t+\Delta t}}{(d \cdot \rho_s)_N^t \cdot d_g \cdot (c_i)_N^{t+\Delta t}} \cdot \left[\frac{C_{H2} \cdot \left(T_g^{t+\Delta t} - T_N^{t+\Delta t} \right)}{(c_i)_N^{t+\Delta t}} + 1.0 \right] \quad . \tag{A.17}$$

The partial derivative of the bottom layer equation with respect to the amount of liquid-water in the bottom layer at time t + Δt is

$$\frac{\partial E_N}{\partial W_N^{t+\Delta t}} = \frac{L_f \cdot \rho_w}{10 \cdot (d \cdot \rho_s)_N^t \cdot (c_i)_N^{t+\Delta t}} \tag{A.18}$$

*U.S. GOVERNMENT PRINTING OFFICE:1976 210-801/185 1-3

(Continued from inside front cover)

NWS 16 Storm Tide Frequencies on the South Carolina Coast. Vance A. Myers, June 1975. (COM-75-11335)

NWS 17 Estimation of Hurricane Storm Surge in Apalachicola Bay, Florida. James E. Overland, June 1975. (COM-75-11332)

NWS 18 Joint Probability Method of Tide Frequency Analysis Applied to Apalachicola Bay and St. George Sound, Florida. Francis P. Ho and Vance A. Myers, November 1975.

NOAA—S/T 76-1938